UNIVERSITÀ
DI PAVIA

Ph.D. IN BIOMEDICAL SCIENCES
(XXXV Cycle)

DEPARTMENT OF BRAIN AND BEHAVIORAL SCIENCES
UNIT OF NEUROPHYSIOLOGY

Investigating the complex integration processing of input patterns in the cerebellar cortex using HD-MEA and computational tools

Supervisors:
Prof. Lisa Mapelli, Supervisor
Prof. Egidio D'Angelo, Co-Supervisor

Tutor:
Dott. Stefano Masoli

Doctoral Dissertation of
Alessandra Ottaviani

a.a 2021/2022

Declaration

I hereby declare that the contents and organization of this dissertation constitute my own original work and do not compromise in any way the rights of third parties, including those relating to the security of personal data.

Alessandra Ottaviani

2022

Summary

The cerebellum is a remarkable structure with a well-organized cytoarchitecture that allows it to perform parallel operations and process information in a few milliseconds to retransmit them to different brain areas. The main functions of the cerebellum perform are posture control, gait, motor coordination, and learning. In recent decades, the study of the cerebellum has also focused on other functions besides motor functions: emotional and cognitive functions, corroborating the idea that this structure, although highly organized, is capable to perform complex functions. The presence of numerous and different cell types performing excitatory or inhibitory functions and the presence of feedback and feedforward loops, make the cerebellum an interesting object of study on multiple scales of resolution, from the microscale to the macroscale.

At the microscale level, I focused on studying the biophysical aspect of the Golgi cell, one of the main interneurons of the granular layer that plays a key role in the control of information integration. In fact, the Golgi cell is involved in the spatiotemporal organization of inputs and regulates the transmission of the excitatory signal between mossy fibers and granules. The presence of apical and basal dendrites makes the Golgi cell able to perform a dendritic integration and a process of synaptic plasticity called spike-timing-dependent plasticity (STDP). These predictive properties were identified through the construction of a detailed computational model of a single neuron, used here to make up for the lack of experimental information

on Golgi cell connectivity and dynamics. The computational model made it possible to provide a prediction about the interplay of basal and apical dendrites, whose functioning is modulated by different patterns of excitation and inhibition regulated by synaptic NMDA and AMPA receptors. STDP may be controlled by information provided by parallel fiber and integrated into apical dendrites, supporting the fact that spike timing is important to control synaptic plasticity at the input stage.

At the mesoscale level, I focused on the *ex vivo* spatiotemporal study of the cerebellar cortex circuit, and how the signal from the mossy fibers is transmitted and integrated at the level of the granular layer and the Purkinje cell layer, the only output of the cerebellar cortex. The focus has been on how the circuit manages to integrate information at different input frequencies by stimulating the mossy fibers electrically. We recorded the extracellular signals of the neuronal population using the HD – MEA (high-density multielectrode array), a new technology that allows high spatial and temporal resolution, especially in terms of a population study. The spatiotemporal profile of the extracellular responses of granules and Purkinje cells was then analyzed by applying a Lempel - Ziv compression algorithm that allowed us to identify all significant activations of cells after each last pulse of the stimulation train across trials, at different input frequencies (0.1Hz, 6Hz, 20Hz, 50Hz, 100Hz). Subsequently, we calculated the Perturbational Complexity Index (PCI) an index, mainly used to investigate the different complexity states of the cerebral cortex, here applied to an *ex vivo* condition, to define the state of integration and segregation that determines the connectivity of cerebellar neurons and the complexity of information transmission.

Table of Contents

Chapter 1

Introduction

1.1 From movement to cognition

The remarkable diversity of molecular, cellular, and circuit mechanisms enclosed in a dynamic circuit architecture contributes to make the cerebellum an essential structure in information processing (De Zeeuw et al., 2021). This functional richness can predict events with precise timing, acting like a forward controller (D'Angelo, 2018).

The internal connections of cerebellar neural networks and the intrinsic features of cerebellar neurons define how the wide range of sensory inputs can be integrated to generate motor–related outputs (Apps and Garwicz, 2005). The cerebellum receives motor commands from the primary motor cortex and predicts the sensory feedback triggered by the command based on motor coordination. The prediction is then compared with the actual feedback from sensory inputs, including tactile, visual, vestibular, and auditory information. The prediction error is relayed back to the motor cortex, which adapts the motor program from one movement to the next (Bastian, 2006). In fact, the cerebellum helps to detect and correct errors between intended movement and their actual execution. However, its

invlvement not only in motor and coordination control but also in higher cognitive functions like attention, language skills, motion perception, and emotional processing has been reported (Nguyen et al., 2023).

Cerebellar networks show different types of synaptic plasticity, which indicates that learning processes and experience-dependent adaptions are salient features of their functioning.

New technologies for experimental research and the development of computational modeling led to new theories on the cerebellum, defined as a “supervised learning machine”, and how it contributes to both movement and cognitive processes (Albus, 1971). In neuronal networks, the pivotal role of supervised learning is that feedback concerning the system performance is used to regulate internal settings and improve future performance. This means that the cerebellum develops an internal prediction scheme that is compared to the feedback from the sensory systems to direct anticipatory behaviors (Keller and Mrsic-Flogel, 2018; Hull, 2020).

The cerebellar network contains multiple neuronal types, connected to each other to create a highly recurrent architecture. The information is integrated with neuronal ensembles that have linear input/output computation (Raymond and Medina, 2018). The cerebellar network comprises three elements: (i) an adaptive filter; (ii) input preprocessing, and iii) an instructive signal. (i) To be able to learn, in response to each input, the network needs to have internal parameters that can be adaptively changed. This change is obtained by modifying the properties of cerebellar neuron connectivity and the different types of synaptic plasticity. The input signal is processed in order to transform one set of temporally signals into another signal (Dean and Porrill, 2008). The main example is the mossy

fiber input that is split into components (parallel fibers signals), before reaching the Purkinje Cells, which represent the filter's output. The Purkinje cells behave as an adaptive processor, producing the output and sending it to various brain areas, via the cerebellar nuclei (Apps and Hawkes, 2009); (ii) The preprocessing of the input is driven by the granule cell layer, the first stage of the cerebellar cortex, characterized by the granule cells, the most abundant neurons in the central nervous system (CNS). The processing of mossy fiber inputs by granule cells suggests that this internal circuit performs a pattern separation (Marr, 1969), exploiting synaptic connectivity, spike thresholding, multimodal integration, and broad feedback inhibition (Marr, 1969; Albus, 1971; Cayco-Gajic and Silver, 2019). The mossy fiber input was shared with a large number of granule cells, and each granule cell receives synaptic input from an average of four mossy fibers. In addition, Golgi cells, the granular layer interneurons, provide feedback inhibition. The same mechanism is conserved in the different cerebellar regions, suggesting that the cerebellar cortex architecture and circuitry play a key role in learning. (iii) Errors are important during supervised learning, which depends on instructional signals that lead to appropriate adjustments in the adaptive filter. Climbing fiber projections, responsible for evoking complex spikes in Purkinje cells, play a crucial role in conveying neural instructive error signals in the cerebellum (Silva et al., 2022) and their activity is related to sensorimotor errors for several behavioral tasks. The Purkinje cell simple spike activity can also provide instructive signals, and the output is correlated with the corrective mechanism. Indeed, the Purkinje cell high-rate pacemaker activity can instruct plasticity in the cerebellar nuclei and influences network responses through firing increases and pauses (Raymond and Medina, 2018).

The acquisition of new motor skills usually implies passing from a “controlled” to an “automatic” processing, where movements that initially demand problem-solving and attention become increasingly efficient, stereotyped, and significantly less dependent on attention (Koziol and Lutz, 2013). A similar mechanism is used during cognitive processing, where the development of automatic operations similarly requires the involvement of cerebellar functional systems (Castellazzi et al., 2018).

In recent years, the discussion has been focused on how the cerebellum participates in cognitive functions. The internal cerebellar modular architecture allows for parallel processing of different specific activities. The reason can be found in the complex connectivity between the cerebellum and different brain areas, as neuroimaging functional studies confirmed. Beside the main motor-related structures, the cerebellum receives information from the hypothalamus, the parahippocampal gyrus, the cingulate gyrus, the superior temporal cortex, the posterior parietal cortex, and the prefrontal cortex (Koziol and Lutz, 2013). These data have been confirmed by fMRI and tractography studies. This is confirmed by the consequences of lesions in cerebellar regions receiving different inputs. Lesions of cerebellar motor regions cause ataxia, limb dysmetria, and dysarthric speech; impairments at cerebellar vestibular sites generate the vestibular syndrome; while lesions of cognitive regions manifest the cognitive-affective syndrome (Schmahmann, 2019) characterized by deficits in executive function, linguistic processing, spatial cognition, and affect regulation.

To summarize, cognitive and motor functions represent forms of behavior and use anticipatory control loops developed for overt actions, and the fact that cognitive processing is ultimately grounded in sensorimotor anticipation suggests that the cerebellum plays a pivotal role in the shaping,

coordination, and fine-tuning of action, cognition, and thought (Koziol and Lutz, 2013).

1.2 The anatomical and physiological principles of the cerebellum

The cerebellum consists of ~ 10% of the total brain mass in humans (Azevedo et al., 2009) (https://bionumbers.hms.harvard.edu/bionumber.aspx?s=n&v=3&id=106398), holding ~ 80% of the neurons (D'Angelo, 2018; Van Essen et al., 2018), most of which are granule cells packed into the input layer. As a part of the CNS, it is located behind the brainstem, sends and receives information through the inferior, middle, and superior peduncle, and occupies nearly all the space of the posterior cranial fossa. It consists of an outer layer of tightly folded grey matter forming the cerebellar cortex, with the white matter located beneath. Four deep cerebellar nuclei are embedded in the center of the white matter in mice (Apps and Garwicz, 2005; D'Angelo, 2018). Some animals, including humans, present only three DCN, due to the fusion of emboliform and globose nuclei in the interposed nucleus (Diedrichsen et al., 2011).

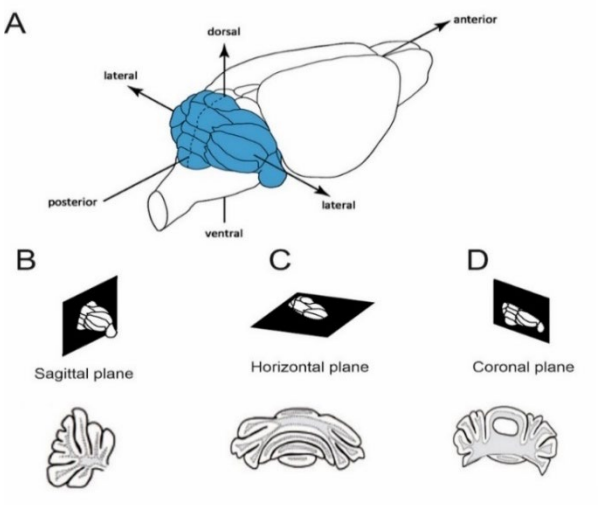

*<u>Figure 1</u>: Anatomical plane in the mouse cerebellum. (**A**) Mouse cerebellum (in blue). (**B – C – D**) Orientation used in vitro experiments and resulting slices in sagittal, horizontal, and coronal orientation. Adapted from Özcan, 2018 and Valera, 2015.*

The cerebellar cortex is arranged spatially along two main axes (Figure 1): the anterior-posterior axis divides the cortex into lobules, while the mediolateral axis separates it into a vermis and two hemispheres. The mediolateral axis is also known as the long axis of the folium, embracing both the coronal and the horizontal/transverse plane. Because of the cerebellar folding, acute slices in either coronal or horizontal/transverse planes have a similar organization. However, each slicing plane will allow the study of several groups of lobules. In general, using the horizontal plane is more convenient since it allows easier lobules recognition instead of the coronal plane.

The cerebellum is partied by three longitudinal regions, running along the rostral to caudal orientation, that represent the three main areas based on the origin of the afferent fiber (Figure 2):

i) *Vermis* and *paravermial zones* (formerly known as *spinocerebellum*). They are located in the medio lateral zone of the hemispheres and are the sole region that receives afferent fibers directly from the spinal cord. The lateral part controls the movements of distal muscles similar to the limb movement while walking. The vermis controls the movements of proximal muscles and regulates eye movements in response to vestibular inputs.

ii) The lateral zone of the *hemispheres* (formerly known as *cerebrocerebellum*). It is the largest subdivision that occupies most of the lateral hemisphere in humans and primates. It receives afferent information from multiple areas of the cerebral cortex, and sends information through the dentate nucleus, to the motor, premotor, and prefrontal cortex concerning the regulation of highly skilled movements, especially the

planning and execution of complex spatial and temporal sequences of movements and cognitive tasks.

The *medial zone* (nodulus) controls the axial musculature, while the flocculus are involved in eye movements and hand–eye coordination. These caudal lobes, in regard to phylogenesis, represent the *achicerebellum*, and are strictly connected with the vestibular nuclei (the oldest subdivision is the *vestibulocerebellum)* sending output to these structures.

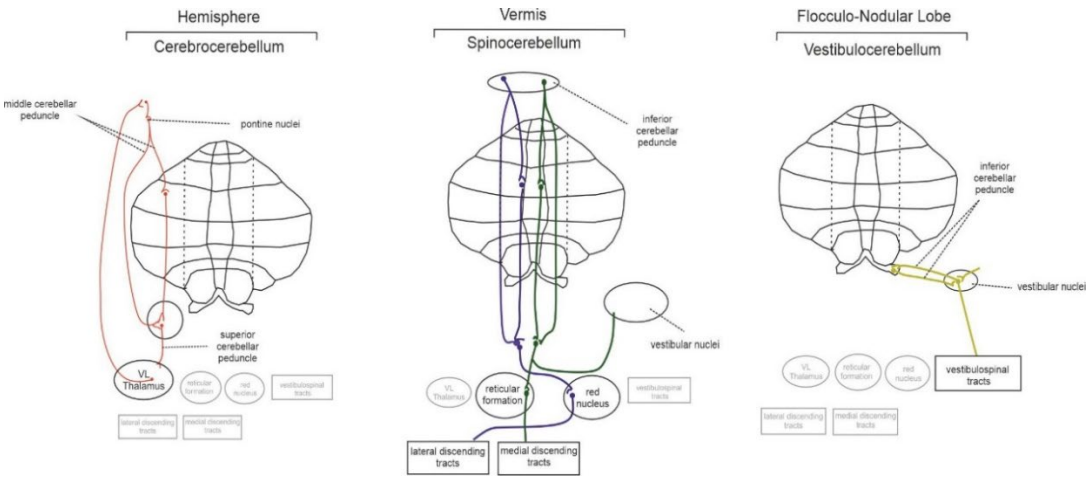

Figure 2: Functional organization of cerebellum and its connectivity. Adapted from Purves D., 2012.

The inferior and middle peduncles connect the CNS and the Peripheral Nervous System (PNS) to the cerebellum, while the superior peduncle connects the cerebellum to the cerebral cortex:

i) The inferior peduncle is the smallest and the most complex, with many afferent and efferent pathways. The afferent fibers are axons from the vestibular nuclei, the spinal cord, and several regions of the brainstem tegmentum. The main tracts are the olivocerebellar, paraolivocerebellar, vestibulocerebellar, reticulocerebellar, posterior spinocerebellar, cuneocerebellar, and trigeminocerebellar tracts. Additionally, the efferent pathways include the cerebelloolivary, cerebellovestibular, and cerebelloreticular tracts, which project to the vestibular nuclei and the reticular formation.

ii) The middle peduncle is primarily an afferent pathway to the cerebellar network; the majority of the cell bodies are located at the base of the pons, where they generate the pontine nuclei, which receive inputs from a wide variety of sources, including almost the entire cerebral cortex and the superior colliculus. The pontine nuclei axons, named transverse pontine fibers, cross the midline and enter the cerebellum as the pontocerebellar tract. The two middle peduncles contain over 20 million axons each and are thus among the largest pathways in the brain (Purves et al., 2001).

iii) The superior peduncle is mostly composed of the efferent pathway originated by the neurons in the DCN, which axons project to upper motor neurons in the red nucleus, deep layers of the superior colliculus, and, through a relay in the dorsal thalamus, primary motor and premotor areas of the cortex. The afferents to the cerebellum are the anterior

spinocerebellar tract, which works in parallel with the posterior spinocerebellar tract, to convey the subconscious proprioceptive information from the peripheral areas to the cerebellum and the Tectocerebellum. The efferent path comprises the Cerebellorubral, Dentatothalamic, and Fastigioreticular fibers.

1.2.1 Cerebellar cortex microcircuit

At the microscopic level, the cerebellum is divided into three cortical layers (from inner to outer): i) granular layer; ii) Purkinje cell layer, and iii) molecular layer with seven major types of neurons, all defined by a specific morphology and localization: granule cells, Golgi cells, Lugaro cells, unipolar brush cells, Purkinje cells, basket cell, stellate cell (Figure 3). In these seven neuronal types, considerable subtypes were distinguished by biochemical properties. Under the granular layer, there is the white matter,

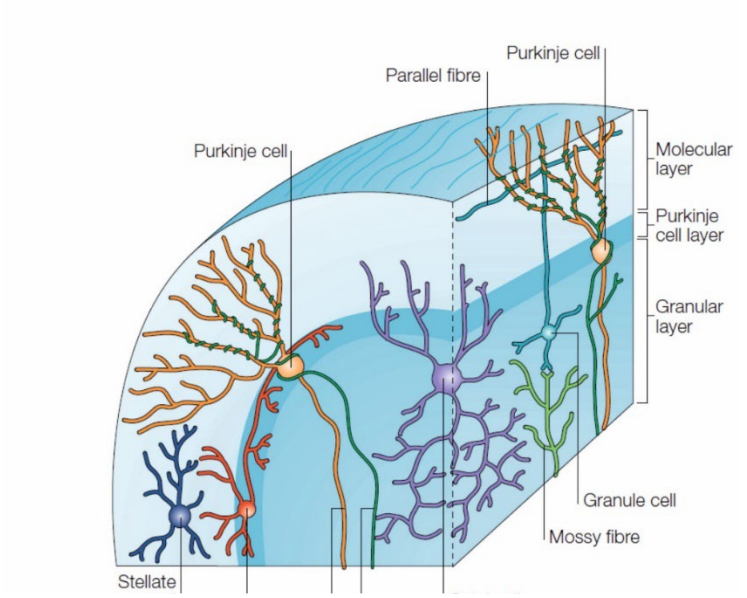

Figure 3: Cerebellar cortex cytoarchitecture. From Apps and Garwicz, 2005

or *arbor vitae*, containing all the afferent and efferent fibers of the cerebellar cortex.

The granular layer contains granule cells, the most numerous cells in the cortex, Golgi cells, Lugaro cells, and unipolar brush cells (mostly in the posterior lobules). The granular layer average thickness is ~ 149 μm in rats (Harvey and Napper, 1991), but the depths could be variable, depending on the curvature of the cortical sheet. The granular layer processes the input coming from mossy fibers, the major excitatory inputs to the cerebellar cortex. Originating from the pre-cerebellar nuclei (e.g., the vestibular and pontine nuclei), they are glutamatergic and make a multitude of synapses with granule cells dendrites and Golgi cells axons inside the *glomeruli* (Mapelli et al., 2014). Mossy fibers are tailored to promote rapid and consistent excitatory synaptic transmission that contributes to the granule cell responses. Granule cells have a small soma (~ 5 μm) (Manto et al., 2013) with four short dendrites and are specialized to differentially contribute to processing across regions. They send their axons into the molecular layer where they bifurcate to originate the parallel fibers.

The distribution of Purkinje cells soma forms a monolayer with the dendritic tree extending into the molecular layer and their axon passing through the granular layer.

The molecular layer is the external layer of the cerebellar cortex. The thickness is around 225 μm (Harvey and Napper, 1991). The main neurons are the stellate cell and basket cell, both named molecular layer interneurons. The parallel fibers run along the coronal orientation, intersecting the flat dendritic tree of Purkinje cells, the apical dendrites of Golgi cells, and the dendrites of molecular layer interneurons.

1.2.1.1 *Excitatory Input*

Mossy fibers and climbing fibers are the afferent projections of the cerebellar cortex. The input information follows two pathways that are both converging onto the Purkinje cells, the sole output of the cerebellar cortex. Mossy fiber originates from pre-cerebellar nuclei (e.g., the vestibular and pontine nuclei) and conveys various types of information, including vestibular, somatosensory, tactile, proprioceptive, or motor information to the cerebellar input layer (Powell et al., 2015; Cayco-Gajic and Silver, 2019). Climbing fibers, originating from inferior olive, project directly to the Purkinje cells (de Zeeuw et al., 2011), evoking the *complex spike*.

1.2.1.2 *The granule cell*

Granule cells are the most abundant of all neurons in the mammalian brain. They are excitatory neurons located at the cerebellar input stage. Granule cells are also the smallest brain neurons (Cesana et al., 2013; Mapelli et al., 2014; D'Angelo, 2018), with a soma of around 5 μm in rats and an average of four short dendrites (Galliano et al., 2013). The dendrites are embedded in the *glomerulus* that contains dendrites from many granule cells, the mossy fiber terminal, and Golgi cell axons. Each granule dendrites receive excitatory input from a single afferent mossy fibers bouton (Mapelli et al., 2014) or from the same mossy fiber terminal. Granule cells originate an ascending axon that develops vertically and bifurcates in a T–shaped fibers, called parallel fibers, in the molecular layer. The ascending axon follows the dendritic plane of the Purkinje cell and creates synapses with the apical dendrites of Golgi cells, the dendritic tree of Purkinje cells, and molecular layer interneurons. Parallel fibers run along the mediolateral plane for several millimeters in the molecular layer. They are unmyelinated and cross orthogonally the dendritic tree of the Purkinje cell, making *en passant* synapses with Golgi cells, Purkinje cells, stellate cells, and basket cells.

Granule cells are silent at rest and are endowed with a K^+ inward rectifier current that allows near–threshold oscillation and theta frequency resonance (D'Angelo et al., 2001). Theta–frequency bursting and resonance in granule cells are critical in defining synchronization, rhythmicity, and learning at this stage (D'Angelo et al., 2001). The mossy fiber - GrC synaptic connection shows high fidelity of transmission (Rancz et al., 2007) and a single mossy fiber input is able to trigger a spike in the postsynaptic granule cell. Moreover, the wide range of mossy fiber discharge, from slow firing modulation to high discharge, was shown to be transmitted to granule cells (Schwartz et al., 2012). The multimodal information provided by mossy fibers promotes a multimodal integration in granule cells, supported by intrinsic properties generating a rich repertoire of firing patterns (Jörntell and Ekerot, 2006; Masoli et al., 2020).

1.2.1.3 *The Golgi cell*

The main inhibitory interneuron in the cerebellar granular layer is the Golgi cell, which plays an important role in controlling cerebellar processing. It is well established that these cells represent the main the source of GABAergic-glycinergic inhibition (Guo et al., 2016) to the granule cells and are located at various depths in the granular layer. Golgi cells are connected by electrical synapses (gap junctions) and to the other neuronal types by chemical synapses, forming feedback and feedforward inhibitory loops in the granular layer. The temporal pattern of granule cell discharge in response to the mossy fiber input is under the control of Golgi cells (Mapelli et al., 2014).

The Golgi cell morphology displays a rounded soma with a complex dendritic organization: apical dendrites that extend along the molecular layer, and basal dendrites, which are bounded to the granular layer (Dieudonné, 1998; Hull and Regehr, 2012). The axonal plexus ramifies profusely in the granular layer, descending toward the white matter. It

extends in parasagittal and mediolateral orientation to contact thousands of granule cells, which are inhibited at the level of the glomerulus (Dieudonné, 1998; Tabuchi et al., 2018). Because of the extent of the axon, Golgi cells play an important role in providing lateral inhibition. Besides, in response to the stimulation of mossy fiber, Golgi cells control the spatial pattern of granule cell depolarization (Mapelli and D'Angelo, 2007; Mapelli et al., 2009). Functionally, the inhibition operates through GABA receptors, allowing effective spike timing control, and in some cases, glycine (Hull and Regehr, 2012). The mossy fiber – granule cell – Golgi cell pathway is involved in the feedback inhibition of granule cells, while the direct path mossy fiber – Golgi cell controls the feedforward inhibition (Cesana et al., 2013). The interplay of basal and apical dendrites under various patterns of excitation and inhibition provides dendritic integration, unveiling complex synaptic plasticity mechanisms (Masoli et al., 2020b). Golgi cells present important variations in size, shape, or biochemical markers. The neurochemical heterogeneity of Golgi cells suggests that the granular layer has a more complex organization than initially thought (Simat et al., 2007).

1.2.1.4 *Molecular layer interneurons*

Stellate and basket cells are GABAergic interneurons of the molecular layer, observed initially by Ramon y Cajal (Cajal and Ramón y Cajal, 1909), specialized in controlling the Purkinje cell discharge. The stellate cell soma is located in the outer two-thirds of the molecular layer, while the basket cell soma is located in the deep molecular layer, close to Purkinje cells. They display a parasagittal orientation of the axon and dendritic tree. These two types of molecular interneurons are usually considered as a single population. However, the morphological features revealed some differences in the axonal plexus. Stellate cell presents a stellate shape with numerous short and thin dendrites and large axonal plexus with collaterals (Sultan and

Bower, 1998). The axonal collateral of the stellate cells makes synapses with the shaft of Purkinje cell dendrites (Palay and Chan-Palay, 1974). Axon terminals from multiple basket cells contact Purkinje cells through a pericellular basket and from a pinceau, innervating the axonal initial segment. Each pinceau is composed of around 50 collaterals from basket cells, creating ephaptic connections with the Purkinje cell (Blot and Barbour, 2014). Both basket and stellate cells have an irregular pacemaking activity (15 – 30 Hz) and they perform feedforward inhibition on the Purkinje cell and other molecular layer interneurons. The position in the cerebellar cortex allows them to integrate glutamatergic input from parallel fibers and climbing fibers, to perform lateral inhibition onto other interneurons and Purkinje cells.

1.2.1.4 *The Purkinje cell*

Discovered in the 19th century by Jan Evangelista Pukinje (Žárský, 2012), Purkinje cells are the most complex GABAergic interneurons in the brain and play a crucial role in cerebellar cortex functions (Eccles et al., 1966; Llinás and Sugimori, 1980). Indeed, this cell represents the sole output of the cerebellar cortex and, therefore, the last step of information integration. Purkinje cells have a pear-like soma of about 20 µm (Palay and Chan-Palay, 1974), organized in a single layer forming the Purkinje cell layer. Each cell has tree-shaped dendritic arbors, extending in parasagittal microzones. The dendritic tree has one or two primary trunks, which are subdivided into secondary smooth branches and tertiary spiny branches. Microzones are innervated by climbing fibers, ascending from the inferior olive. Moreover, the microzones establish the functional loop between the cerebellar cortex, deep cerebellar nuclei, and inferior olive. The myelinated axon runs through the white matter, reaching several deep cerebellar nuclei. The terminal of each axon targets a specific area in the deep cerebellar

nuclei. Thus, there is both a high degree of convergence and divergence of Purkinje cells onto cerebellar nuclei neurons (Person and Raman, 2012). The axon presents collaterals that contact other Purkinje cells, Lugaro cells, and also basket cells.

Experimental recordings *in vivo* and *in vitro* described Purkinje cells at multiple functional aspects. The physiological properties of ion channels distributed along the Purkinje cell sections generate a regular and spontaneous firing at a frequency between 10 and 100 Hz (Jaeger et al., 1997). The presence of the voltage Na^+ channels and calcium-activated channels generates different firing patterns. The extensive dendritic tree arises into the molecular layer and receives excitatory inputs from climbing and parallel fibers.

Two distinct types of action potentials were described in the Purkinje cell: i) *simple spikes*, which occur at a high rate and are the regular spontaneous activity of the Purkinje cell, due to the intrinsic pacemaking, both investigate *in vitro* (Raman and Bean, 2001; Khaliq et al., 2003) and *in vivo* (Shin et al., 2007); ii) *complex spikes*, a low-rate activity, in which the initial action potential is followed by smaller spikelets, occurring in response to climbing fiber input.

Purkinje cells are heterogeneous in the expression of some molecular markers (Wise et al., 2010). In particular, they are classified based on the expression of Zebrin II, that is the aldolase C enzyme. Purkinje cells expressing Zebrin II (called Zebrin +) alternate with those not expressing it (Zebrin -). This expression pattern of Zebrin II gives rise to the parasagittal stripes of the cerebellar cortex (Zhou et al., 2014). Moreover, the Purkinje cell discharge can be modulated by the expression of Zebrin II proteins. These molecular phenotypes establish a patterned organization of the cerebellar circuits (Apps and Hawkes, 2009; White et al., 2014). The map is

organized into parasagittal microzonal compartmentations, critical for motor coordination and motor learning (Attwell et al., 1999; Horn et al., 2010).

The cerebellar circuit can be schematically illustrated below (Figure 4). The granular layer constitutes the cerebellar cortex's input layer, and it is mostly composed of granule cells. Mossy fibers, which originate from multiple sources, provide excitatory input to granule cells. They also stimulate unipolar brush cells and Golgi cells, which contribute to feedforward excitatory and inhibitory input to granule cells, respectively. Golgi cells are also regulated by inhibitory input from Lugaro cells. Granule cells send axons into the molecular layer, where they bifurcate, giving rise to parallel fibers that run along the coronal plane, providing excitatory input to Purkinje cells, Golgi cells, basket cells, and stellate cells. Purkinje cells are under the inhibitory activity of basket and stellate interneurons. Purkinje cells receive also a strong excitatory activity by climbing fiber input from the inferior olive. Purkinje cells provide inhibitory input to neurons in the deep cerebellar nuclei (DCN) and vestibular nuclei, which integrate the input with

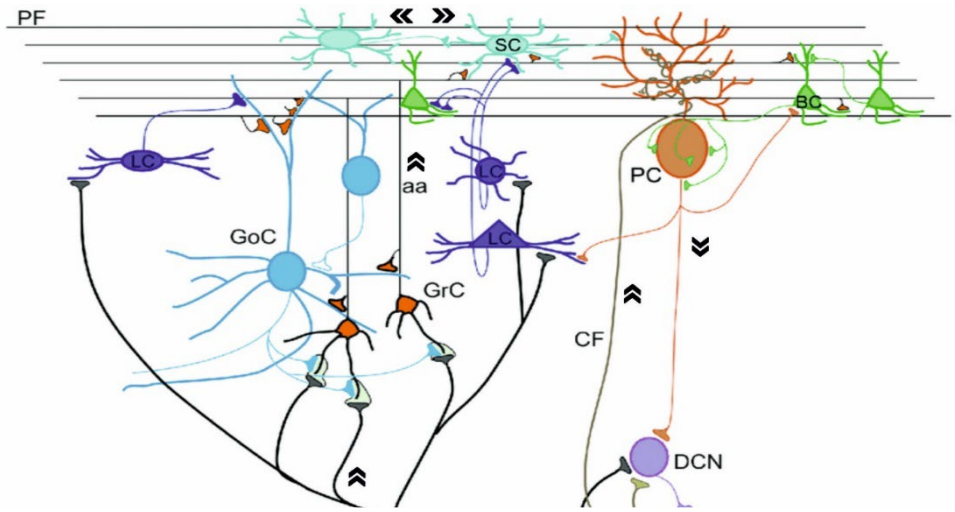

Figure 4: Schematic view of the cerebellar circuit. From Prestori et al., 2019

other signals, including collaterals of mossy fibers and climbing fibers, to produce the cerebellum output.

1.3 Cerebellar cortex input processing

Incoming signals are first processed in the input stage of the cerebellar cortex, the granular layer, which integrates inputs with a variety of dynamic properties (D'Angelo and De Zeeuw, 2009; Courtemanche et al., 2013). Mossy fibers typically carry frequency-modulated discharge bursts to the cerebellum (Chadderton et al., 2004; Rancz et al., 2007). Mossy fibers make synaptic contacts with granule cells and Golgi cells, providing the spatial and temporal reconfiguration of the incoming input (D'Angelo, 2011).

Concerning the spatial organization of granule cell processing of mossy fibers input, it has to be considered that Golgi cells are activated by mossy fibers simultaneously with granule cells. The Golgi cell axonal plexus provides lateral inhibition, which plays a fundamental role in the center-surround organization, and spatial distribution of granular layer responses (Mapelli and D'Angelo, 2007). The center-surround organization, similar to the typical of the retina, shows excitation prevailing in centers and inhibition prevailing in the surrounding areas (Mapelli and D'Angelo, 2007; Gandolfi et al., 2014). This organization enhances the spatial discrimination of the signal transmission: the center shows bursts with a higher frequency and a shorter delay compared to the surround (Solinas et al., 2010). The spatial organization of synaptic plasticity is also affected: the strong excitation in the core drives long-term potentiation, while the weak excitation in the surround results in long-term depression (D'Angelo and Casali, 2012).

The temporal organization of cerebellar processing is determined by the feedforward inhibition provided by Golgi cells, which allows the

generation of a permissive time window, during which granule cells are not yet inhibited (since inhibition will arrive on granule cells with a disynaptic delay compared to excitation). This so-called “time-window effect” is strictly dependent on Golgi cell feedforward inhibition (D’Angelo and De Zeeuw, 2009), and the combination of multiple transmission delays throughout the mossy fiber-Golgi cell-granule cell pathway results in a permissive time window of 5 ms. This allows granule cells to fire 1-3 spikes before Golgi cell inhibition. Long-term synaptic plasticity can contribute, together with the time-window mechanism, to shape the granule cell responsiveness. Long-term potentiation (LTP) and long-term depression (LTD) play a critical role in the regulation of granule cell first spike delay (Nieus et al., 2006).

Therefore, synaptic plasticity at the mossy fiber-granule cell synapse contributes to this sophisticated input processing (D’Angelo and De Zeeuw, 2009). Bidirectional plasticity has been indeed demonstrated at the cerebellum input stage, modulated by mossy fiber discharge (D’Errico et al., 2009), and correlated with the duration of the stimulus train (Gall et al., 2005). Both LTP and LTD occurring at the mossy fibers-granule cells synapses have been associated with changes in the intrinsic excitability of granule cells (Sola et al., 2004; Gall et al., 2005; Nieus et al., 2006), supporting the role of plasticity in shaping the cerebellar network activity and impact on the timing of granule cell responses. Thus, LTP and LTD cooperate to determine the number of spikes released by granule cells in the time window. This kind of mechanism is known as the “window-matching effect” (D’Angelo and De Zeeuw, 2009). Time-window and window-matching coordination have a significant impact on burst retransmission toward the molecular layer, favoring short bursts of information (Arleo et al., 2010). Both components of Golgi cell inhibition called phasic and tonic (Mapelli et al., 2014), influence granular layer activity. Phasic inhibition

refers to the γ-aminobutyric acid (GABA) release from the Golgi cell presynaptic terminal, which regulates the delay and precision of granule cell firing (Nieus et al., 2014). The second component depends on the level of tonic GABA, released at the synaptic cleft or derived from spillover from neighboring synapses. The tonic inhibition exerts control of synaptic transmission between the mossy fibers and granule cells (Mitchell and Silver, 2003). These synaptic inhibition mechanisms may modulate the granule cell excitability as well as the information transmission. Furthermore, the granular layer acts as a high-pass filter and shows a marked frequency dependence, enhancing the transmission of the high-frequency bursts (above 50Hz) to the molecular layer (Mapelli et al., 2010a). NMDA receptors might be involved (D'Angelo and Rossi, 1998; Mapelli et al., 2010b, 2010a; Solinas et al., 2010), suggesting that excitation and inhibition concur in the regulation of the temporal dynamics of input processing.

The granular layer can modify the response to incoming input at different frequencies, showing resonance in the theta-band (Gandolfi et al., 2013) and high-pass filtering above 50Hz (Mapelli et al., 2010a).

Granule cells and Golgi cells act as multiple resonators (D'Angelo and Casali, 2012): on one side the granular layer resonance reflects the intrinsic properties of the granule cell (D'Angelo, 2011) and amplifies the responses to input currents at around 6Hz (Gandolfi et al., 2013); on the other side, Golgi cells show pacemaker activity at around 10 Hz (Forti et al., 2006) and phase reset (Solinas, 2008) at the same frequencies, being strongly electrically coupled and displaying low-frequency oscillations (Dugué et al., 2009). Theta-frequency oscillations have been observed during resting state activity *in vivo* (Courtemanche et al., 2013), and synchronization has been found between this rhythmic activity and

cerebrocortical up and down states (O'Connor et al., 2002; Ros et al., 2009; Popa et al., 2013). Extracellular field recordings in freely behaving animals have shown that the granular layer can be also entrained in synchronous oscillations encompassing the beta frequency (7-25 Hz) (Courtemanche et al., 2013). This frequency band has been recorded *in vivo* as a "background activity" within the granule cell layer (Pellerin and Lamarre, 1997), and subsequent studies have revealed its relevance for sensorimotor processing (Courtemanche and Lamarre, 2005; Courtemanche et al., 2009) and vestibular-ocular reflex performances in humans, but these mechanisms have not been characterized locally in the granular layer (Rössert et al., 2014). A computational model has been developed to investigate granular layer activation during sensorimotor stimulation, observing a physiological modulation in the granule and Golgi cell discharge (Solinas et al., 2010).

An *in vitro* investigation has been conducted to reconstruct the excitation of the granular layer and signal transmission towards the molecular layer at higher frequencies (50Hz and 100Hz) (Mapelli et al., 2010a). The granular layer has been described as a high-pass filter, enhancing transmission of higher frequencies compared to lower ones, in agreement with the frequency dependence of the time window. An amplification of burst responses has been described along the vertical axis. This vertical transmission is in line with the spot-like activation of PC observed *in vivo*, following MFs bursts with frequencies over 100Hz (M. Bower, 2010).

In *in vivo* and *ex vivo* investigations, the molecular layer sustains synchronous oscillations in the gamma band (30-80 Hz) and higher (80-160 Hz) (de Solages et al., 2008; Middleton et al., 2008). Even if the contribution of these high-frequency oscillations to signal processing in the cerebellar

system has been already hypothesized (de Zeeuw et al., 2008), their specific role in concert with low-frequency patterns remains unknown. Although the coexistence of all these mechanisms is needed to enable pattern recognition and information processing in the cerebellum, a comprehensive study of the cerebellar cortex responsiveness at different input frequencies is still missing and deserves experimental assessment using both high spatial and temporal resolutions.

1.4 The spatiotemporal organization of activity in the cerebellum

In neuroscience, space and time are two coordinates, which are quantified and remain separate; space means distance and displacement, while time refers to duration and interval (Buzsáki and Llinás, 2017). The critical question is to understand the relationship between the properties of single neurons embedded in a microcircuit. Neurons constantly change their firing frequency, communicating with each other. Recently, it has become fundamental to consider the exact time point of the neuron spike (the spike time) as a critical element in relaying and storing information (de Zeeuw et al., 2011). Moreover, inputs and outputs are topographically organized in both the anterior-posterior axis and the mediolateral axis (Cerminara et al., 2015). Different levels of the organization were observed in the cerebellar cortex, following the *one–map hypothesis*, which confirms that regional differences are present in the cerebellar cortical microcircuit and lead to fundamental differences in information processing (Apps and Hawkes, 2009).

The spatiotemporal patterns of the cerebellar microcircuit integrate rate coding, allowing precise control in motor and cognitive information processing. To better understand this, a description of signal processing is

necessary, in terms of how the information is encoded and how the input affects the output.

1.4.1 The spatial organization of the cerebellum

In the cerebellar cortex microcircuit, the spatial organization consists of the compartmentalization into multiple modules, considered as the unit with specific functionality J. Voogd (Voogd, 2011) defines the term “module” as a longitudinal Purkinje cell zone that is repeated several times. Particularly, cerebellar interneurons present heterogeneous molecular expression, which is linked to the functional cerebellar modular organization. Indeed, modules consist of an array of microcircuits with a specific identity. Each module can be described as a subgroup of Purkinje cells that receive climbing fiber input from a particular subsection of the inferior olive nuclei to the sagittally orientated zone of the Purkinje cell (Sugihara and Shinoda, 2004). The Purkinje cell is also influenced by the mossy fiber, through the input conveyed from the granule cell to parallel fiber and molecular layer interneurons.

Instead, “microzones” represent the cortical element of cerebellar modules, that contain a small group of Purkinje cells with distinct climbing fibers with a thickness of 100 – 200 μm. One climbing fiber collateral contacts a single Purkinje cell but the same climbing contact multiple Purkinje cells. The projections run along the parasagittal orientation with one climbing fiber projecting in a single zone. The parasagittal projection of climbing fibers with the same input is processed all along a lobule, and across lobules, resulting in a comparable architecture of multiple lobules, each performing a parallel and simultaneous computation based on the same input. All the microzones are linked to the same group of DCN and inferior olivary neurons. Mossy fibers projecting through the granular layer

to a specific group of Purkinje cells likewise project to the same DCN neurons, receiving input from those Purkinje cells.

The modules are connected exclusively through parallel fibers, which run along the transverse plane, contacting Purkinje cells and molecular layer interneurons. This organization promotes communication between microzones and coordinates the Purkinje cell output.

To examine the anatomy and physiology of cerebellar modules, another organization element named stripes has been described. Mossy and climbing fibers terminate in stripes, revealed by immunostaining for different types of molecules (Figure 5). Particularly, high contrast between negative and positive longitudinal stripes was described with a monoclonal antibody that recognizes the antigen zebrin II, the isozyme of enzyme aldolase C. The stripes are oriented in the parasagittal plane, as the module, and the zebrin II expression pattern is correlated with modules.

Recent studies confirmed the different intrinsic properties of Purkinje cells in ZII+/- stripes (Schonewille et al., 2006). The Purkinje cell spontaneous firing is higher in ZII- than in ZII+. The difference in Purkinje cells intrinsic excitability underlines different firing patterns of ZII+ and ZII- Purkinje cells. Since the morphology remains unchanged, ionic mechanisms (presence of TRP3C and Mglur1) are responsible for the different firing rates between ZII+ and ZII-.

Zebrin II +/- Purkinje cells respond to afferent inputs in a similar manner, but present changes in the synaptic plasticity. The topography of climbing and mossy fibers describes highly integrated and complex somatosensory information (Apps et al., 2018).

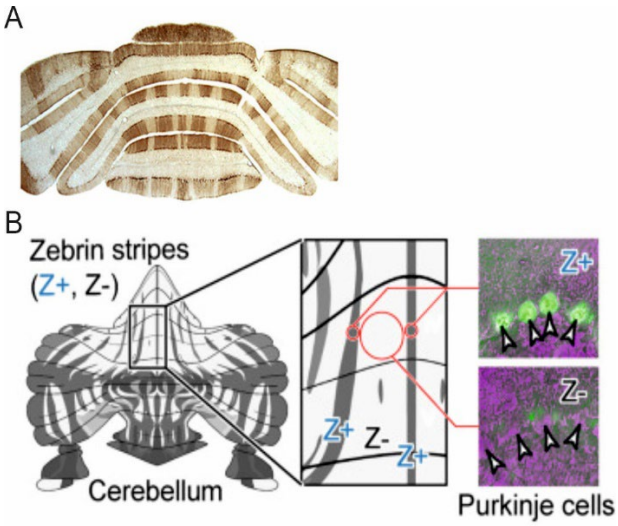

*<u>Figure 5:</u> Stripes in the adult mouse cerebellar cortex revealed various Purkinje cell subset markers. (**A**) A coronal section through the immunoperoxidase stained using anti–zebrine II (Adapted from Marzban et al., 2004 and Hawkes, 2014) (**B**) Scheme of zebrin zones in the unfolded cerebellar cortex and Z+ and Z – Purkinje cells (Adapted from Viet et al., 2022)*

which are important to encode the adaptation and coordination of movements (Medina and Mauk, 2000; Ohyama et al., 2003). The uniform well – organized architecture provides parallel computation, performed in a few milliseconds to adjust the movement and requires precise temporal timing. The cerebellar processing includes some relevant elements: the precise time pattern of spikes in the different neurons and the synaptic plasticity inside the circuit. The mossy fiber–granule cell–Purkinje cell pathway regulates the Purkinje cell discharge, which encodes all the information transmitted downstream to the DCN neurons.

The mossy fiber firing pattern depends on the specific aspect of the input source and the stimulus state (D'Angelo and De Zeeuw, 2009). Some examples are (i) the vestibular input is encoded by mossy fibers using a spike rate in the range of 0 – 40 Hz (Bagnall et al., 2009); (ii) the trigeminal

input generates a burst in response to stimulation and induces burst in granule cells (Chadderton et al., 2004); (iii) the oculomotor input produce both burst and tonic discharges.

The spatiotemporal organization of granular layer activity is due to the feed-forward and feedback inhibitory loops. Granule cells and Golgi Cells process the temporal sequence generated by the mossy fiber spikes. They sustained bursting and repetitive activity at different frequency bands (Mapelli and D'Angelo, 2007). The granule cell is resonant and shows synchronous discharge at 7 – 25 Hz; the Golgi cell with its spike activity is resonant at low frequency (Solinas, 2008).

Purkinje cells have unique and complex electrophysiological properties due to the capability to generate two different types of action potentials. Simple spikes are associated with spontaneous activity or in response to the activation of the mossy fiber–granule cell – Purkinje cell pathway. They are classical Na^+ spikes generated from the initial segment. In different preparations, including acute cerebellar slices, spontaneous activity frequency ranges from 10 Hz to 60 Hz but can reach a maximum of 250 Hz (de Zeeuw et al., 2011). The firing rate of simple spikes might depend on the spatial localization of Purkinje cells in the cerebellar cortex. Indeed, ZII- bands have a higher PC firing frequency than ZII+ bands. Furthermore, PC intrinsic membrane features were observed to differ in lobules receiving diverse sensory input, such as spinocerebellum lobules III to V versus vestibulocerebellum lobule X. The pacemaking activity is driven by the intrinsic properties and the synaptic inputs from parallel fiber and molecular layer interneurons. The complex interplay of different cerebellar neuronal types determines the simple spike patterns of Purkinje cells. These excitatory and inhibitory inputs modulate the spontaneous activity or the pause. Complex spikes are generated by the climbing fiber input at

remarkably low – frequencies (Rasmussen et al., 2014; Burroughs et al., 2017; Tang et al., 2017). The Ca^{2+} spikes in the Purkinje cell dendrites activate Ca^{2+} - dependent K^{+} conductance (BK and SK channel) and modulate the simple spike activity. Also, the Ca^{2+} spikes are involved in plasticity functions (Warnaar et al., 2015). Following complex spikes, the PC shows long pauses (20 ms) in the autorhythmic firing. These pauses are referred to the depolarization related to the refractory period, resulting from the hyperpolarizing currents and climbing fiber collaterals that inhibit the molecular layer interneurons. Complex fibers might induce long-term depression mechanisms at parallel fiber synapsis on PCs, but the functional role of complex spikes still remains unclear (Davie et al., 2008). *In vivo* recordings showed two stable states of Purkinje cell activity: the upstate is the autorhythmic activity; the downstate is a hyperpolarized state due to the inactivation of the voltage-dependent Na^{+} channel. The climbing fiber input controls the passage from the upstate to the downstate. The transition of these Purkinje cell two-stable states is under the control of climbing fibers which behave as a switch. However, the physiological mechanisms of downstate are still a subject of discussion because it is more evident in *in vitro* recordings and in anesthetized animals (Schonewille et al., 2006).

1.5 Theories on the role and function of the cerebellum

The cerebellum plays a major role in motor and non - motor learning and control at the functional level (Eccles, 1967; Ito, 1982; 2008; Boven et al., 2022, Van Overwalle e al.2014, 2019a; Heleven et al. 2019, 2020b). Historically, cerebellar functions have been primarily understood due to lesions. In (Riku, 1995), the authors mapped different regions of the cerebellum based on various impairments in motor control and timing-

related activities. Cerebellar information processing can be defined as a computational operation performed by the cerebellar cortex, although inputs and outputs can differ greatly in their origins and targets (Walpert et al. 1998). However, the knowledge of cerebellar functions has lagged behind the understanding of the anatomical cerebellar circuitry. The modules composing the cerebellum are each a *unit learning machine* (Ito, 2008), that is made up of uniformly structured neuronal circuits. The cerebellum encodes internal models with the aim to help coordinate fluent motor and – non-motor sequences and predict the consequences of the action. Originally proposed by (Ito, 1970), the fact that the brain along with the spinal cord is able to perform complex tasks involving a large number of joints and muscles at high speeds calls for an internal model that can generate commands in a feed-forward mode to avoid delays due to sensory feedbacks. The cerebellum learns the inverse dynamics model of the control objective under supervised learning conditions and then uses this model to produce motor commands.

In the motor control theory, internal models are identified as forward and inverse model controls (Wolpert et al. 1998). The forward models describe the forward or causal relationship between inputs and the output: it can predict the consequences or future sensory states which would arise because of the current motor action. This prediction allows the brain to avoid waiting for the sensory feedback to correct itself. In contrast, inverse models act as controllers as they can provide the motor command due to achieve some desired changes in state. The inverse model hypothesis has its own drawbacks. It requires an error signal in motor commands to train the cerebellum, but if the motor error is a priori then there is no requirement for an inverse model in the first place. For example, during limb movement, forward models could predict the position of the limb, while inverse models

form the desired trajectory into appropriate joint forces/torques. Previous studies were focused on the internal modelling of body movements. In (Cerminara et al., 2009), authors show that the cerebellum presents internal models of the movement of external objects in the environment, and predicts the future position of these objects. In fact, Purkinje cell simple spike activity in the lateral cerebellum responds to visual inputs during visual tasks, and also remains active during the occlusion of the visual target, describing an internal representation of the target.

The basic structure of a control system is represented in Fig 6: a controller manipulates a controlled object, an instructor gives an instruction to the controller, and a sensory system mediates feedback to the controller (Ito, 2008). This external feedback is represented using a dashed line as it can be spared when internal models are functional forward-model control systems. In this system, a forward model mimics the dynamic properties of the controlled object. Error signals are derived by comparing the outputs of the controlled object (monitored by the sensory system (a) with those of the forward model (b) in the inferior olive (IO) and are sent into the forward model to modify it. An inverse-model control system mimics the reciprocal of the dynamic properties of the controlled object. Feedback errors are derived from the command signals that are generated by the controller.

Assuming that the cerebellum contains an internal model is very important for simulation studies. Simulations do not include all brain regions in detail, which are often abstracted to simple blocks capturing only their top-level functionality. Therefore, one needs to decide where and how the inputs and outputs of the cerebellum connect in a given control. Depending on these choices, the role of the cerebellum would be either a forward or inverse model. One may argue that, if one knows the inputs and outputs of a block, then it is possible to conclude if the system operates as a forward

or inverse model. Unfortunately, understanding how neurons encode information is yet another unclear area in neuroscience. This has raised difficulties in correlating neural activity to engineering dimensional quantities such as position, velocities, and forces.

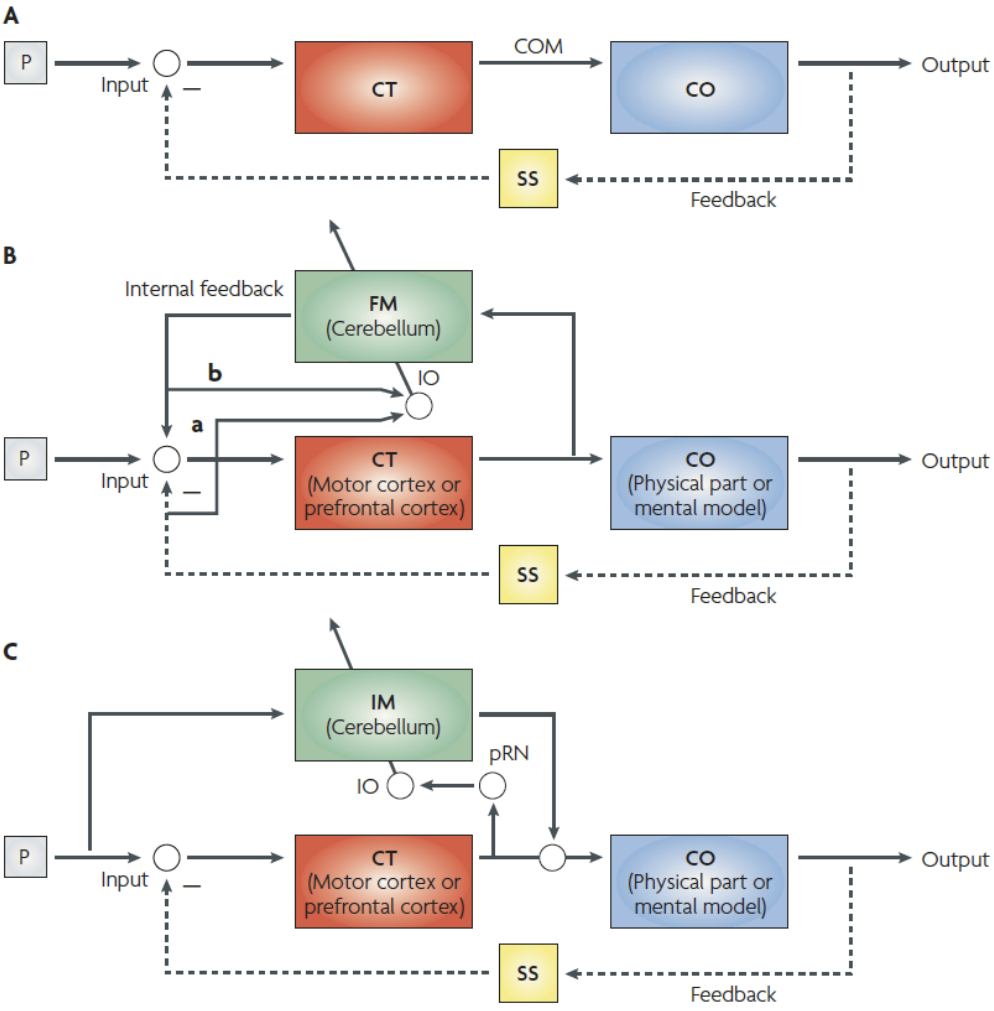

*Figure 6: Internal models in the cerebellum. (**A**) The cerebellum acts like a control system, consisting of an instructor (P) that gives input to the controller (CT), which shapes an object (CO) through a command signal (COM). The sensory system (SS) mediates the feedback (-) to the CT. (**B**) Forward models (FM) mimic the CT dynamics. The comparison between CO outputs has given error signals and the inferior olive (IO) is the site of this comparison. (**C**) Inverse models (IM) mimic the CO dynamics properties. Feedback errors are derived from the COM generated by the CT. These COMs are sent to the cerebellum through the pRN (parvocellular red nucleus) and IO and drive the learning process in the IM. From Ito, 2008.*

Aim of the work

During my Ph.D. years, I worked on two projects, aiming to understand the physiological mechanisms underlying information processing in the cerebellar network. In my first year, with my tutor Stefano Masoli, I focused on the multi-compartmental model reconstruction (*Chapter 4*) of the Golgi cell, which plays a fundamental role in controlling cerebellar processing. The multi-compartmental model of the Golgi cell was developed in this part of my thesis, with a focus on the modeling of the biophysical and synaptic mechanism of this inhibitory interneuron. The model can faithfully reproduce a large set of experimental findings and reveal some aspects of synaptic dynamics. This multi-compartmental model is described with systems of differential equations able to reproduce ion channel activity using the Hodgkin and Huxley mathematical scheme or the Markovian chains. The sections composing the morphology can be solved using the cable theory. These equations describe how the currents, generated by the ion flow, can produce action potential and its ability to propagate along the sections. The Golgi cells model was reconstructed using the NEURON+Python to reproduce the rich pattern of electrophysiological properties recorded *in vivo* and *in vitro*. This work was published with the title: *'Cerebellar Golgi cell models predict dendritic*

processing and mechanisms of synaptic plasticity' (Masoli et al., 2020a) (*Chapter 5*).

During the second and third years of my Ph.D., I started the second project focused on the analyses of spatiotemporal patterns of granule cells and Purkinje cells population in acute cerebellar slices (*Chapter 4*). This research was conducted on previously acquired data (Monteverdi et al., *in preparation*), using a high–density multielectrode array (HD – MEA, 3Brain AG). In parallel, my experimental training and the use of the HD – MEA were useful to contribute to the development of the new 3D HD – MEA resulting in the article 'Design, implementation, and functional validation of a new generation of microneedle 3D high-density CMOS multi-electrode array for brain tissue and spheroids', currently under revision (Mapelli et al., 2022).

The extracellular recordings of evoked activity in parasagittal and coronal slices at different input frequencies in the cerebellar cortex allowed us to investigate the complex dynamic and functionality of information processing. The advanced technology of the HD – MEA has been used to record extracellular neuronal activity with a high spatial and temporal resolution (*Chapter 2*). The work points out the characterization of the spatiotemporal activity of the input stage and the Purkinje cell population, and their firing modulation at different input frequencies. The simultaneous recording through the HD – MEA has been used to investigate the interaction of cerebellar neuron ensembles activity after mossy fiber activation. The well-organized cerebellar cytoarchitecture presents different neurons with specialized functionality (D'Angelo, 2018), and their interaction makes the cerebellar cortex circuit a complex structure, that contributes to

complex brain processes. The connectivity across neurons is fundamental for attending a high level of cerebellar complexity. Herein, the cerebellar functional complexity was explored by applying a measure of complexity to the *ex vivo* network: the perturbational complexity index, PCI (Casali et al., 2013; D'Andola et al., 2018; Colombi et al., 2021; Dasilva et al., 2021). This measure quantifies the integration and segregation balance (Tononi and Edelman, 1998; Tononi et al., 2016) and the consequent richness pattern, generating afterward the stimulation of mossy fibers at different input frequencies.

The cerebellar cortex network and the physiological neuronal mechanisms operate in a complex manner and the use of computational tools is necessary to investigate the dynamics. The reconstruction of the multi-compartmental neuron model and the application of the PCI to quantify the system complexity, are fundamental approaches to explore several characteristics of neural dynamics, especially with rich experimental datasets. On the other hand, the models are the strategy to create experimental hypotheses, predict emerging properties, and drive the research forward (*Chapter 6*).

Chapter 2

Neurotechnology methods applied to cerebellar extracellular signals

The novel neuroscience approaches aim to understand the relationship between the functional connectivity of neuronal circuits and their physiological and pathological functions (Spira and Hai, 2013). The cerebellar microcircuit shows an activity that extends over temporal and spatial scales and requires advanced methodologies to elucidate its finer functions.

Electrophysiological techniques are the gold standard for recording and analysis of neuronal activity. These techniques, ranging from single cells to whole brain resolution, can be summarized as follows: (i) the patch-clamp or sharp microelectrode technique is used to measure the intracellular current and voltage changes in single neurons with high temporal resolution; (ii) the *in vivo* and *ex vivo* multielectrode array technique enables recordings of extracellular multiunit activity and field potentials, to provide information about neuronal ensembles during network functions; (iii) optical imaging and stimulation technologies; (iv) functional magnetic resonance imaging (fMRI), positron emission tomography (PET), and electroencephalography (EEG) enable large – scale measurements of

brain's activity. The latter tools are used to determine the functional connectivity among the brain areas (Obien et al., 2015).

In this part of the work, the mesoscale–extracellular recording has been considered, to investigate the cerebellar network dynamics. Detailed information about single neuron properties cannot be ascertained with this methodology and is less important compared to the simultaneous recordings and analysis of large neuronal populations. Cell non-invasive methods and long-term recordings of the extracellular field potential of neuronal populations give more information about how neurons encode stimulus and how information, that cannot be clearly defined at the single-cell level, can be better interpreted when considering the whole population (Buzsáki, 2004; Quian Quiroga and Panzeri, 2009).

Multi-electrode arrays have both benefits and drawbacks as a method of recording neuronal activity. The main advantages of multi-electrode arrays for *in vitro/ex vivo* experiments are the simultaneous registration of activity from a large number of neurons, allowing the analysis of the activity of neural networks, and having a broad application in drug testing. In experiments *in vivo*, multi electrode arrays allow recording neural activity in the target areas of the brain in awake animals during behavior and detecting changes in neural correlations among different areas. The main drawbacks of using multielectrode array for these purposes are the reduced information about intracellular phenomena as compared to patch-clamp, neuronal cell death and tissue inflammation *in vivo*, with a reduction in the number of working electrodes due to their gradual overgrowth with connective tissue.

2.1 Extracellular recording in the cerebellar cortex

Extracellular field potential recording refers to *local field potential* and is an epiphenomenon of the electric potential in the extracellular space surrounding the neurons (Herreras, 2016). The local field potential has an amplitude resolution of 200 – 400 μV and a temporal resolution in the order of milliseconds (Meyer-Baese et al., 2022). At the level of the soma, neurons generate action potentials that give rise to large transmembrane potentials (Buzsáki, 2004). The ionic currents flowing across the membrane create a flux between the extracellular and intracellular space and vice versa, determining a voltage deflection on the electric field. Extracellular currents of excitable membranes superimpose at a given spatial point, in the extracellular space, and contribute to the generation of a potential (V_e). The difference between two spatial points creates an electric field, defined as a negative spatial gradient of potential (V_e) (Buzsáki et al., 2016). Extracellular electrodes are used to record the changes in the electric field to reconstruct neuronal network dynamics with a millisecond time resolution (Destexhe et al., 1999).

The extracellular field is defined as a summation of currents, such as fast action potential and glia slowest fluctuations, producing a potential in a specific spatial location and it can be transmitted through volume, a phenomenon better known as *volume conduction*.

The local field potential presents a waveform that depends on multiple sources, and the information is more significant when the recording electrode is near the microscopic current source. The amplitude, the spatial density, and the synchrony of the electric current create the extracellular field.

The major contributor to the local field potential is synaptic activity. Glutamate neurotransmitter activates AMPA and NMDA receptors, leading

to the genesis of excitatory currents, mainly determining the inward flux of Na^+ or Ca^{2+} ions. Cations flow from the extracellular to the intracellular space and generate a local extracellular *sink*. The equilibrium in the intracellular space is maintained by local diffusion and by an opposite flux from the intracellular to the extracellular space. The latter process generates a local extracellular *source* defined as the return current (Buzsáki et al., 2016). The sink current and the source current, their location, and the distance between each other contribute to creating a dipole (Figure 7). The inhibitory neurotransmitter, acting on $GABA_A$ receptors mediating inhibitory currents, might be involved to a small extent in generating the extracellular field, due to the Cl^- equilibrium potential close to the membrane resting potential (Einevoll et al., 2013; Buzsáki et al., 2016).

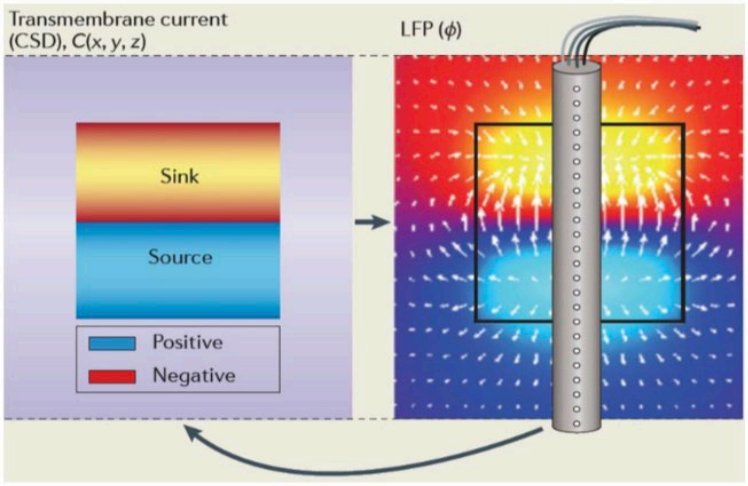

Figure 7: Current source-sink dipole. Cations flow from the extracellular to the intracellular space and generate a local extracellular sink. The equilibrium in the intracellular space is maintained by local diffusion and by an opposite flux from the intracellular to the extracellular space. The latter process generates a local extracellular source defined as the return current. Adapted from Einevoll et al., 2013.

The modeling investigation has shown how the shape, amplitude, and sign of the local field potential strictly depend on the position of the recording electrode. The extracellular potential presents a maximal negative amplitude close to the synaptic contact but has a positive peak near the soma, due to the strong return current (Einevoll et al., 2013). This condition suggests a sizable current dipole (Figure 8).

Another factor that contributes to the genesis of the local field potential is the action potentials, which generate currents across the cellular membrane, and can be detected as Na^+ spike activity in the extracellular field. The synchronous firing of multiple neurons contributes to the high-frequency components of the local field potential (Buzsáki et al., 2016). Ca^{2+} spikes triggered by the NMDA receptor-mediated excitatory postsynaptic potentials (EPSP) and by the back-propagating somatic action potential also contribute to the extracellular events.

Neuronal synchrony is enhanced by direct electrical communication mechanisms through gap junctions and ephaptic coupling. While the gap junction allows the ionic flux across neurons and is not implicated in the extracellular current, the ephaptic coupling affects the population activity, generating strong spatial gradients in the extracellular voltage.

The neuronal morphology, the spatial distributions of the neurons, and the temporal synchrony of the dipole generated are fundamental to define the extracellular field. Adult neurons have a stable morphology and produce countless sources of current because of synaptic activations (Herreras, 2016). In a compact cytoarchitecture, such as the cortex, in which neuron dendrites lie parallel to each other and the input is conveyed perpendicular to the dendritic tree, local field potential shows a large amplitude. The brain size and how it is folded can affect the magnitude of extracellular currents, too. Another element that contributes to the

magnitude of extracellular currents is the temporally synchronous activity, and the cerebellum is a perfect example to explain the influence of these two factors. The cerebellar cytoarchitecture is an ordered structure that generates small extracellular fields. However, the synchronous activity of cerebellar neurons gives rise to large amplitude local field potentials.

The electric field is transmitted through the volume, which means that the extracellular medium is homogenous, isotropic, and ohmic, so the potential induced by a current dipole is based on the magnitude and the location of the current source, and on the conductivity of the extracellular medium.

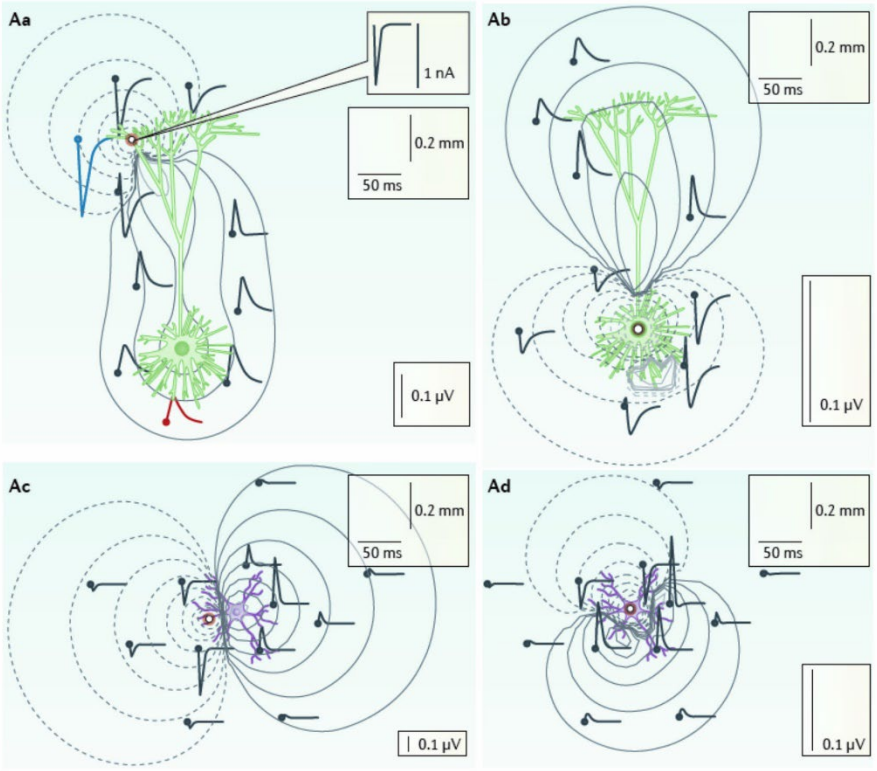

Figure 8: Local field potentials (LFPs) of single neurons. Extracellular signals depend on neuronal morphology and electrode position. The LFP amplitude changes according to the position of the electrode near the apical branch or the soma, and according to the position of active synapses. The LFP amplitude shows a negative deflection near the synaptic input, while a positive shape is present near inactive regions. Adapted from Einevoll et al., 2013.

The cerebellar cytoarchitecture with its regular organization, the autorhythmic activity of inhibitory interneurons, and the evoked activity of granule cells work together to generate a local field potential.

Purkinje cell, Golgi cell, and molecular layer interneurons action potentials are characterized by rapid depolarizations of the neuronal membrane sustained by voltage-dependent sodium and calcium currents, followed by repolarization and a hyperpolarization phase sustained by voltage-dependent potassium and calcium-dependent currents. Depending on the relative position of the recording electrode and the region of spike generation, the extracellular recording of a spike can present a positive or negative overshoot, with the latter being the most common case. As already mentioned above, the shape and amplitude of detected signals are influenced by the distance between neuronal sources and the recording electrodes. The difference in the waveforms reflects the fact that each neuronal source can contribute to a linear summation of currents and presents a different weight. Weights and distances are inversely proportional. Moreover, the spiking activity of multiple neurons can be detected by the same electrode. In this case, the signal is called “multi-unit activity” (MUA), as opposed to the single-unit activity when the spiking of a single neuron is detected. In the case of MUA signals, further analysis of the waveform and amplitude of the recorded signals can be implemented to discriminate the different units contributing to the total signal.

The local field potential is the evoked activity of the granular layer, triggered by mossy fiber stimulation. In his pioneering work (Eccles et al., 1968), Eccles investigated the electrical responses generated in the anterior lobe of the cerebellar cortex by electrical stimulation of peripheral nerves of both hindlimb and forelimb *in vivo*, differentiating the characteristic climbing fiber and mossy fiber responses. Moreover, few investigations

have characterized the local field potential in the granular layer, using (i) a single extracellular electrode (Maffei et al., 2002), (ii) *in vitro* low-density multielectrode array (MEA) (Mapelli and D'Angelo, 2007), (iii) a single electrode during *in vivo* recordings (Roggeri et al., 2008). This signal has been thoroughly characterized both pharmacologically and using theoretical models, too (Diwakar et al., 2011).

Granule cells and Golgi cells contribute to the evoked response, but most of the current generating the local field potential response depends on granule cells, which are silent at rest. The *in vitro* local field potential model describes that the granule cell Na^+ spikes current is the current *sink*, which causes a sink in the initial segment, while the current *source* is in the soma and in the dendrites (Diwakar et al., 2011). Granule cells generate spikes following mossy fibers activation and extracellular electrodes are not able to resolve single spikes from single granule cells, but they show the average changes in the potential of the field surrounding the electrodes. This field potential then reflects the activity of the granule cells emitting spikes in the same narrow time window (usually a few milliseconds).

In MEA recordings, the granular layer evoked activity is described by a typical N_1 – N_2 – P_2 complex as a negative potential variation, where N_1 corresponds to presynaptic volley activation, N_2 is split into two components (the N_{2a} and N_{2b} peaks), that are informative of granule cell synaptic activation, and P_2 represents the currents returning from the molecular layer (Figure 9) as confirmed *in vivo* (Eccles et al., 1968) and in vitro studies (Mapelli and D'Angelo, 2007).

Spike generation in granule cells is primarily correlated to N_{2a}-N_{2b} peaks. In particular, N_{2a} peak amplitude is proportional to the synaptic current derived from AMPA receptor activation and firing synchrony. On the

other hand, the N2b wave is regulated by synaptic inhibition and NMDA receptor activation (Mapelli and D'Angelo, 2007).

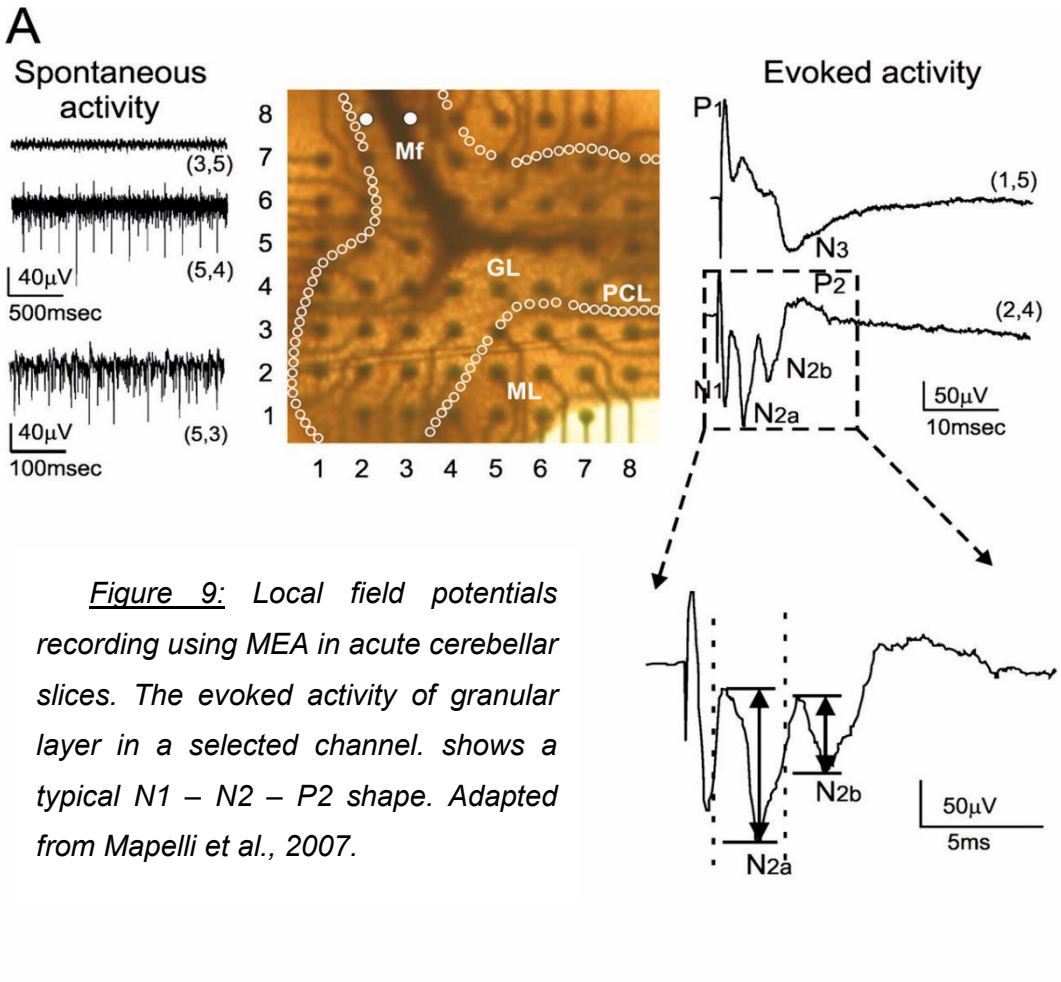

Figure 9: Local field potentials recording using MEA in acute cerebellar slices. The evoked activity of granular layer in a selected channel. shows a typical N1 – N2 – P2 shape. Adapted from Mapelli et al., 2007.

2.2 The High Density multi - electrode array

An important ambition of large-scale recordings of neuronal activity is to unveil information about the interaction of neuronal ensembles (Buzsáki, 2004). Though losing details about single neuron computation, extracellular recordings using high-density multielectrode arrays (HD-MEA) provide information about the activation of the whole network, simultaneously. In the last decade, this technology has been used to record extracellular activity from *in vitro* neuronal cultures and tissue slices over time, maintaining the information on the signal location (Meyer-Baese et al., 2022).

The development and the first use of a planar array of microelectrodes started in the 1970s and 1980s, to measure the spontaneous electrophysiological activity of neuronal populations. In addition, technological efforts improved the quality of recordings and increased the robustness of the data. The ability to record multiple evoked responses in parallel at different electrodes increases the reliability of the data and their subsequent statistical processing. Planar MEAs are used to record cultured excitable cells and acute brain slices, becoming useful to investigate the spatiotemporal pattern of the neuron population activity. However, it presents some critical limitations referred to recording signals that derive from the surface with low access to the 3D tissue; i.e., acute brain slice and organoids (Mapelli et al., 2022). To overcome the issue of the unstable recorded signal due to the dead cell layer at the surface of the slice caused by cutting, and to make the majority of the neuron in organoid tissue more accessible during the recording, penetrating 3D electrodes have been developed (Thiébaud et al., 1997; Liu et al., 2012). The 3D MEA provides an improved signal quality in the recording of spike activity and local field potential and the recently developed technology of 3D HD - MEA

(3Brain AG) implements some features like the high quality of recordings and penetrating capability, and high spatiotemporal resolution (Mapelli et al., 2022).

Signal shapes and amplitudes depend on the spatial distribution of electrodes and the nature of the neurons (Frey et al., 2009). Neurons with larger soma yield larger signals because of the depolarization of the membrane. A second element is a distance between the electrode and the excitable cell. The resistivity of the extracellular medium influences the signal amplitude. Large electrodes would measure a potential averaged across the area, reducing peak signal amplitudes. However, using smaller electrodes may result in increased noise levels in the signals, which may counterbalance or even outweigh the advantage. This new technology allows recording neuronal activity with unprecedented detail, requiring advanced analysis techniques (Nieus et al., 2015).

The complementary metal-oxide-semiconductor (CMOS) based planar HD-MEA (Biocam X, 3Brain AG) was used in this work. The BioCAM X platform is a high-resolution electrophysiology system capable of performing *in vitro* electrophysiological measures on electroactive cells and tissues. The CMOS technology allows the building of active electrodes that integrate into a few micrometers, electrodes, amplifiers, and signal conditioning circuits. Field potentials and spikes recording from a large bandwidth signal are possible thanks to the circuit implemented in BioChips.

HD-MEA integrates a Biochip with an array made of 4096 microscopic metal recording electrodes, arranged in a 64 x 64 grid distributed across a small and compact surface area (2.67 mm x 2.67 mm). These microelectrodes have a size of 21µm x 21µm with a pitch of 42 µm

(Figure 10). The whole chip is packaged onto a substrate together with a glass reservoir with a diameter of 25 mm and 7 mm in height.

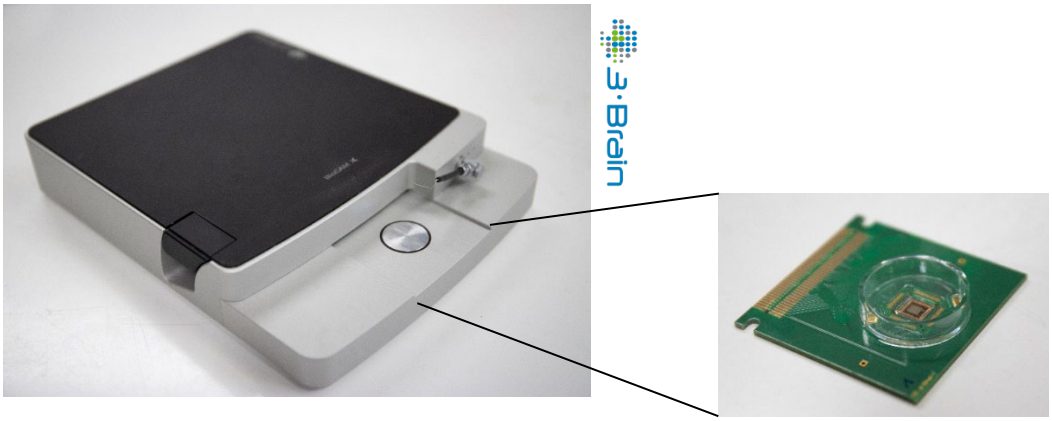

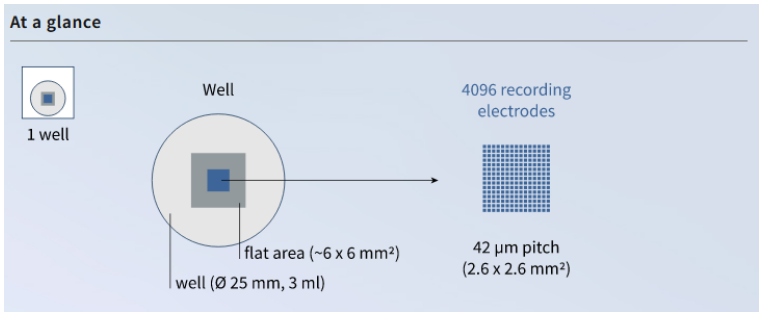

Figure 10: High – Density multielectrode array (3Brain AG). Biocam X is used for the acquisition of extracellular signals of the cerebellar acute slices. The Arena BioChips are plugged into the Biocam X and integrate 4096 electrodes arranged in a 64x64 matrix. Electrodes have a pitch of 42 µm. Adapted from 3Brain.com

2.3 An integrated information measure in the brain

The investigation of neuronal population dynamics shed a light on the complexity of the brain. A large number of neurons generate signals that are integrated into a coherent and multimodal system. The information, arriving from the external environment, is rapidly integrated by the brain's internal structure, to encode the neural output. Questions about what, how, and with what precision the information is being encoded, are still under discussion. Initially, to explain the information encoded, the common approach used was the measure of stimulus and response. In fact, measuring how much information a neural response carries about the stimulus enables the validation and comparison of behavioral performance, suggesting that the encoded information is relevant and directly involved in generating behavior (Tononi and Edelman, 1998; Borst and Theunissen, 1999).

The information theory poses the theoretical basis to quantify the neural code. It is a probabilistic theory that was developed to explain the complexity of the system as the integration of information (Tononi and Edelman, 1998). In the brain, neurons are functionally organized at multiple spatial scales and this neuronal segregation leads to different brain regions being activated by specific cognitive tasks or by a specific stimulus (Fan, 2014; Wang et al., 2020). The information encoded by the activity of neurons is functionally integrated to guide adaptive behavior. Functional specialization and integration are major elements that result at different spatial and temporal scales to build a unified conscious experience.

The anatomical organization of the brain, and in particular the reciprocal and parallel connectivity between functionally segregated neuron populations, is the general mechanism of neural integration. The firing rate

of groups of neurons and the precise temporal spiking pattern are the fundamental elements to encode the information.

The information theory measures the statistical significance of how neuronal responses differ at different stimuli, considering the conditional probability distribution of responses of the neuronal population. Physiologically, the stimulus has a probability of occurrence and is defined as a 'bit', or strings of 'zeros' and 'ones', required to transmit the information. Moreover, information theory is used to calculate the rates of transmission. The number of 'bits' required to specify all the possible responses (R) given the stimulus (S), is described as the entropy of the neural response H (R|S).

Entropy is the information needed to encode all the variability or to eliminate all uncertainty about a variable. This measure is important to evaluate the maximal rate of information transfer. The amount of entropy of a system, accounting for the interactions among its elements, is measured by the interaction complexity related to neural complexity (Tononi and Edelman, 1998). The complexity is high if the system is highly segregate and integrated (Casali et al., 2013; Tononi et al., 2016), where the functional segregation extends to the level of a group of neurons, that can be activated by specific stimuli attributes during cognitive or motor tasks. The information conveyed by the activity of a specialized group of neurons needs to be integrated to exert adaptive behavior (Tononi et al., 1998). The signal transmitted from a large number of specialized neurons over the brain area are integrated to generate coherent and multimodal experience.

The theoretical definition of complexity can be applied to data obtained from neurophysiological experiments. For example, the complexity refers to the correlation dimension of EEG signals. EEG signals reflect a mixture of synchronization and desynchronization: if the segregation and

integration are balanced, the complexity is high. The complexity is low if all groups of neurons fire independently.

These assumptions are fundamental to explain the complexity of the cognitive function of the brain. The Integrated Information Theory (IIT) (Tononi and Edelman, 1998; Tononi et al., 2016) was a new way to approach the understanding of neural complexity. The IIT establishes some essential properties, or axioms, of conscious experience rather than starting from a group of neurons and arguing how they could contribute to consciousness. This kind of strategy emphasizes two main properties of consciousness: conscious experience is an integrated whole because it cannot be subdivided into a subset of disjoint components, and at the same time is highly differentiated because a significant number of different conscious states can be experienced within a short time (Tononi et al., 2016). Besides, the conscious experience is accomplished at a particular spatiotemporal scale, in which it flows in time at a certain speed that cannot be faster or slower because the conscious thought can require a longer time compared to the sensory experience, developed in 100 – 200 ms (Tononi, 2004).

Thus, neuronal processes, both integrated and differentiated, contribute to conscious experience. A measure of the level of information integration (called Φ) could be used to establish whether a physical system takes part in the generation of consciousness. In a system, different groups of elements called complexes can be identified, each one with a corresponding value of Φ. Higher Φ values are associated with a higher ability of the complex to give rise to a conscious experience (Tononi, 2004).

A parameter inspired by the main concepts underlying the IIT and needed for the evaluation of Φ is the Perturbational Complexity Index (PCI) (Casali et al., 2013).

2.3.1 Perturbational Complexity Index

The level of information integration of the brain circuits is measured by the Perturbational complexity index (PCI), introduced in clinical practice as a tool to measure the loss and recovery of consciousness (Tononi et al., 2016; Storm et al., 2017). In fact, the complex cortical dynamic appears to be associated with the conscious and unconscious experience. PCI is an empirical electrophysiological metric used to parameterize the capacity of cortical circuits to integrate information (Arena et al., 2021). Briefly, transcranial magnetic stimulation (TMS) triggers a cortical activity, and the spatiotemporal pattern recorded by electroencephalography (EEG) (Arena et al., 2021) describes the responses. These can be temporally differentiated and distributed among cortical areas (PCI is high), or, in contrast, can be local and stereotyped (PCI is low) (Casali et al., 2013).

Responses are analyzed with nonparametric bootstrap-base statistics in order to extract a matrix containing the significant activations following the perturbation at different times samples and are measured using algorithmic complexity defined “Lempel – Ziv” compression algorithm. This algorithm (Lempel and Ziv, 1976) scans the matrix and approximates the amount of non-redundant information contained in a string, estimating the minimal size of the information necessary to describe the string. Lempel – Ziv algorithm has become a standard routine to compress data. In this case, it was implemented to scan a binary sequence with a length L, and the Lempel Ziv complexity accounts for the number of times the element in the matrix is encountered. The algorithm runs through columns of the matrix, searching for patterns or motifs.

The Lempel Ziv complexity can be defined as:

$$C_L = LH(L)/\log_2 L$$

Where H (L) is the source entropy.

The Lempel Ziv complexity of TMS evoked spatiotemporal patterns of cortical activation is normalized by the source entropy SS (*x*, *t*), defining the PCI. Indices *x* and *t* describe the spatial and temporal dimensions, respectively; while L is the total number of spatiotemporal samples of SS (*x*, *t*). PCI is then equated to the Lampel Ziv complexity of the bi-dimensional sequence of L, $C_l\,(t = L_2)$, and can be defined as:

$$PCI = C_l\,(t = L_2) \times \log_2 L/LH(L)$$

The complexity value is dependent on the spatiotemporal activation patterns present in the data. Interestingly, this parameter has been demonstrated to be representative of the level of consciousness in patients: the PCI is high only if brain responses are both integrated and differentiated, leading to a high complexity value. A lower PCI has been reported in cases of reduced connectivity among cortical areas (loss of integration) or in the presence of a stereotypical hypersynchronous activation (loss of differentiation). In both cases, the perturbation response is not transmitted among interconnected areas and does not give rise to complex spatiotemporal patterns.

The complexity of brain responses quantified by the PCI was tested in human subjects, in rodents, and in acute brain slices. A simplified model and *in vitro* adapted version of the PCI have been developed to investigate and measure the network complexity (D'Andola et al., 2018). The slice PCI (sPCI) has been computed directly from extracellular signals recorded *ex vivo.* At the microscale level, the sPCI represents an approach to evaluate electrical and pharmacological perturbations of the system used to mimic

different states of consciousness. These results might confirm a link between macroscale measurements and microscale neuronal events.

In this work, the estimation of the PCI value for the cerebellar network appears to be particularly interesting. Since cerebellar activity in humans cannot be assessed with non-invasive measures, an *ex vivo* evaluation of complexity needs to be performed, using the sPCI as a new tool to explore the network complexity. The computation of sPCI would provide a deeper understanding of cerebellar input processing and shed new light on its contribution to the cognitive experience. The cerebellum is not only a coordinator of motor actions but also of reasoning and, most recently discovered, of emotional and cognitive states. Despite the idea that the cerebellum cannot be involved in the conscious experience, due to its modular organization, the cerebellar interaction between modules shows that information processing is adaptable and dynamic, and can operate in parallel in different lobules and modules (Apps and Hawkes, 2009) or interact with others lobules achieving a coordinated Purkinje cells output (Valera et al., 2016).

Chapter 3

Article I

High density multielectrode array recordings reveal computational complexity in cerebellar cortical processing

In preparation

In collaboration with:

Thierry Nieus, Anita Monteverdi, Marcello Massimini, Lisa Mapelli and Egidio D'Angelo

Author contribution

Alessandra Ottaviani performed experiments and analyzed the data

Thierry Nieus analyzed the data and provided statistical analyses support

Anita Monteverdi performed experiments.

Lisa Mapelli, Marcello Massimini, Egidio D'Angelo conceived experiments, provided experimental support and supervised the work.

3.1.1 Abstract

The cerebellar cortex has a prominent architecture that performs a complex spatiotemporal reorganization of mossy fibers input. Over the years, it has been assumed that the cerebellar well–organized architecture and parallel computation were indicative of low – complexity.

Here, we characterize the complexity of the cerebellar responses, stimulating mossy fibers at different input frequencies (0.1, 6Hz, 20Hz, 50Hz). Mossy fibers convey multimodal information to the granular layer, which is filtered and transmitted vertically, converging on PC, the sole output of the cerebellar cortex. We recorded the spatial organization and temporal pattern of GrC and PC responses using HD-MEA (3Brain, AG), which provides an extremely high spatial and temporal resolution of *ex vivo* cerebellar neuronal activities with remarkable details. The simultaneous recording in sagittal and coronal planes of GrC and PC highlighted the frequency-dependence mechanisms, suggesting the involvement of inhibitory processes to modulate the GrC and PC discharge. The complex pattern of activity that emerged from the stimulated cerebellar cortical network, allows us to adapt the PCI applied in humans to acute cerebellar slices under different frequency conditions. The PCI reveals the contribution of inhibitory inputs to shape the GrC and PC spatiotemporal patterns and suggests that high frequencies yield cerebellar circuit functionality and information processing.

3.2 Introduction

In theoretical neuroscience, the investigation of complex spatiotemporal activity patterns takes into account two main properties: functional integration and differentiation. Integration describes the brain's propensity to engage in neural interactions, while differentiation refers to the functional specialization of neurons that interact with each other to produce a complex pattern of activity. An optimal balance between these two properties is thought to be fundamental to brain complexity. Different measurements were used to gauge the neural complexity based on the investigation of neuronal activity with regard to mutual information or graph models (Tononi and Edelman, 1998; Deco et al., 2015). A common approach to measure brain complexity is the Perturbational Complexity Index (PCI), primarily used in human subjects during transcranial magnetic stimulation (TMS), to evaluate the activity of the cortex and the complexity of the resulting electroencephalogram (EEG) responses. PCI value is low if the stimulus-induced activation of different brain areas is stereotyped: the matrix of responses can be easily compressed. Otherwise, PCI value is high when the stimulus is transmitted to integrated areas that react differently, creating a complex spatiotemporal pattern of responses: the matrix cannot be reduced. It has been shown that PCI correlates with the loss and recovery of consciousness of subjects in both physiological and pathological conditions. These findings have been paralleled by animal experiments (D'Andola et al., 2018), confirming that the circuit organization and the brain state are crucial to sustain complex patterns of activity.

The well–organized modular cytoarchitecture and parallel computation typical of the cerebellar network are considered predictors of low complexity of spatiotemporal activities compared to the cerebral cortex (Tononi and Edelman, 1998). However, the cerebellar processing reveals

complex dynamics among the different neuronal types, but the complexity of the cerebellar network has never been assessed experimentally. The prominent forward cerebellar cortex architecture has long been thought to perform two principal tasks: the spatiotemporal mechanism of input signals in the granular layer followed by pattern recognition in the molecular layer. These operations have been proposed to regulate the gain at the mossy fiber–granular layer relay and consequently, the vertical retransmission to the Purkinje cells, the sole output of the cerebellar cortex (Mapelli et al., 2010a). The multimodal integration of the input (Huang et al., 2013) and how it is processed in the output stage are still unknown, though contribute to the complexity of the spatiotemporal activity of the cerebellar network. The granular layer exerts dynamic input integration, from oscillation to resonance, and allows the spatiotemporal reconfiguration of incoming signals (Solinas et al., 2010; D'Angelo, 2011). These signals are transmitted to the molecular layer and integrated by Purkinje cells, the only output cells of the cerebellar cortex. The relationship between cerebellar neurons' biophysical properties and ensemble network activity is critical to understand the cerebellar microcircuit functions at the local level. A detailed electrophysiological investigation of the cerebellar network and its spatiotemporal pattern of activity is required in order to understand its role in information processing. In particular, the spatiotemporal pattern of activity in the granular layer and how it is related to the pattern activity in Purkinje cells is the main focus of this work.

The goal of this study was to shed light on the functional characteristics of the granule cell and Purkinje cell response patterns following mossy fibers stimulation at different frequencies, to mimic the various range of multimodal information that is transmitted to the cerebellum. Extracellular recordings of cerebellar multi- and single-unit

activity patterns with a high spatiotemporal resolution were recorded during the stimulation of mossy fibers bundles at different frequencies (0.1 Hz, 6 Hz, 20 Hz, 50 Hz, 100 Hz). The evoked activity in the granular and Purkinje cell layers was monitored in acute cerebellar slices in the sagittal and the coronal plane, using a high-density multielectrode array (HD-MEA) (see *Chapter 2*), a device providing a high spatial and temporal resolution (Gagliano et al., 2022) (Monteverdi et al., *in preparation*). The ability of the cerebellar circuits to process and segregate spatial and temporal inputs as a function of the network was investigated with a computational approach, that was determinant for optimizing the presence of segregation and integration of the neuronal activity patterns (Tononi and Edelman, 1998; Haun and Tononi, 2019). In the present work, we explored the spatial organization and temporal responses of the cerebellar network by applying the PCI to measure the complexity of the ex vivo cerebellar cortex network and point out the importance of frequency modulation in information processing. Both the coronal and sagittal planes were considered to investigate the spatial organization of the entire cerebellar cortical circuit and the several connections among the main neuronal types. In the coronal orientation, parallel fibers are intact, allowing the signals processing along this axis and the involvement of the molecular layer interneurons to modulate Purkinje cells discharge (Valera et al., 2016). In the sagittal plane, the white matter bundles radiate distally into the lobules and the organization of the circuit showed the feedforward connection between ascending axons and Purkinje cells. The observed data from both sagittal and coronal planes allowed the reconstruction of the cerebellar network functioning during the modulation at different input frequencies. This allowed to characterize the integration of this information. The modulated responses of granule and Purkinje cells exhibited a frequency dependence,

reconstructing a spatial distribution of the correlated evoked activity in the cerebellar input and output layers.

3.3 Materials and Methods

Preparation and maintenance of acute cerebellar slices

Animal maintenance and experimental procedures were performed according to the international guidelines of the European Union Directive 2010/63/EU on the ethical use of animals and were approved by the local ethical committee of the University of Pavia (Italy) and by the Italian Ministry of Health (following art.1, comma 4 of the D.Lgs. n.26/2014 approved on December 9th, 2017).

The investigation of the cerebellar circuit has been conducted by recording extracellular signals in acute 220 μm parasagittal and coronal slices obtained from the cerebellar vermis of C57BL/6 mice (18 – 23 days old, either sex) (Monteverdi et al., in preparation), following the standard procedure, as reported previously (Soda et al., 2019; Gagliano et al., 2022). Mice were deeply anesthetized using halothane (Sigma - Aldrich) and killed by decapitation. Acute slices of the cerebellar vermis were cut (220μm thickness) using a vibroslicer (Leica VT1200S, Leica Microsystem). During the whole procedure, slices were maintained in ice-cold oxygenated Krebs solution containing (mM): 120 NaCl, 2 KCl, 1.2 MgSO4, 26 NaHCO3, 1.2 KH2PO4, 2 CaCl2,11 glucose, equilibrated with 95% O2–5% CO2 (pH 7.4). Slices were then recovered for 1 hour in the same solution at room temperature, before recording. During recordings, slices were gently placed on the recording electrodes matrix in the glass reservoir (Arena chip, 3Brain AG) and were constantly perfused with Krebs solution (2 ml/min) using a peristaltic pump (Ismatec), to maintain tissue vitality. During the recording

session, the temperature was maintained at 32 ºC with a Peltier feedback temperature controller (TC-324B; Warner Instrument Corporation).

Electrophysiological multielectrode array recordings

Simultaneous electrophysiological recordings of Purkinje cells spontaneous activity and granule layer evoked responses were performed using a complementary metal-oxide-semiconductor (CMOS) based high-density multielectrode array (HD-MEA; Biocam X, 3Brain AG) (Figure 1A). The chip provides 4096 electrodes arranged in a 64x64 grid with an electrode pitch of 42 µm. Slices were stabilized using a platinum anchor with wires, to provide the coupling on the electrode's matrix. A total of 11 cerebellar parasagittal acute slices and 8 cerebellar coronal acute slices were obtained from 14 animals. Extracellular signals were sampled at ~ 18 kHz/electrode, with a high-pass filter at 100 Hz. External electrical stimulation was provided using a bipolar tungsten electrode (WPI). Spontaneous activity was monitored for 10 minutes, sampled acquiring 20 seconds every 2 minutes, and followed by electrical stimulation in correspondence with the mossy fiber bundle in the cerebellar lamina at the level of central lobules (IV – V – VI). The intensity of monophasic stimulation was set at 50 µA with a duration of 200 µs. The granular layer evoked response or local field potential was obtained by stimulation of 30 single stimuli at 0.1 Hz, followed by 30 trials of 5 impulses at 6Hz, 20Hz, 50Hz, and 100Hz, given in a mixed order to avoid plasticity and repeated every 10 seconds. We assumed that the stimulation did not activate climbing fibers because there was no evidence of the presence of Purkinje cell *complex spikes* activity during recording sessions. Therefore, we cannot exclude the antidromic effect on Purkinje cells but this did not affect the analysis of PC

responses, considering that a time blanking of 1.3 ms after the stimulus onset was set for each experiment.

Data Analysis

Two main extracellular signals were recorded from cerebellar cortex microcircuits in the coronal and sagittal orientation: local field potential (LFP) and multi-unit activity (MUA) (Figure 1A – 1D – 1E). Local field potentials represent the granular layer evoked responses, following mossy fibers stimulation (see Electrophysiological multielectrode array recordings). The MUA represents the spiking activity of the Purkinje cells population nearby the stimulated granular layer. In this work, we analyzed both LFP and MUA, by following the workflow reported in (Figure 1B – 1C). Data were displayed online and stored using BrainWave X (3Brain AG) (Monteverdi et al., in preparation) and data analysis was performed with BrainWave 4 (3Brain AG) and ad hoc routines written in Python 3.8.

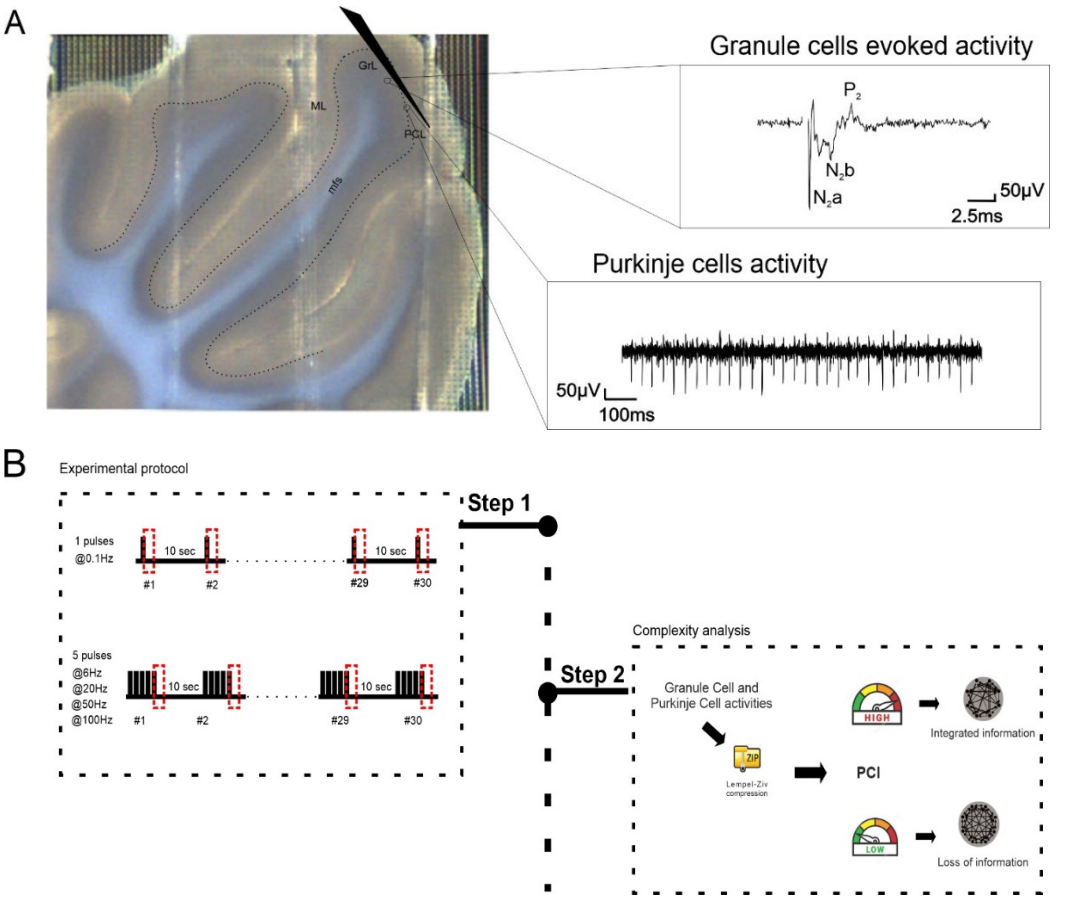
A
GrL
ML
PCL
mfs
Granule cells evoked activity
P2
N2b
N2a
50μV
2.5ms
Purkinje cells activity
50μV
100ms
B
Experimental protocol
Step 1
1 pulses
@0.1Hz
10 sec
#1
#2
#29
#30
5 pulses
@6Hz
@20Hz
@50Hz
@100Hz
Step 2
Complexity analysis
Granule Cell and
Purkinje Cell activities
Lempel-Ziv
compression
PCI
HIGH
Integrated information
LOW
Loss of information
C
Raw Data
LFP analysis
Filtered Data
Blanking artifact
PC firing analysis
Spike detection
Spike sorting
Permutation test
PCI

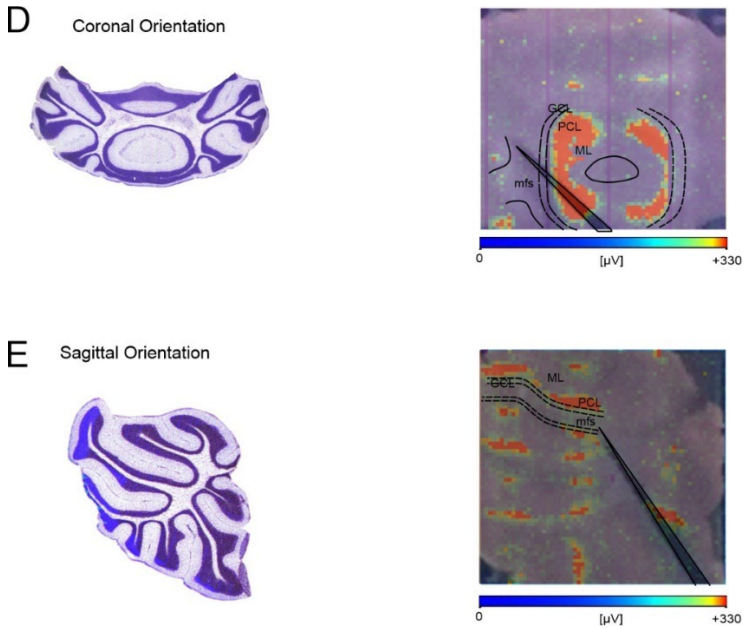

Figure 1: HD-MEA recordings in a cerebellar acute slice and analysis workflow. ***(A)*** *Parasagittal slice of the cerebellar vermis (thickness 220 µm) placed on the 64x64 electrodes matrix. mfs indicate the white matter bundles stimulated by an external bipolar electrode. GrL, the granular layer. The left raw trace on the top show evoked activity with the typical N2a – N2b – P2 complex, on one selected electrode at the granular layer level. PCL, Purkinje cell layer. The left raw trace on the bottom exhibits the Purkinje cell autorhythmic activity on one selected electrode. ML, refers to the molecular layer.* ***(B - C)*** *Experimental protocol and .data analysis workflow. Step 1: Experimental protocol. Two different evoked activities were considered: the local field potential and Purkinje cell discharge were analyzed. We considered the first 5 ms after the last stimulation pulse in each train of stimulation across trials to analyse the N2a peak amplitude of granule cells evoked activity. To analyse the Purkinje cells activity, we considered the first 20 ms after the last stimulation pulse in each train of stimulation across trials. Step2: Complexity analysis. The compression algorithm Lempel- Ziv is used to compute the PCI of the granule cell and Purkinje cell activity. The workflow in* ***(C)*** *show the pre – processing of the raw data.* ***(D - E)*** *Representative images of coronal and sagittal cerebellar slices on a chip with a map of HD – MEA highlighting PCs position.*

Local field potential analysis

In the 64x64 matrix, we selected a region of channels corresponding to the granular layer of the stimulated lobule. The raw data was low–pass filtered with a cut-off frequency of 5KHz, to avoid aliasing. The data were decimated by a factor 9 reaching a resolution time of 0.05 ms and we discarded the first 1.3 ms, after the stimulus, to eliminate the artifact. The statistical significance of the responses was assessed using a nonparametric permutation test with the acceptance value $\alpha = 0.001$ to have conservative statistics (Nieus et al., 2018). To analyze the LFP, we calculated the amplitude of the maximum negative peak, corresponding to N2a, as the granule cell significant activation in the first 5 ms after the last pulse of the stimulation train across trials.

The perturbational complexity index which quantifies the richness of the patterns displayed by the granular layer population, was computed on the significant post-stimulus granule cells activities matrix.

Purkinje cells firing analysis

The analysis of Purkinje cell autorhythmic and evoked activity required a detection phase and a clustering phase. A concatenation procedure of each raw data acquired, at different frequencies, was performed to apply homogeneous spikes detection and clustering algorithm in a single concatenated file for each experiment.

The spike detection was performed in BrainWave 4 (3Brain AG) using the hard threshold at -100 µV with a refractory period of 1 ms. Spike detection was followed by the waveform extraction in a temporal window of 0.5ms pre-spike and 3ms post-spike. The spike sorting process was performed using the clustering algorithm based on K - means & PBM index, selecting three principal features related to the spike characteristic (Min Peak, Max

Peak, and Slope). As a result of these processes, one or more clusters of spikes were assigned to each channel showing Purkinje cell activity. Clusters correspond to different units, thus collecting spikes originating from different Purkinje cells. The inter-electrode tip distance of 42 μm and the diameter of Purkinje cell soma (20 μm) (Weber and Schachner, 1984) allow the detection of more than a single unit for each electrode. The sorting process includes a procedure to avoid the same Purkinje cell being represented in different electrodes, assigning each unit to the channel where the spike amplitude is larger. The statistical significance of Purkinje cell responses was assessed using a nonparametric permutation test with the acceptance value $\alpha = 0.001$ to have strictly conservative statistics. The responses to stimulation were characterized by computing the mean firing rate of each unit before the stimulus and the mean firing rate in the early 80 ms after the last pulse of the stimulation across trials. Only units with a basal mean firing rate of ≥ 10 Hz were considered for analysis (Ostojic et al., 2015). The spatiotemporal pattern of Purkinje cell responses with respect to the basal frequency was calculated on the significant activation in the early 20 ms after the last stimulus of the train at different input frequencies.
The perturbational complexity index was computed on the binary Purkinje cells matrix to quantify the richness of the spatial-temporal patterns displayed by the Purkinje cell layer population.

Adaptation of the Perturbational Complexity Index for in vitro recordings

The perturbational complexity index represents one of the complexity indices, which aims to quantify the richness of the spatiotemporal patterns displayed by neural networks. We quantified the PCI with an adapted version for in vitro recordings of the original algorithm (Casali et al., 2013), describing EEG responses in humans to TMS stimulation. In this work, the

spatiotemporal pattern of cerebellar granule cells and Purkinje cells in response to different input frequencies (0.1Hz, 6Hz, 20Hz, 50Hz, 100Hz) were analyzed. Note that the post-stimulus phase, here, is intended as the response following the stimulation train. A binary spatiotemporal distribution of significant activity (SS(x,t)) was extracted to represent the spatial (channel x) and temporal (time t after the last pulse of the stimulation train) activation given by the electrical stimulation (Casali et al., 2013; Colombi et al., 2021). Channels in the matrix were sorted as in works (Casali et al., 2013; Colombi et al., 2021) based on the amount of significant activation during the post-stimulus time. The minimal amount of redundant information contained in the compressed binary matrix was quantified using the Lempel - Ziv complexity measure (see Chapter 2). The PCI, subsequently, was defined as the normalized (between 0 and 1) Lempel – Ziv complexity measure, to compare PCI across different input frequencies (e.g., 0.1Hz, 6Hz, 20Hz, 50Hz, 100Hz).

3.4 Results

The stimulation of mossy fiber bundles excites granule cells, generating the extracellular evoked responses or local field potentials, that travel along the ascending axon and parallel fibers, activating Purkinje cells and molecular layer interneurons responses as demonstrated in (Mapelli and D'Angelo, 2007; Mapelli et al., 2010a; Gandolfi et al., 2014). Local field potentials also propagate along the granular layer, spreading to almost the entire lobule. The temporal and spatial organization of granule cells and Purkinje cells population activities was investigated with an HD – MEA in coronal and parasagittal slices of the cerebellar vermis. Neurons were identified based on their average frequency of firing, and their position in the layers. The

electrodes recorded regular autorhythmic activities in multiple locations: a) in the granular layer generated by Golgi cell, b) in the Purkinje cell layer generated by the soma of Purkinje cells, and c) in the molecular layer reflecting the presence of stellate and basket cells with spontaneous discharge at relatively high frequency (10 – 60 Hz) (Dieudonné, 1998; Forti et al., 2006; Schonewille et al., 2006). The presence of spontaneous and evoked activities confirmed the vitality of the slice circuitry (see Materials and Methods). The extracellular signals of the neurons population were determined by (i) the synaptic activity with a substantial contribution of Ca2+ currents; (ii) the voltage-dependent intrinsic events as action potential (iii) the architectural organization of network and synchrony of neurons (Diwakar et al., 2011; Buzsáki et al., 2016). The HD – MEA technique allowed to record the fundamental properties of field potentials and to define the spatial and temporal organization of activity patterns of granule cells and Purkinje cells.

3.4.1 Characterization of granule cell spatiotemporal activity in the coronal and the sagittal plane

The stimulation of the mossy fiber bundle with a train of five pulses at different frequencies induced characteristic activation patterns in the granular layer. The granular layer was usually at rest since granule cells do not have any autorhythmic activity. Field potentials were evoked in response to the mossy fiber stimulation, at different input frequencies, showing a typical $N_1 – N_2 – P_2$ complex. N_1 describes the presynaptic volley and cannot be discriminated from the stimulus artifact as was confirmed by (Mapelli and D'Angelo, 2007). The N_2 corresponds to the granular layer postsynaptic activity and is split into two different components named N_{2a} and N_{2b}. P_2 refers to the return current from the molecular layer (Maffei et al., 2002).

The analysis was focused on the N_{2a} peak amplitude as a measure of granule cell synaptic activation (see *Material and Methods for details*) in order to compute the complexity of the population of the granular layer. The spatial distribution of evoked responses in the granular layer after mossy fiber stimulation was reconstructed by plotting maps indicating the average amplitude across trials after the last stimulus of the train at different input frequencies (Figure 2A-B). Evoked activity travels from the stimulated mossy fiber bundle and the activation of granule cells is regulated by the excitatory synapse from the mossy fibers and the inhibitory one from Golgi cells. Granule cell local field potential revealed changes in N_{2a} peak amplitude increasing the stimulation frequencies. The amplitude decreased proportionally to the increasing input frequencies and this trend was similar in coronal and sagittal orientations. The variation of the peak amplitude with respect to the amplitude generated at a single pulse shown in Figure 2C, summarizes this trend. In the coronal orientation, the N2a peak amplitude % change is similar at 6Hz and 20Hz (6Hz: - 0.05 ± 0.04%; 20Hz: - 0.05 ± 0.05%), while at high frequencies the variation of the amplitude decrease (50Hz: -0.10 ± 0.08%; 100Hz: - 0.16 ± 0.05%). In the sagittal orientation, the variation of the amplitude decreases at different input frequencies (single: 6Hz: - 0.12 ± 0.03%; 20Hz: - 0.12 ± 0.04%; 50Hz: -0.14 ±0.04%; 100Hz: -0.19 ± 0.05%). No significant differences in amplitudes (unpaired *t*-test, 6Hz: $p = 0.1$; 20Hz: $p = 0.28$; 50Hz: $p = 0.68$; 100Hz: $p = 0.65$) were shown in both coronal or sagittal planes, reflecting the presence of the same recruitment of granule cells regardless of the several differences in the cerebellar cortex circuitry. Lower frequencies of stimulation showed a higher impact on slow oscillatory activity in the granular layer (Tremblay et al., 2019).

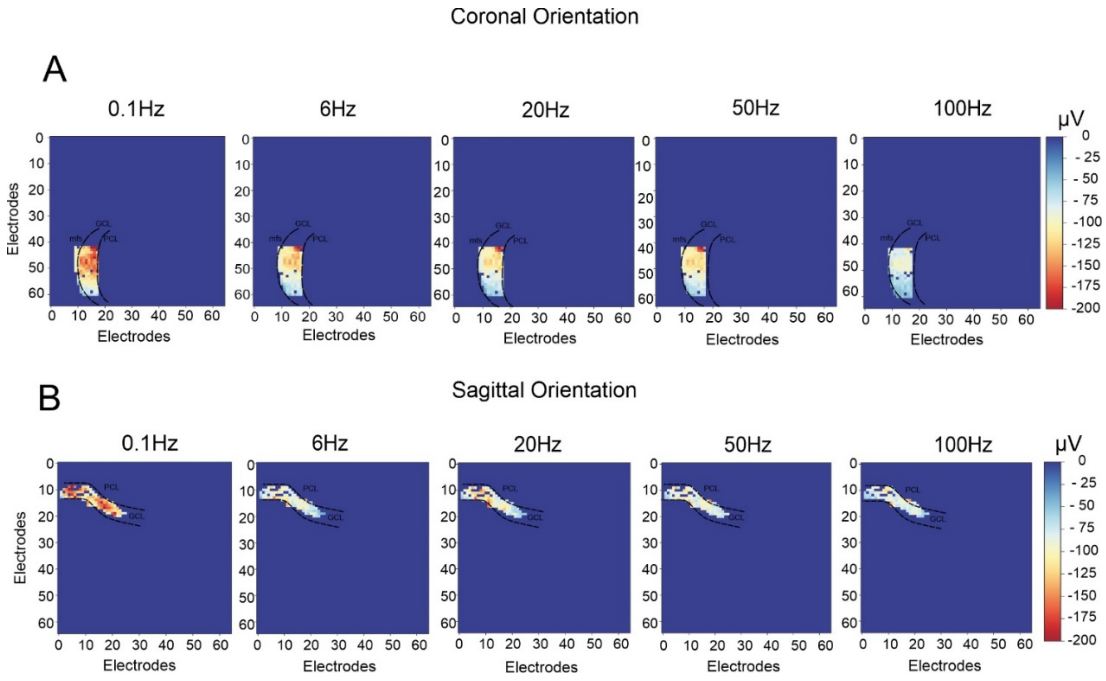
Coronal Orientation
A
0.1Hz
6Hz
20Hz
50Hz
100Hz
μV
0
- 25
- 50
- 75
-100
-125
-150
-175
-200
Electrodes
Sagittal Orientation
B
PCL
GCL
mfs

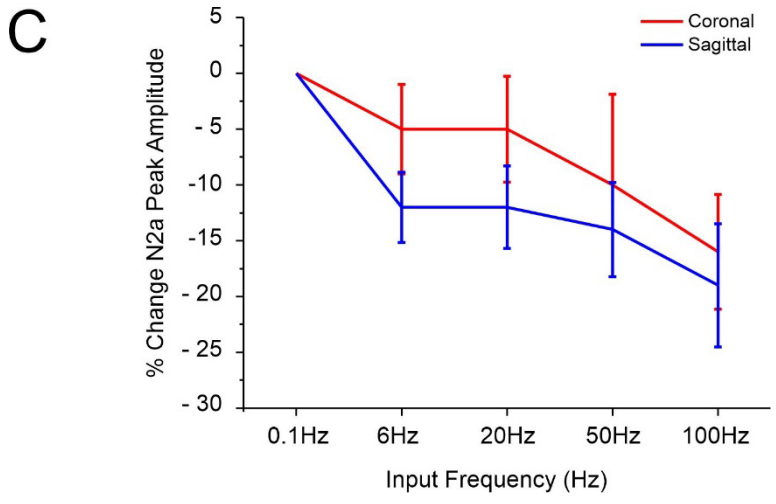
C
Coronal
Sagittal
% Change N2a Peak Amplitude
5
0
- 5
-10
-15
- 20
- 25
- 30
0.1Hz
6Hz
20Hz
50Hz
100Hz
Input Frequency (Hz)

Figure 2: Characterization of the GrC spatiotemporal activity in the ***coronal orientation*** *and* ***sagittal orientations****. (****A- B****) Heatmaps show the N_2a peak amplitude (μV) recorded in the coronal cerebellar acute slice using the HD – MEA, selecting the mask of granular layer local field potential near the external stimulus electrode at different input frequencies (0.1Hz, 6Hz, 20Hz, 50Hz, 100Hz). in coronal and sagittal orientation. (****B****) Heatmaps show the variation of MFR with respect to the basal firing rate at different stimulation frequencies (****C****) The plot shows the relationship between the input frequency and the average % change of N_2a peak amplitude for all the experiments in the coronal (red line) ad sagittal (blue) orientation).*

3.4.2 Purkinje cell spatiotemporal activity in the coronal and the sagittal plane

Given the possibility to record simultaneous multiple neuronal responses, our work was also focused on the study of the Purkinje cell pattern activity (Figure 1C). These detected units were identified from their characteristic regular spontaneous activity and their spatial localization in the Purkinje cell layer in the multielectrode array matrix.

The stimulation of the mossy fiber bundle with a train of five pulses at different frequencies induced characteristic activation patterns of responses in Purkinje cells (n units = 1709; parasagittal slices = 11, coronal slices = 8). To compute the complex dynamic of the information processing in the output stage of the cerebellar cortex, the non - parametric permutation test was used to estimate the statistical significance of unit responses to stimulation. We considered only units located in a specific region of interest (ROI, figure x, A-B) near the stimulation point, with a basal mean firing rate (MFR) ≥ 10 Hz, and that showed a significant increase or decrease of the

MFR in the first 20 ms after the last stimulus of the train (n units = 632; parasagittal slices = 11, coronal slices = 8).

The Purkinje cells are controlled both by synaptic input and by intrinsic properties that are responsible for spontaneous firing (Womack et al., 2004). The spatial organization in the electrodes matrix revealed a high variability of Purkinje cells firing, recorded in the 500 ms before the stimulation (MFR range 10 Hz – 150 Hz). The firing activity differs within the Purkinje cells population, presumably due to the distribution in bands of zebrin II positive (Z+) and negative (Z-) cells over the cerebellar cortex (Zhou et al., 2014). In our experiments, zebrin expression was not characterized but the different Purkinje cells firing patterns might represent this property. Indeed, in the coronal slice, the firing activity of the Purkinje cell population followed the band distribution, while in the sagittal orientation, the organization in bands of activity was not evident (Figure 3A – 4A).

The electrophysiological intrinsic and synaptic properties of Purkinje cells revealed excitatory and inhibitory patterns of responses to a strong current input (Valera et al., 2016). Herein, the characterization of Purkinje cell responses was analyzed for each stimulation frequency (0.1Hz, 6Hz, 20Hz, 50Hz, 100Hz). Purkinje cell responses showed a variation of the MFR, with respect to the basal one, at different stimulation frequencies in both coronal and sagittal slices (Figure 3B – 4B). Purkinje cells with a lower basal frequency (10 Hz – 50 Hz) revealed larger responses (Fig 3C – 4C), while at higher basal frequency (> 50 Hz), the responses were smaller. In many cases, a correlation was found between the basal MFR and the responses as shown with the fitting function.

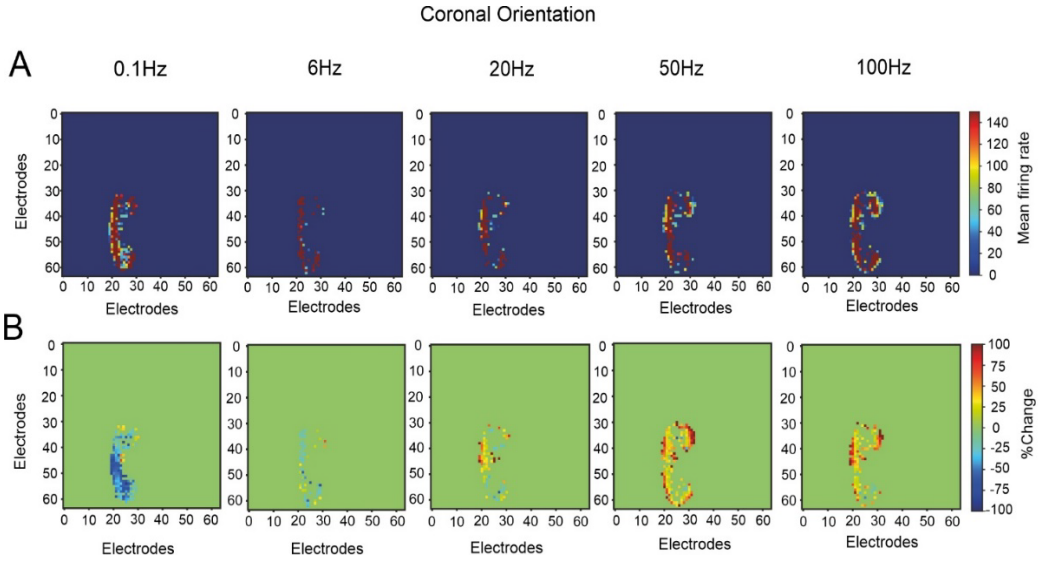
Coronal Orientation
A
0.1Hz
6Hz
20Hz
50Hz
100Hz
Electrodes
Mean firing rate
B
%Change

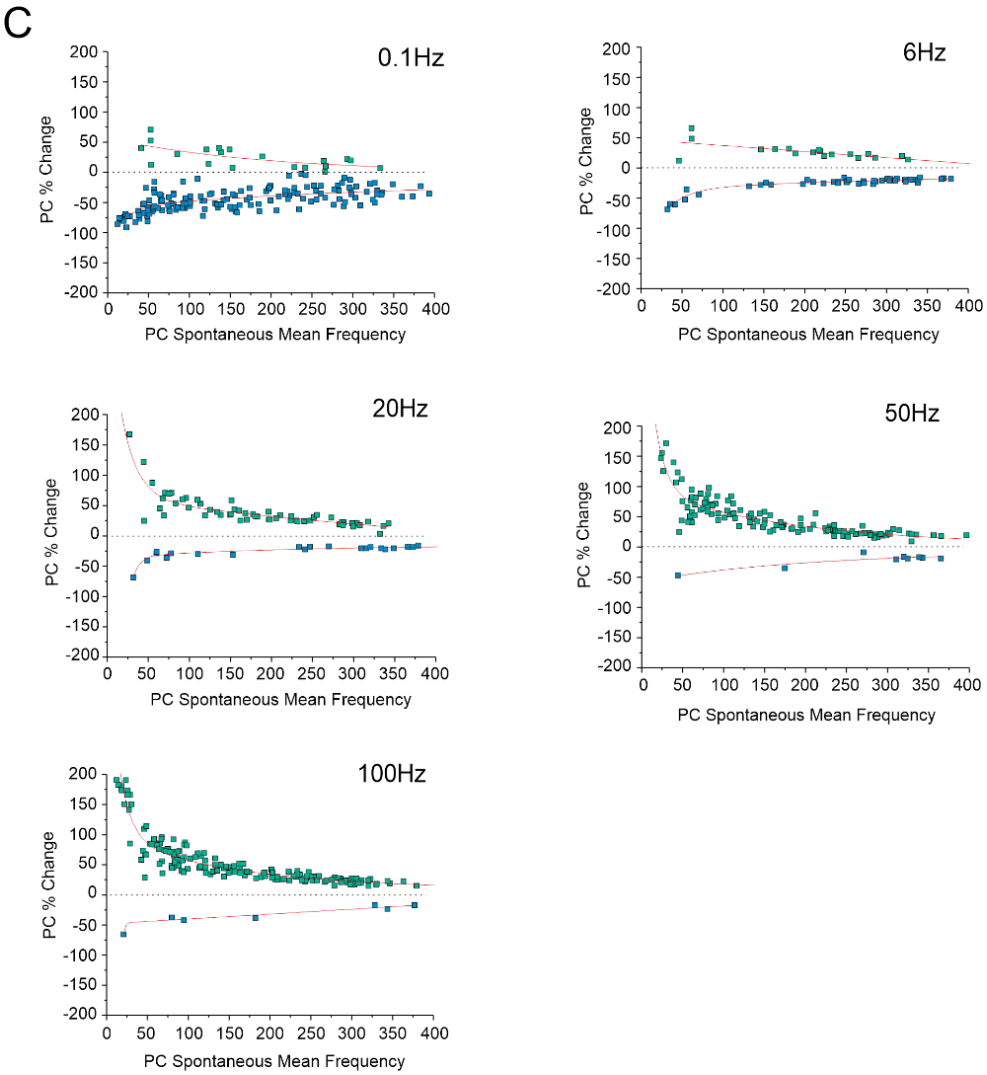
C
0.1Hz
6Hz
20Hz
50Hz
100Hz
PC % Change
PC Spontaneous Mean Frequency

*Figure 3: Characterization of the PC spatiotemporal activity in the coronal orientation. (**A**) Heatmaps show the mean firing rate of the PC spontaneous activity recorded in the coronal cerebellar acute slice using the HD – MEA, selecting one region of interest (ROI) near the external stimulus electrode at different input frequencies. (**B**) Heatmaps show the variation of MFR with respect to the basal firing rate at different stimulation frequencies (single pulse, 6Hz, 20Hz, 50Hz, 100Hz). (**C**) The plot shows the relationship between the spontaneous mean frequency and the % change at different frequencies (biexponential fit). The dots distribution refers to PC units recorded; the fitting curve (red line; 0.1Hz: R2=0.31, R2=0.43; 6Hz: R2=0.32, R2=0.92; 20Hz: R2=0.95, R2=0.91; 50Hz: R2=0.82, R2=0.62; 100Hz: R2=0.88, R2=0.88) describes the correlation between spontaneous mean frequency and the variation of the firing calculated for the significant activation in the first 20ms after the last stimulus of the train. The distribution of the dot indicates the PC firing increase (green) and decrease (indigo).*

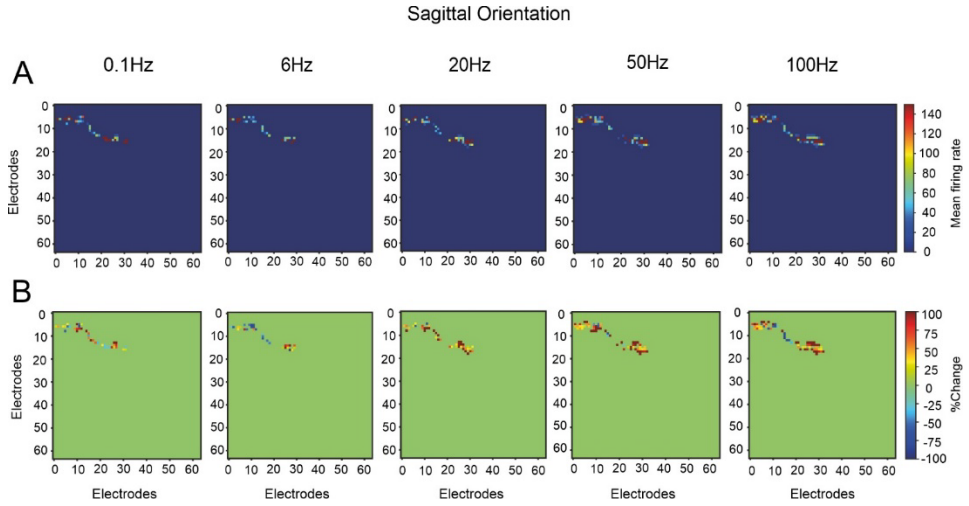
Sagittal Orientation
A
0.1Hz
6Hz
20Hz
50Hz
100Hz
Electrodes
Mean firing rate
B
Electrodes
%Change

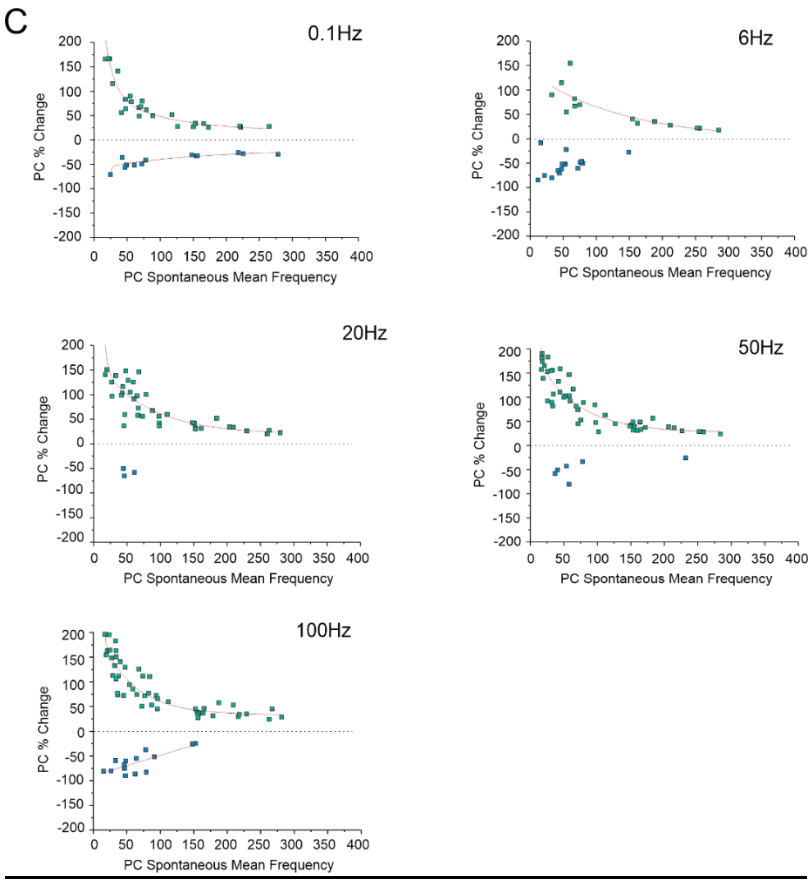
C
0.1Hz
6Hz
20Hz
50Hz
100Hz
PC % Change
PC Spontaneous Mean Frequency

*Figure 4: Characterization of the PC spatiotemporal activity in the sagittal orientation. (**A**) Heatmaps show the mean firing rate of the PC spontaneous activity recorded in the sagittal cerebellar acute slice using the HD – MEA, selecting one region of interest (ROI) near the external stimulus electrode at different input frequencies. (**B**) Heatmaps show the variation of MFR with respect to the basal firing rate at different stimulation frequencies (single pulse, 6Hz, 20Hz, 50Hz, 100Hz). (**C**) The plot shows the relationship between the spontaneous mean frequency and the % change at different frequencies (biexponential fit). The dots distribution refers to PC units recorded; the fitting curve (red line; 0.1Hz: R2=0.88, R2=0.75; 6Hz: R2=0.52; 20Hz: R2=0.82; 50Hz: R2=0.84; 100Hz: R2=0.86, R2=0.42) describes the correlation between spontaneous mean frequency and the variation of the firing calculated for the significant activation in the first 20ms after the last stimulus of the train. The distribution of the dot indicates the PC firing increase (green) and decrease (indigo).*

The analyses of average Purkinje cells responses to different input frequencies showed marked differences in coronal and sagittal slices (Figure 5A). In the sagittal orientation, units tended to respond with a larger variation of the firing compared to the coronal orientation, with MFR increases always prevailing over the decreases. In the coronal plane, Purkinje cell responses were characterized by a predominant MFR decrease at lower frequencies and smaller increases at the other frequencies compared to the sagittal plane. At 0.1 Hz, the difference between the two planes was evident (*sagittal*: 21.9±11.7%; *coronal*: -32.4±7.3%; p = 0.001) as well as at 20 Hz (*sagittal*: 56.7±15.9%; *coronal*: 15.4±12.0%) and 50 Hz (*sagittal*: 73.2±9.9%; *coronal*: 31.7±16.6%; p = 0.03). Purkinje cell responses at 100 Hz were not statistically different (*sagittal*: 79.7±18.3%; *coronal*: 45.6±18.3%) in coronal and sagittal orientations. These results might be explained by the fact that at high-

frequency Purkinje cells activity tends to be synchronized, as shown by *in vivo* experiments (de Solages et al., 2008).

The results also showed similarities in the theta band, at 6Hz (*sagittal*: -1.1±11.7%; *coronal*: -9.3±11.5%) where the average variation of the activity with respect to the basal firing is near 0%. This might underlie the slowly oscillating spike activity of the Purkinje cells (de Zeeuw et al., 2008).

Purkinje cell responses following the mossy fiber stimulation at different frequencies reflected a strong frequency dependence of Purkinje cells activity. We calculated the percentage of units showing two different responses: the MFR increased and decreased after the stimulation. This evaluation is based on the significant responses in the first 20ms after the last stimulus of the train, estimating with the non – parametric permutation test (see *Material and Methods*).

In the coronal plane, the majority of Purkinje cells decreased the MFR with low-frequency stimulations, and this effect became less evident the higher the stimulation frequency (Figure 5B). At 0.1 Hz, the percentage of units (85.1±4.6%) that decreased their basal discharge was significantly larger (unpaired *t*-test, $p = 3.74 \times 10^{-8}$) compared to those units that increased their basal firing (14.8±4.6%). Significant differences were also observed at 6 Hz and 100 Hz. In particular, at 100Hz the majority of Purkinje cells increased their MFR (71.0±12.9%) compared to the units that decreased their basal discharge (28.9±12.9%; p=0.036).

In the sagittal plane, a similar number of Purkinje cells either increased or decreased the MFR, but the two response patterns became more differentiated at increasing stimulation frequencies (Figure 5C). At 0.1 Hz, the number of units that showed MFR increase (53.7±10.0%) was similar to those units that decreased the MFR (46.4±10.0%; p= 0.6 (ns)),

suggesting the equal contribution of direct excitatory granule cell pathway and the inhibitory activity of the molecular layer interneurons. At frequencies > 20Hz, the majority of PC increased their MFR in response to stimulation (20 Hz: 75.5±8.9%, p = 0.0006; 50 Hz: 84.3±4.7%, p = 2.34×10^{-9}; 100 Hz: 80.6±7.0% p = 5.4×10^{-6}).

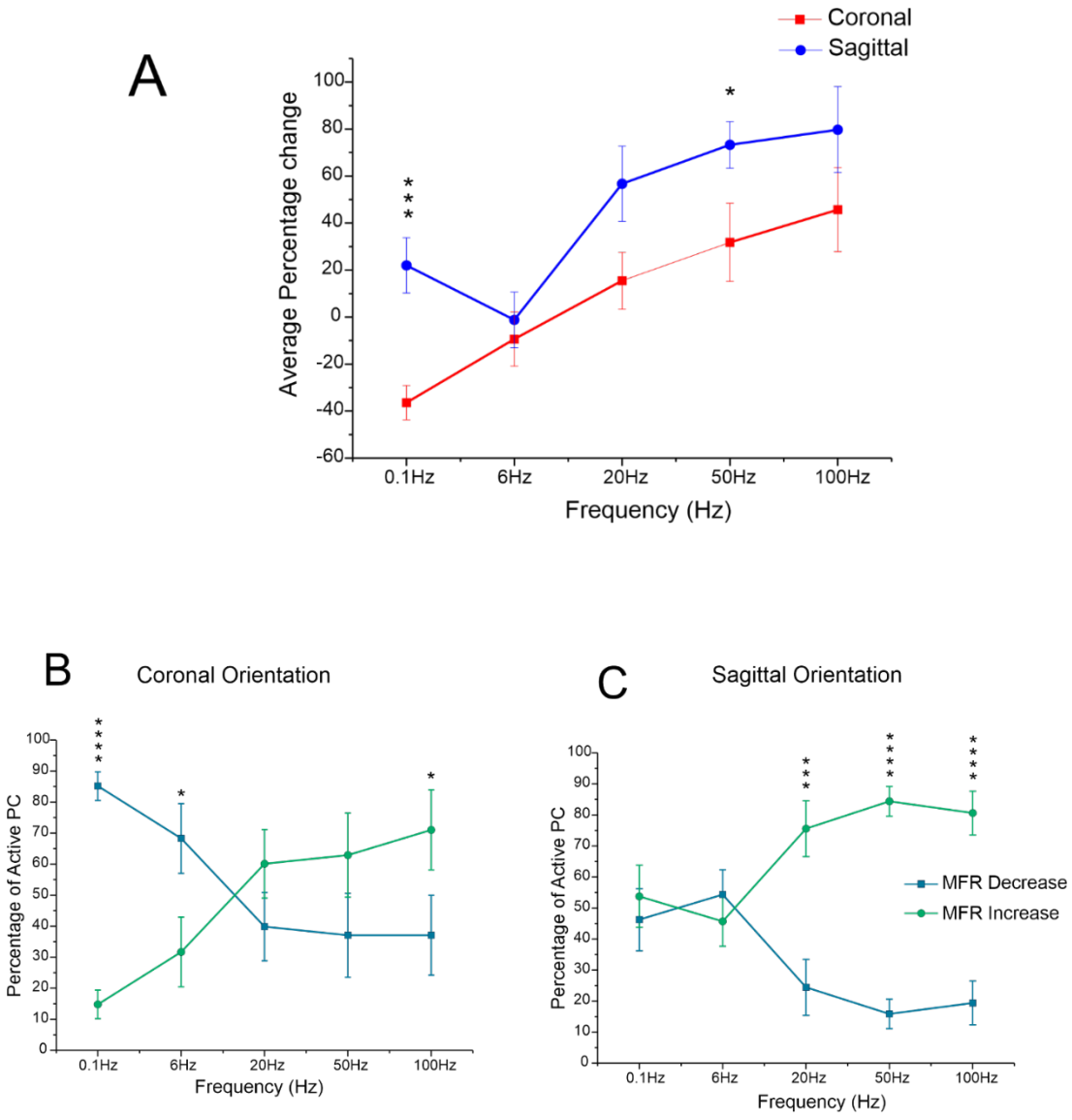

*Figure 5: PC changes of firing rate following mf stimulation at different frequencies. (**A**) The plot describes the average of variation of the mean firing rate with respect to the basal firing rate at different input frequencies. PC firing shows a frequency dependence relative to all experiments in both coronal (red) and sagittal (blue) orientation at different frequencies. At different stimulation frequencies, plots (**B - C**) describe the number of units with significant activation that present an increase (green) and decrease (indigo) in the firing rate in coronal and sagittal orientation.*

3.4.2 Spatiotemporal activation of granule and Purkinje cell population

The complexity measures of evoked activity aimed at investigating the richness of the spatiotemporal patterns displayed in the cerebellar network. For each channel showing a response to stimulation, the permutation test was applied to determine the presence of a significant activation (See *Material and Methods*). To be noted, a significant activation can be either an increase or a decrease in Purkinje cells MFR. At different frequencies, the computation of the compressed algorithm (see *Material and Methods*) generated a binary matrix of significant sources across trials in the granular layer and in the Purkinje cell layer, for each experiment in both coronal and sagittal orientation.

The binary matrix of the significant source relative to the coronal plane (Figure 6A) showed the significant activation in granule and Purkinje cell populations at different input frequencies. Mossy fibers convey input signals to the cerebellar cortex, modulating the granular layer discharge (Chadderton et al., 2004; Jörntell and Ekerot, 2006). We investigated the impact of these characteristic patterns during the granular layer evoked activity in response to trains of stimuli. The significant activation of granule cells in response to stimulation (t=0) showed the instantaneous and

simultaneous temporal changes of the local field potential. The stimulation at 0.1Hz marked the significant activation of granule cell responses for ~ 10 ms, followed by the temporal changes in Purkinje cell responses lasting for 80 ms. Increasing the input frequencies, the granular layer activity showed a remarkable temporal summation in which the responses were extended until 100 ms at 100 Hz. The number of sorted units in the Purkinje cell population incremented with respect to the input frequencies, showing a frequency dependence. At 0.1 and 100 Hz, we observed the maximal significant activation of Purkinje cell responses that occurred across trials. At 6 Hz we noted that the PC responses lasted for 40 ms, (Figure 6A – 6Hz) and were reduced with respect to the other input frequencies.

In the sagittal plane, a single stimulus determined the significant activation of granule cell responses for ~ 10 ms, followed by Purkinje cell responses lasting for 60 ms (Figure 6B). The fraction of Purkinje cells population, sorted in space, significantly activated by the stimulus increased at increasing frequencies, which could be explained considering (i) the granular layer adaptive filter function and (ii) the number of units activated in response to the granular layer evoked activity. Increasing the stimulation frequency, a considerable temporal summation of the granular layer evoked activity was revealed, as observed in the coronal plane, followed by progressive recruitment of the number of units activated in the Purkinje cell population and the response lasted for 80 ms.

These considerations displayed the complex dynamic of evoked activity in granule cells and Purkinje cell populations and their spatiotemporal integration after stimulation.

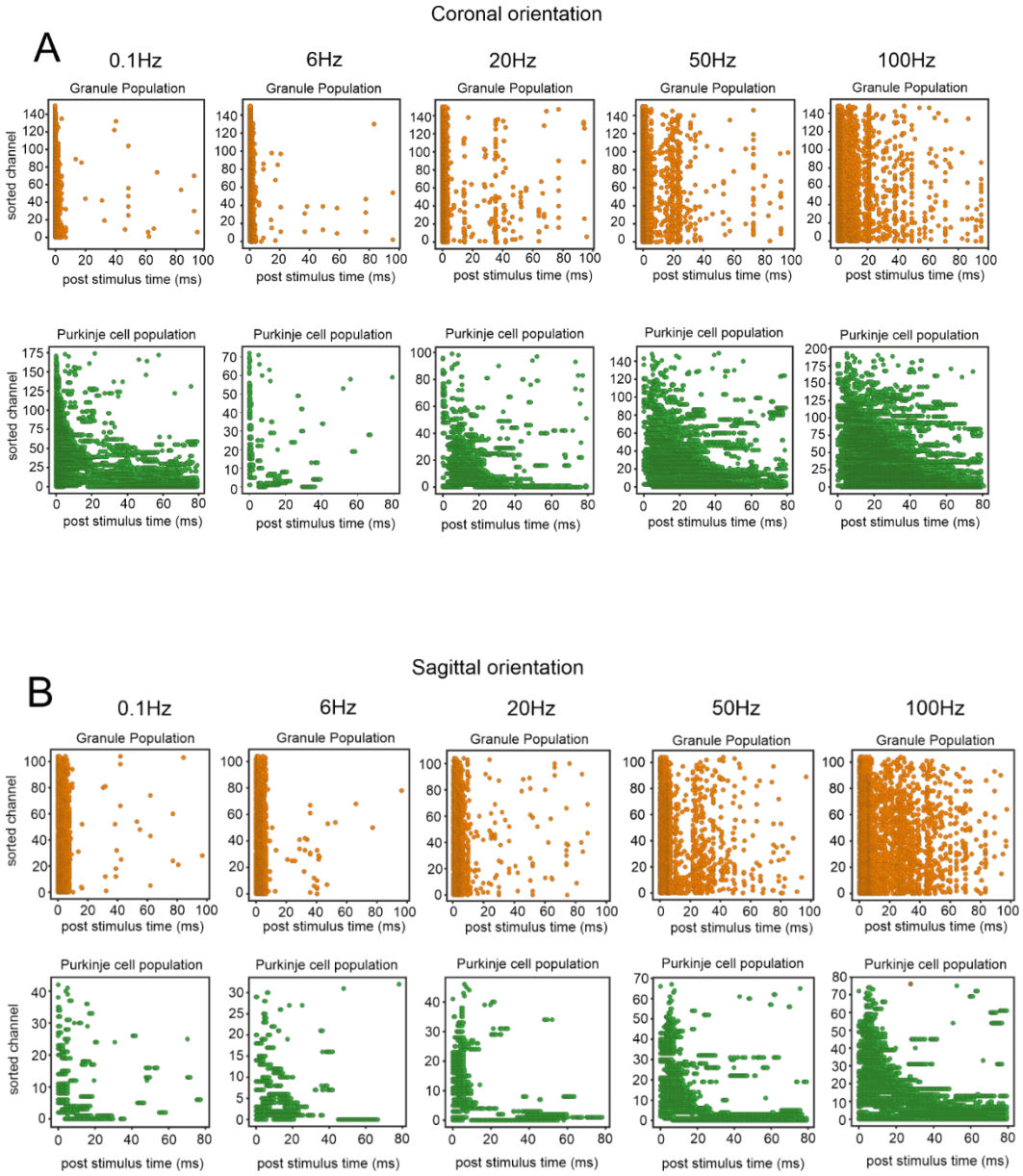
Coronal orientation
A
0.1Hz
6Hz
20Hz
50Hz
100Hz
Granule Population
Purkinje cell population
sorted channel
post stimulus time (ms)
Sagittal orientation
B
0.1Hz
6Hz
20Hz
50Hz
100Hz
Granule Population
Purkinje cell population
sorted channel
post stimulus time (ms)

Figure 6: Binary matrices of spatiotemporal activation of evoked activities of granule cells and Purkinje cell populations. (A) The binary matrix of significant activation sources of the granule cell population (orange) and Purkinje cell population (green) at different input frequencies, relative to a representative coronal slice. (B) The binary matrix of significant activation sources of the granule cell population (orange) and Purkinje cell population (green) at different input frequencies, relative to a representative sagittal slice. Time (t = 0) corresponds to the stimulus and the dots describe the spatiotemporal activation.

3.4.3 Preturbationa Complexity Index (PCI) of the granule and Purkinje cell populations

PCI was computed for the evoked activity of both granule cells and Purkinje cell populations considering all experiments in coronal and sagittal orientation at different input frequencies.

At the granule cell population level, the PCI increases with the stimulation frequency (Figure 7A). In sagittal slices, PCI is larger than in coronal slices (*0.1Hz*: 0.39; *6Hz:* 0.40; *20Hz:* 0.45, *50Hz:* 0.54; *100Hz:* 0.57). In the coronal orientation, PCI is lower than in sagittal orientation but increases at different input frequencies (0.1Hz: 0.31; *6Hz:* 0.35; *20Hz:* 0.38, *50Hz:* 0.52; *100Hz:* 0.49). Significant differences were observed at 0.1 Hz (unpaired *t*-test, p = 0.004) and 100Hz (unpaired *t*-test, p = 0.004).

The PCI calculated at the level of the Purkinje cell population changed dynamically with the input frequencies and orientation of the slice (Figure 7B). In the sagittal orientation, the PCI decreased at higher frequencies (*0.1Hz:* 0.32; *6Hz:* 0.31; *20Hz:* 0.33; *50Hz:* 0.32; *100Hz:* 0.26). In the coronal orientation, the PCI was larger with respect to the sagittal plane (*0.1Hz:* 0.23; *6Hz:* 0.35; *20Hz:* 0.43; *50Hz:* 0.40; *100Hz:* 0.40). We noticed significant differences at 0.1 Hz, 20 Hz, 50Hz and 100Hz (unpaired

t-test, $p_{0.1Hz} = 0.020$; $p_{20Hz} = 0.007$; $p_{50Hz} = 0.015$; $p_{100Hz} = 3.3x10^{-5}$). At high frequencies the PCI is larger in the coronal orientation, compared to the sagittal plane.

We calculated the total PCI of the joint granule cell and Purkinje cell populations in sagittal and coronal orientation at different frequencies (Figure 7C). In this case, PCI increased with the stimulation frequency and the increase was more pronounced in coronal slices presumably due to the intense spread of the activity along the parallel fibers (*sagittal*: *0.1Hz:* 0.39; *6Hz:0.41; 20Hz: 0.44; 50Hz: 0.50; 100Hz:* 0.48; *coronal*: *0.1Hz*: 0.27; *6Hz: 0.36; 20Hz: 0.39; 50Hz: 0.49; 100Hz: 0.47*) with significant differences at 0.1 Hz (unpaired *t*-test, p = 0.0001).

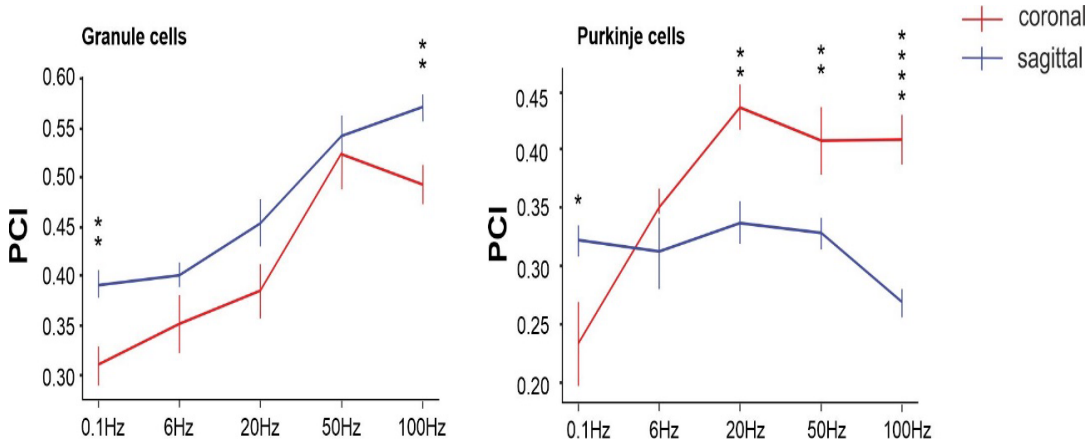

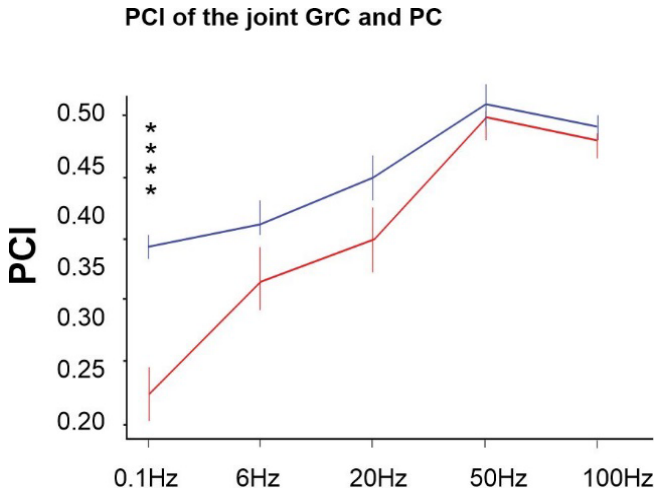

*Figure 7: Perturbational complexity index (PCI) measure of evoked activity in sagittal (blue) al coronal plane (red). (**A**) PCI of granule cell population increase at different input frequencies (**B**) PCI of Purkinje cell population change dynamically with the input frequencies and orientation of the slice. (**C**) PCI of the joint granule cell and Purkinje cell population.*

3.5 Discussion

HD – MEA recordings provided a measure of extracellular activity in acute cerebellar slices in the coronal and sagittal orientation, allowing the investigation of evoked discharge of the cerebellar neurons elicited by the stimulation of the mossy fiber bundle. In this paper, we characterized the spatiotemporal activation of evoked activities of granule cells and Purkinje cells populations, in the effort to highlight the cerebellar network pattern dynamics and, consequently, the cerebellar information processing in response to different input frequencies. Spatiotemporal operations at the input stage are fundamental to understand cerebellar motor coordination and learning function (Mapelli et al., 2010a). Moreover, the propagation of

the input signals activates the firing pattern dynamics of Purkinje cells (Valera et al., 2016), revealing a frequency dependence of responses. The complex information processing along the mossy fibers – granule cells – Purkinje cells pathway and the pattern of interaction among cerebellar neuronal types had been studied using a complexity index (PCI) to evaluate the integration levels of neurons responses in space and time.

3.5.1 Spatiotemporal filtering properties of the granular layer

At the cerebellum input stage, the circuit functioning is related to its topological organization. The granular layer has been suggested to perform a spatiotemporal reconfiguration of input signals. One of the two major inputs pathways is conveyed by mossy fibers, originating from the brainstem nuclei, to granule cells, the most numerous, small, and closely packed neurons (D'Angelo, 2018; Hull and Regehr, 2022; Masoli et al., 2022). Granule cells emit four short dendrites and a single axon, that ascend vertically into the molecular layer, where it bifurcates to form parallel fibers that run along the orthogonal plane. The granular layer includes a feed-forward (mossy fibers – Golgi cells – granule cells) and feedback (mossy fibers – granule cells – Golgi cells – granule cells) inhibitory loop. These inhibition mechanisms control the temporal window during which granule cell integrates excitatory input and facilitates the oscillation in the theta frequency band. The permissive time window lasts about 4 – 5 ms (D'Angelo and De Zeeuw, 2009) and controls the granule cell response.

Granule cells are silent at rest, but when depolarized, respond with doublet spikes after mossy fibers stimulation (D'Angelo et al., 1995; Maffei et al., 2002). In the extracellular recordings, the granular layer activity is represented by local field potential, which showed the typical N1 – N2 – P2

complex (Eccles et al., 1967; Mapelli and D'Angelo, 2007). The presence of multiple peaks in the granular layer field potential reflected the evoked activity of granule cells. According to the literature, the N_2 wave is split into two peaks, N_2a and N_2b, denoting the major determinant elements for the spike generation in granule cells. These two waves were correlated with the postsynaptic activity and indicated the recruitment of the mossy fibers (Mapelli and D'Angelo, 2007).

The characterization of granule cell responses in coronal and sagittal slices was focused on the N_2a peak amplitude, which was related to the strength of the mossy fibers – granule cell synaptic transmission (Mapelli and D'Angelo, 2007). The N_2a peak refers to the early fast AMPA receptor–mediated components and to spike synchrony, and it provides the gain mechanism at the mossy fiber–granule cell synapses.

The stimulation of the mossy fiber bundle with a train of five impulses, repeated for 30 trials, at different frequencies, induced a particular activation pattern in the granular layer. The spatiotemporal organization of the granular layer, in fact, indicated that the number of mossy fibers recruited in input transmission changed, increasing with the input frequency (Figure 3A – B). A higher number of stimulated fibers can enhance the number of mossy fibers – granule cell synapses, however, the substantial build-up of glutamate concentration in the cleft determines only moderate AMPARs desensitization at high frequencies (DiGregorio et al., 2007).

This finding was corroborated by the analyses of the variation of the N_2a peak amplitude with respect to the single stimulus, which decreased at higher frequencies. Single pulse stimulation had a major effect on granule cells, confirmed by the maps (Figure 3A-B) in which the theta and beta bands are preferred frequencies (D'Angelo et al., 2001; D'Angelo and De Zeeuw, 2009), confirmed the fact that the information processing is highly

nonlinear, generating oscillation, bursting, and resonance, especially in response at preferential frequencies. The results reported that the granular layer response to mossy fibers followed a frequency–dependent transmission. Therefore, the gain function of the granular layer demonstrated its ability to behave as an adaptive filter and the transmission of the input enhances spatiotemporal coding.

3.5.2 Frequency dependence of Purkinje cell population

The cerebellar output layer is composed of a monolayer of adjacent Purkinje cells with dendrites that branch out in the molecular layer and are contacted by granule cells ascending axons, parallel fibers, and molecular layer interneurons in the molecular layer. Granule cells provide excitation to Purkinje cells. Purkinje cells also receive inhibitory inputs from basket cells and stellate cells, which are molecular layer interneurons that play an essential role in controlling the cerebellar cortical output.

The characterization of the spatiotemporal pattern of Purkinje cell activity was conducted in coronal and sagittal slices. The propagation of the signal followed the anatomical organization. In the sagittal orientation, activation spread from the mossy fiber bundle and ascended vertically toward the molecular layer. In the coronal orientation, the molecular layer showed a strong pattern of activity due to the signal propagation longitudinally along parallel fibers. The high spatial and temporal resolution of the HD-MEA allowed us to highlight the zebrina-like distribution pattern of Purkinje cells in coronal slices, in contrast to the sagittal slice, in which it was not possible to distinguish this pattern. Based on our findings, were observed variability of Purkinje cell pattern responses elicited by mossy fiber inputs. This variability is coherent with the functional encoding of the

cerebellar cortex, here emulated at different input frequencies, and is not related to the intrinsic single neuron noise as confirmed in (Sauerbrei et al., 2015). The wide range of Purkinje cell complex patterns of activity was likely due to the complex intrinsic oscillator, spontaneous firing, and high rhythmicity in the absence of synaptic input, as previously characterized (Häusser and Clark, 1997). In response to different input frequencies, Purkinje cells incremented or decremented their firing in the first 20 ms after the last stimulus of the train, showing a complex spatiotemporal pattern of activity. Our results showed that high-frequency mossy fiber input plays a crucial role in the rapid integration of information processing at the cerebellar output stage. In fact, the synapses parallel fibers – inhibitory interneurons were reported to depress with high-frequency stimulation (Rizza et al., 2021), while the synapsis parallel fibers - Purkinje cells showed facilitation, implementing a time dependence of the cerebellar network. The mossy fiber stimulation at different frequencies modulated the Purkinje cells discharge, through various types of pathways of excitation and inhibition that converged on Purkinje cells implementing information processing. The difference between both planes suggested that in the coronal orientation at low frequency, the inhibitory pathway prevailed to provide a decrease of Purkinje cells MFR. The opposite condition was visible at high frequency. In the sagittal plane, at high frequency, the excitatory pathway was more influential to modulate the PC discharge probably due to the tonic glutamate spread around the extracellular space. Interestingly, in both planes, the amplitude of Purkinje cells response negatively correlated with the basal MFR. This might suggest that Purkinje cells that received more inhibitory input (i.e., with lower basal MFR) were more able to modulate their discharge in response to synaptic inputs, and vice versa. This observation confirms and further expands the knowledge about the critical role of local

inhibition to boost the processing power of principal neurons. Additionally, at 6 Hz the Purkinje cells responsiveness is lower in both orientations, suggesting an oscillatory activity, that usually occurs at 2 to 10 Hz as confirmed by (de Zeeuw et al., 2008). These lower frequency bands are the preferred frequency of PC oscillation activity and in conjunction with the granule cells resonance, could contribute to implement a temporal coding scheme in the cerebellar network (Gandolfi et al., 2013; Bauer et al., 2022). These findings suggest the frequency dependence of the Purkinje cell dynamic and provide important clues to confirm the important role exerted by molecular layer interneurons to control Purkinje cells information processing (Kim and Augustine, 2021).

3.5.3 Perturbational complexity index as a measure of cerebellar information processing

The complexity of the interaction among neurons in the cerebellar cortex was investigated using adapted complexity measurements that can explain the spatiotemporal pattern of activity in the granular layer and Purkinje cell population at different stimulation frequencies. The PCI is a reliable index that can correlate the level of integration and segregation of neurons, and it was applied at macroscale level studies to gauge the complexity of the causal interaction in the brain (Tononi and Edelman, 1998; Casali et al., 2013; Dasilva et al., 2021).

Here, for the first time, we described the spatiotemporal activities in the cerebellar cortical circuitry and measured the complexity of neuronal interactions by applying a perturbational approach to cerebellar acute slices at different input frequencies. At this microscale level, we found (i) substantial differences in spatiotemporal complexity patterns in both the

coronal and sagittal planes; (ii) granule cells and Purkinje cells population activity patterns depended significantly on different input frequencies; (iii) the joint granule cells and Purkinje cells population increased with stimulation frequency, (iv) complexity of granule cells and Purkinje cells population suggested that high frequencies maximize the efficiency of the cerebellar circuit with respect to low frequencies, in which the neuronal population showed a stereotyped activity.

The spatial organization of cerebellar cortex circuits is a highly organized 3D structure and provides insights into the mechanisms that regulate information processing. It is necessary to take into account the spatial localization of cerebellar neurons in both orientations: Purkinje cells dendrites and BC axons are oriented in the sagittal plane, while pf run along the coronal plane. The spatial organization can reflect the connectivity and functionality of the cerebellar cortex (Figure 8).

The increased complexity value in the granular layer at increasing stimulation frequencies confirmed the frequency-dependent transmission of mossy fibers input in the granular layer. The difference between the coronal and sagittal planes suggested that signal transmission follows the anatomical interaction of cerebellar neurons. In this case, the PCI is higher in the sagittal slices than in the coronal slices, probably reflecting the spread of Golgi cells axonal plexus in the sagittal plane. On the contrary, in the coronal plane, the Golgi cell axon ramifications were limited because of the cutting procedure; however, the molecular layer showed a strong activation which propagate along the undamaged parallel fibers.

The PCI computed in the Purkinje cells population is higher in the coronal plane with respect to the sagittal, with a preferred frequency of 20 Hz, 50 Hz, and 100Hz. This finding might suggest that these frequencies are the optimal frequencies in which the circuit presents the higher

integration among Purkinje cells and other neuronal elements in the network. Purkinje cells receive feedforward inputs from two pathways: excitatory inputs from granule cells and inhibitory inputs from molecular layer interneurons that contribute to control Purkinje cells output (Rizza et al., 2021). The synaptic transmission of parallel fibers – molecular layer interneurons is expected to exert a significant influence on Purkinje cells inhibition at the level of the soma and dendrites. The high-frequency mossy fibers stimulation increased the granule cell activity, which retransmitted the signal along the parallel fibers. The Purkinje cell soma received inhibition from basket cell, while the Purkinje cell dendritic tree was inhibited by stellate cell (Bao et al., 2010). Molecular layer interneurons received multiple excitatory and inhibitory inputs, which were integrated and transmitted to Purkinje cells (Kim and Augustine, 2021). The contribution of the molecular layer interneurons might influence the spatiotemporal activation of Purkinje cells; therefore, Purkinje cells output might reflect molecular layer interneurons - mediated filtering of the inputs. After a single stimulus, the difference between the coronal and sagittal PCI might reflect the richer Purkinje cells patterns in the sagittal orientation. This is confirmed by the relative contribution of Purkinje cells and granule cells to the PCI, comparing sagittal and coronal planes. Contrary to granule cells, Purkinje cells contribution to PCI is strikingly different in the two planes. However, the complexity of the joint granule cells and Purkinje cells population described a linear trend similar to the PCI evaluated in the granule populations. This suggests that the granular layer regulates the transmission gain and generates temporal dynamics during signal processing, with the contribution of Golgi cells.

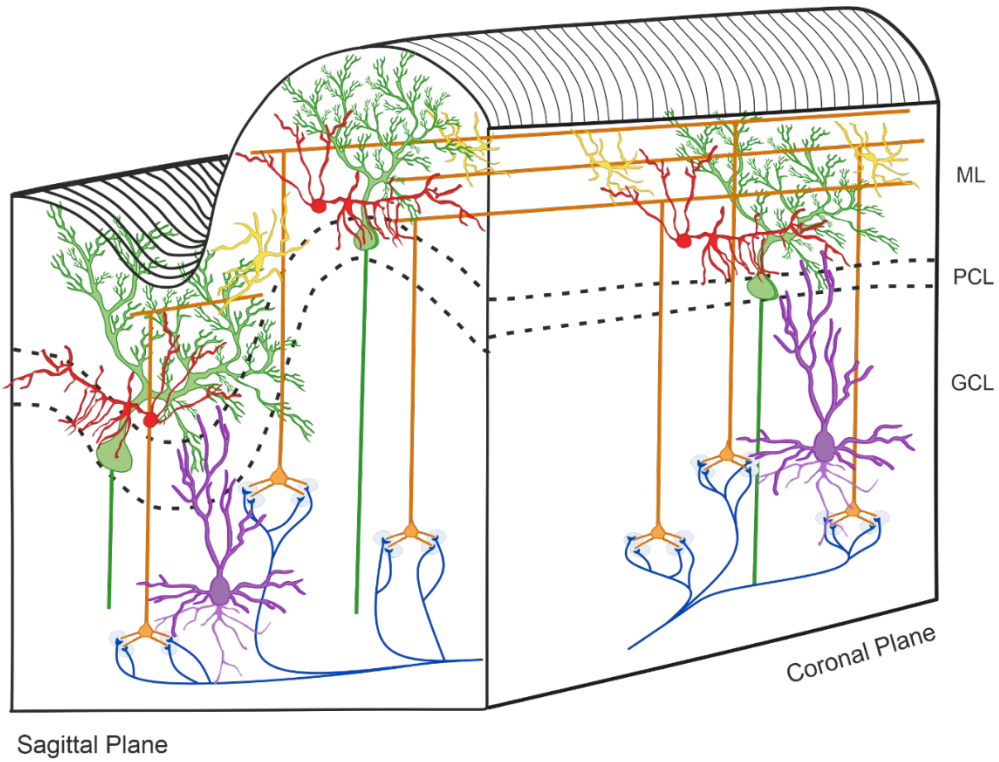

Figure 8: Representation of the cerebellar cortex circuit in sagittal and coronal planes. There are different types of neurons including granule cells (orange), Golgi cells (violet), Purkinje cells (green), stellate and basket cells (yellow, red), Lugaro cells, and unipolar brush cells (not shown). The two main inputs are represented by mossy fibers (blue) originating in various brain stem and spinal cord nuclei, and by climbing fibers originating from the inferior olive (not shown). Signals conveyed through the mossy fibers to the granular layer. The ascending axon of the granule cell bifurcates in the molecular layer forming the parallel fibers. The cerebellar cortical circuit is organized as a feedforward excitatory chain assisted by inhibitory loops: mossy fibers excite granule cells, which activate all the other cortical elements. In the granular layer, inhibition is provided by Golgi cells, in the molecular layer by stellate and basket cells. Finally, Purkinje cells inhibit DCN. The whole system can be seen as a complex mechanism controlling the information processing towards the DCN.

3.6 Conclusions

These findings demonstrated that the use of the HD – MEA technology makes it possible to record extracellular signals correlated with firing frequencies, and provides relevant frequency-dependent evidence about the cerebellar network responses at different frequency ranges. These cerebellar neuronal population data are useful to evaluate the spatiotemporal firing pattern of different neuronal types in the cerebellum. Moreover, the investigations of the spatial and functional organization of the cerebellar circuitry in the sagittal and coronal orientation provide new hints about the role of cerebellar pathways involved in information processing.

The application of computational measurements, like the PCI, is fundamental to understand how the cerebellar cortex complexity changes during different activity states of the network. Here, at the mesoscale level, PCI has no relevance for consciousness, but an ex vivo investigation can contribute to explore the neuronal complexity interactions. This approach can be a confirmation of the complex functionality of the cerebellar well-organized cytoarchitecture. Similar to its role as a “general controller” during movement, the cerebellum has been reported to play important roles in the most sophisticated mental operations (D’Angelo, 2018). The cerebellum might control the synchronization of wave patterns in different brain regions, especially among the midbrain, the thalamus, and the cortex, which contributes to conscious wakefulness (Schmahmann, 2019).

Chapter 4

Modelling of biophysical features of neurons

The biochemical and biophysical characteristics of neurons make these excitable cells highly specialized. Ionic channels and membrane proteins distributed on the neuron's surface are crucial to neuronal activities. Like all other cell types, their cytoplasm is endowed with a sophisticated network of intracellular regulatory systems (Koch and Segev, 2000).

The animal model allows the study of neurons' intrinsic and synaptic properties that cannot be examined in humans, since they cannot be studied due to bioethical limitations (Junhee Seok et al., 2013).

The assumption that the animal model presents similarities with human neurophysiological properties (first deriving from the evolutionary theory) provides the basis to infer human neuronal properties from other vertebrates or mammals, partially overcoming the lack of experimental data on humans. The implementation of computational methods to build accurate models of cells and stimulate their activity in a controlled environment is used to minimize the dependence on animal experimentation and to test properties beyond experimental feasibility. The computational model exploits the

experimental data of animal models to hypothesize and predict brain functionality.

Understanding the dynamics and computations of single neurons and their role within larger neural networks is at the core of neuroscience. Computational models represent advanced methodologies to test hypotheses and theories, and the range of feasible simulations depends on the accessible computational resources and the experimental data to constrain the models. Modeling systems at different scales of complexity can be achieved using one of the multiple available computational methodologies, but it requires even more computational power and experimental data.

Biophysically detailed models reproduce the biological features of real neurons and microcircuits, considering 3D morphology, ion channel gating, and localization. The voltage- and time-dependence of the gating process of membrane ion channels can produce several functional states, such as regular firing, bursting, oscillations, rebounds, and resonance (D'Angelo et al., 2013a). The presence of multiple compartments extends the non-linear effects generated by the gating mechanisms, resulting in local dendritic and axonal computations that integrate with synaptic transmission. Synapses are added as specialized processes that activate receptor-channel models at specific locations. The properties expressed by these neurons can be retrieved in local field potentials (LFPs) that represent the ensemble activity of neuronal populations (D'Angelo and Jirsa, 2022).

The models are used to i) reproduce the electrophysiological properties of a neuron; ii) predict properties that can be used to define newer experimental tests or techniques (Solinas, 2008; Masoli et al., 2015; Masoli and Angelo, 2017) iii) to build networks with millions of neurons connected

with spatial and connectivity rules (Solinas et al., 2010; Lennon et al., 2014); iv) describe properties that are not observable with experiments.

The realistic biophysical modeling approach represents a tool for investigating the inner nature of brain functions and can be used by neuroscientist (Davison, 2012; Markram et al., 2012).

4.1 Top – Down and Bottom-up approach

The complexity of the brain can be studied at different levels of the organization. To create a realistic computational model of the brain and neurons, relevant biological details and biophysical principles are necessary (D'Angelo et al., 2013b). Behaviors that are not added during the construction of the model or during the validation process can be defined as "emerging properties" of the system, which means a prediction that has to be tested and confirmed by experiments.

The brain is organized as a multilevel structure (Figure 11) with functional levels referred to as microscale, mesoscale, and macroscale, and each level has its own complexity that can be investigated through different techniques. The microscale describes the molecular, subcellular, and local microcircuits (D'Angelo and Wheeler-Kingshott, 2017). Experimentally, at the microscale, single-cell properties are analyzed using high-resolution techniques (see *Chapter 2*) that can show intracellular membrane potential and ion concentration changes. In addition to the fundamental relevance of ion channels and receptors, a crucial role is attributed to dendritic integration – a nonlinear process that endows neurons with high-dimensional computational capabilities (Amsalem et al., 2020; Fişek and Häusser, 2020). The mesoscale level represents the interconnected microcircuits

which can be studied with recordings from multiple neurons or neuronal fields providing relevant information regarding the distribution of activity inside local microcircuits. At the macroscale, the function of the large-scale network can be studied using non-invasive techniques even in humans (D'Angelo and Jirsa, 2022). Brain phenomena are analyzed using ensemble recording techniques, including magnetic resonance imaging, fMRI; electroencephalography, EEG; magnetoencephalography, MEG; and positron emission tomography, PET.

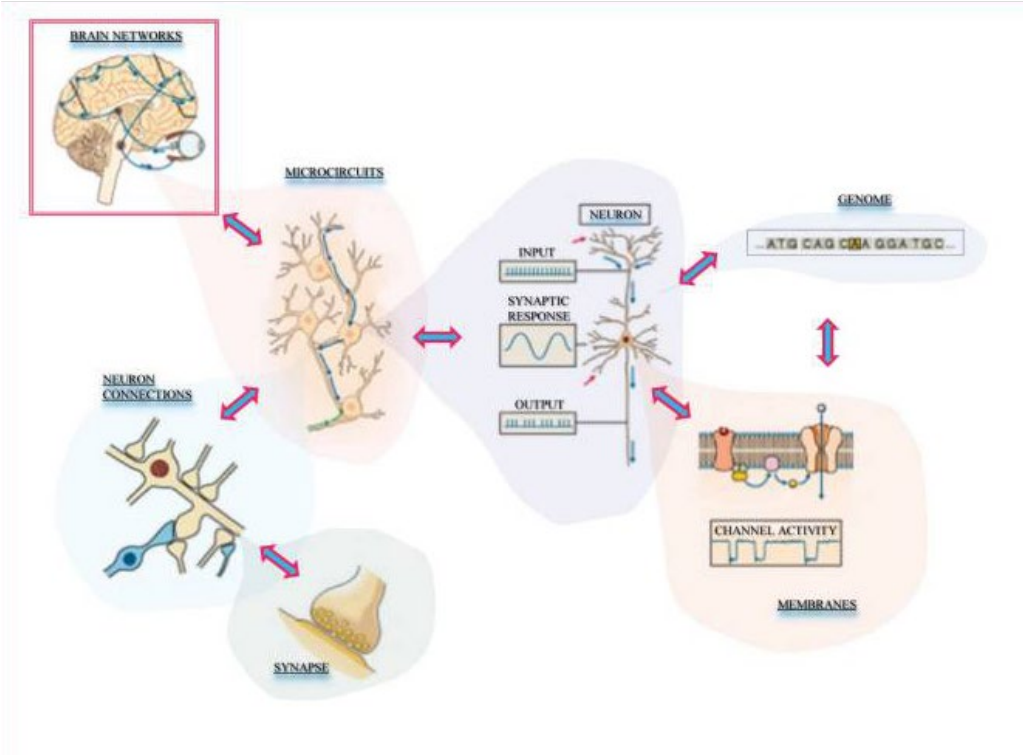

Figure 11: Multilevel organization of the brain. The levels describe different brain functionality from a subcellular resolution that present gene regulation of ion channel and synaptic receptor protein, moving on to single neurons and microcircuits and finally reaching the macroscale resolution in which is represented the complex circuit connection of the whole brain. From D'Angelo et al, 2013.

This multilevel approach rises issues concerning the integration of their large-scale measures with microscopic sources, which can be addressed using multiscale brain modeling, where the properties of one level might predict those of the higher level or can be used to demonstrate the functionality of those in the lower level (D'Angelo and Wheeler-Kingshott, 2017).

Bottom-up approaches have recently received much attention, as opposed to traditional top-down modeling strategies that predict the structure-function relationship of brain circuits with high-level experimental techniques. In fact, the construction of a realistic neuron model is founded on rules of elementary interaction. Top-down approaches are restricted by the brain's excessive complexity, multiscale organization, and overwhelming number of details.

Bottom-up approaches are a good strategy and are essential to create a realistic model of the brain (Angelo et al., 2016). This type of modeling framework has some advantages compared to other approaches: (i) depending on the experimental data availability, it can be implemented with important biological details; (ii) it is possible to monitor all the parameters that can have an impact on the whole system (D'Angelo and Jirsa, 2022); (iii) it can be improved and expanded with new experimental data.

Realistic modeling addresses the common understanding that complexity in biological systems should be utilized rather than rejected (Pellionisz et al., 1977; Jaeger et al., 1997) and can include enough details to generate microcircuit spatiotemporal dynamics and explain them using neuronal and connectivity mechanisms (Brette et al., 2007).

The construction of realistic models follows some steps:

- models of neurons and circuits are *reconstructed*, considering the available experimental data;
- models are *validated* by comparing them with the experimental data;
- models are simulated to see if they can provide *predictions* about functionality that were not originally tested during construction and validation.

To build a multi-compartmental neuron model, it is necessary to have capable software containing specific tools to construct the 3D morphology of neurons with multiple compartments, to characterize the soma, the dendritic, and the axonal trees with their collaterals. The number of compartments depends on the size and morphological resolution of the neuron. In addition, it is possible to implement the connection between every section of the neuron, the location of specific ion channels on the membrane, and the connectivity between the neurons to form a network. The fundamental feature of a model is the simulation of what happens over time. As a result, to determine whether a model is generating the required behaviors, the environment enables accurate simulations when the injection of a current into the soma causes changes in the action potential generation.

NEURON is described as “a simulation environment (Hines et al., 2009; Hines and Carnevale, 2016) for modeling individual neurons and networks of neurons” (http://www.neuron.yale.edu/neuron/). Using the NEURON simulator, it was possible to reconstruct the principal cerebellar neuron types and their synaptic properties (Masoli et al., 2015, 2020b, 2020c; Masoli and Angelo, 2017; Rizza et al., 2021), supported by experimental data for validation. It provides tools for conveniently building, managing, and using models in a way that is numerically sound and computationally efficient. It is particularly well suited to address problems that are closely linked to experimental data, especially those that involve cells with complex anatomical and biophysical properties. The built-in programming language defines every constituent of a model but it is difficult to learn, compared to other script languages. To resolve this problem, the author of NEURON, in 2009, added Python as an optional programming language and now it is the main language for NEURON code development. Python can be described as a general-purpose, interpreted high-level programming language whose design philosophy emphasizes code readability. Its syntax is clear, and expressive, and has a large and comprehensive standard library. Python is a script language, which is highly extendible, simple, and easy to use. Moreover, it takes advantage of the many additional modules like Numpy, Scipy, and Pandas, which permit the management of the mathematical part, to load and save files and analyze the results. The simulator NEURON+Python uses cylindrical sections to define the geometry of neuron morphologies. It can solve the cable equation for the membrane passive currents, and integrate the ionic channels and synaptic currents.

These multicompartmental model and their dendritic processing have been embedded into a network using a Python/NEURON-based code called the brain scaffold builder (BSB) (De Schepper et al., 2022). The

resulting microcircuit model is fine-grained and allows precise reconstruction of local neuronal dynamics, maintaining single neuron and synapse details.

The cerebellar network model can integrate the single neuron biophysical mechanisms with mesoscale functions, allowing the prediction, not only of physiological mechanisms, but of the impact of drugs on the ionic channels and synaptic transmission or of the genetic alteration to membrane ion channels or receptors, explaining how these alterations can change the cerebellar output and can cause ataxia, dystonia, and autism (Peter et al., 2016).

4.2 Conductance based Hodgking and Huxley Model

Hodgkin and Huxley developed a mathematical model to study the activity of ion channels, which were not yet described, in the axon of the giant squid (Hodgkin and Huxley, 1952). They unveiled that the key features were conductance Gi_{max} values able to generate the action potential. The membrane potential is related to currents generated by ion channels distributed along the neuron membrane, and these processes are time and voltage-dependent and are usually represented with the membrane equation, described by the Hodgkin and Huxley (HH) and Markovian or stochastic models (Hodgkin and Huxley, 1952). The study of the mathematical model of action potential in the squid giant axon has allowed to obtain accurate measures of membrane current given by depolarized pulses (Figure 12).

With a system of Ordinary Differential Equations (ODE), the HH model, a conductance-based model, describes the kinetics of single channels and their interaction to generate and propagate action potentials.

Additionally, the model incorporates four currents, Ca^{2+}, K^{+}, Na^{+}, and leakage currents, which are iteratively summed to give a total current, *I,* that predicts the action potential time course (Schwiening, 2012).

The plasmatic membrane and the electrophysiological passive properties can be compared to an electrical equivalent circuit: (i) membrane capacitance (C_m) used to model the charge storage capacity of the membrane; (ii) membrane resistance (R_m), describes as resistors for the various types of ion channels embedded in the membrane; (iii) differential potential is generated between the intra and extracellular space (Vm) describes as batteries to represent the electrochemical potentials established by intra and extracellular ion concentrations. When a current I(t) is injected inside the excitable cell, it flows through the membrane and divides over the capacitor and the conductances. Also, because of the active transport of ions across the membrane, due to the ion pumps, a difference in ion concentration is maintained between the inside and outside of the membrane. The Nerst potential, generated by the concentration difference, is schematized as a voltage generator. The conductance associated with Na^{+} channels and K^{+} channels exhibits a dependence on the membrane potential and, therefore, a nonlinear relationship.

The leak resistance (R) associated with the unspecific channel, which takes into account all other ion channels other than sodium and potassium, has instead a linear or passive relationship, i.e. an independent value of the voltage. When the ion channels are open, they transmit current with a g_{Na}, g_K, and g_l.

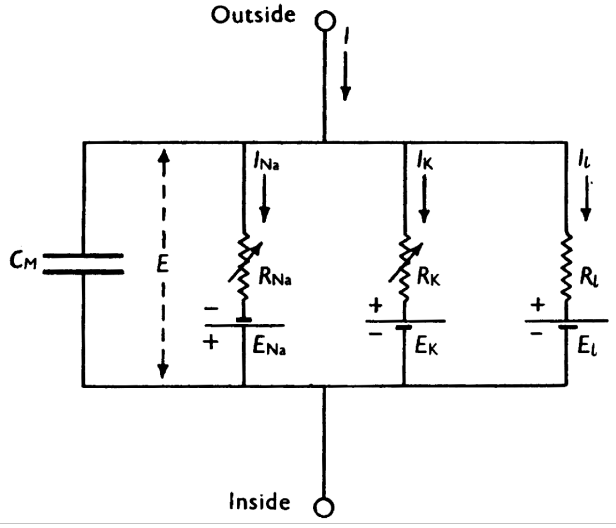

Figure 12: Parallel electrical equivalent circuit. R_{Na} = 1/ g_{Na}, R_K = 1/g_K, R_l = 1/g_l; C_m = membrane capacity. I and E refer to the current (I) and reversal potential (E) of Na^+, K^+, and Leakage. From Hodgkin and Huxley, 1952.

Applying the law of nodes to the circuit in Figure 11, which described the behavior of a portion of the membrane, the current injected I(t) split in a capacity current I_c which charges the capacitor C and further components I_k which pass through the ion channel. Thus:

$$I(t) = I_C(t) + \Sigma\, I_K(t)$$

Where the sum runs all ion channels.

The HH model describes the channel kinetic, which allows the genesis and propagation of an action potential. The presence of different

conductances gK, gNa, and gCl, are indicated for different ions. Each ion presents an equilibrium potential. Therefore, the ionic conductance creates a current that is expressed according to modified Ohm's Law:

$$I = gi(Vm - Ei)$$

where (V_m – E_i) is the driving force.

The HH formulation takes into account the ionic conductances and the activation and inactivation dynamics of the channels. In each compartment, membrane voltage is obtained as the time integral of the equation:

$$dVm/dt = -1/Cm * \{\sum[g_i * (Vm - Ei)] * i_{inj}\}$$

where Vm is the membrane potential, Cm is the membrane capacitance, gi is the ionic conductances, E_i is the reversal potentials and i_{inj} is the injected current.

Ionic conductances are a function of V_m and *t*. According to HH formulation, these are voltage and time-dependent, since each conductance depends on the probability of channel gating. Ion channels can switch between an activated and inactivated state, so ion conductances depend on a value of maximum conductance multiplied by the probability of activation or inactivation:

$$g_i = Gmax_1 * x_i^{zi} * y_i$$

Gating particles are part of a conformational structure of ion channels and control the flow of ions through the channel. When ion flux changes in response to a modification in membrane voltage, the conformational status of the proteins is modified and determines the opening or closing of the

channel. The voltage dependence of gating reflects the energetic properties of the conversion electrochemistry and can be approximated by applying the Boltzmann equation. The channels respond to the change in membrane potential by switching from a closed to a transient open state.

The gating particles of ion channels have activation and inactivation that follows a time constant τ in the order of ms. The pattern of channel opening and closing has two states, C (close) and O (open), and two rate constants, α, and β,

$$C \underset{\beta}{\overset{\alpha}{\leftarrow}} O$$

The time constant (τ) is calculated as:

$$\tau = 1/ (\alpha + \beta)$$

In a neuron, channels have more than two states, and the general rule is that τ is the equal of the reciprocal of the sum of all the rate constants that determine the kinetics of the channels (Eric R. Kandel, 2014; Simms and Zamponi, 2014).

4.3 Additional considerations about limitations of computational modelling

In silico model simulation of a complex system in the form of equations or rules offer significant advantages providing pivotal insights into the mechanism of neuronal processing. Especially, detail models processing morphologically complete dendritic trees, can elucidate the

dendritic processing, as in (Masoli et al., 2020). Furthermore, computational methods limit the use of animal models in research which support the rationale in designing novel, safe drug candidates. Due to the high computational power request for the simulation, detailed models are replaced in neuronal network with simplified neuron models. These reduced models are computationally efficient in particular if used for the simulation of large networks of neurons.

The aim of the computational model is to discover and study the properties that characterize the mechanism of date processing that take place in the brain with a focus on neurons, that have a peculiar ability to communicate by means of voltage propagation.

However, computational modelling presents some limitations and constraints that need to be taken into account, as:

- *Morphology*: the model is reconstructed by detailed branching structure. However, there is no certainty that this represents the same number of compartments of the biological status. In this case the spike waveform can show mismatches compared to the biological asset.
- *Active properties*: while the passive properties reflect the cable theory equation, ion channels and pumps are embedded as *mod file* in the model along the plasma membrane. The opening and closing dynamics of ion channels mimic the biological basis of channel functioning. However, the gating is a complex mechanism and depends on the sensitivity to membrane voltage and to chemical modulator such as neurotransmitters, calcium ions, cyclic nucleotides, and G – proteins that can be represented inaccurately.
- *Synapses*: At the synapses, neurotransmitters are released through a vesicle fusion mechanism activating receptors in the membrane of the receiving neurons. Different neurotransmitters and receptors can

generate a large variety of electrical and metabolic effects on the postsynaptic neurons. The mechanisms regulating neurotransmitter release and receptor activation generate phenomena of short- and long-term plasticity, controlling the temporal dynamics of signal transmission. In models, the finesse of these synaptic mechanism is lacking, in terms of appropriate connectivity rules.

Realistic models obviously lack the instant intuition or any synthetic account of how the brain works, which were the goals of earlier attempts to understand the brain. Such flaws could also result from missing mechanisms, improper connection rules, or erroneous descriptions of synaptic and neural processes. Thus, experimental evaluation is needed for step-by-step validation of realistic models.

Chapter 5

Article II

Cerebellar Golgi cell models predict dendritic processing and mechanisms of synaptic plasticity

Masoli S., Ottaviani A., Casali. S, D'Angelo E.

PLOS Computational Biology 16(12): e1007937. December 2020

https://doi.org/10.1371/journal.pcbi.1007937

PLOS COMPUTATIONAL BIOLOGY

RESEARCH ARTICLE

Cerebellar Golgi cell models predict dendritic processing and mechanisms of synaptic plasticity

Stefano Masoli[1], **Alessandra Ottaviani**[1], **Stefano Casali**[1], **Egidio D'Angelo**[1,2]*

1 Department of Brain and Behavioral Sciences, University of Pavia, Pavia, Italy, **2** Brain Connectivity Center, IRCCS Mondino Foundation, Pavia, Italy

* dangelo@unipv.it

OPEN ACCESS

Citation: Masoli S, Ottaviani A, Casali S, D'Angelo E (2020) Cerebellar Golgi cell models predict dendritic processing and mechanisms of synaptic plasticity. PLoS Comput Biol 16(12): e1007937. https://doi.org/10.1371/journal.pcbi.1007937

Editor: Hermann Cuntz, Ernst-Strungmann-Institut, GERMANY

Received: May 5, 2020

Accepted: November 13, 2020

Published: December 30, 2020

Peer Review History: PLOS recognizes the benefits of transparency in the peer review process; therefore, we enable the publication of all of the content of peer review and author responses alongside final, published articles. The editorial history of this article is available here: https://doi.org/10.1371/journal.pcbi.1007937

Data Availability Statement: The models are available on the Brain Simulation Platform (BSP) of the Human Brain Project (HBP) as a "live paper" containing a selection of routines and optimization scripts and their codebase is uploaded on

Abstract

The Golgi cells are the main inhibitory interneurons of the cerebellar granular layer. Although recent works have highlighted the complexity of their dendritic organization and synaptic inputs, the mechanisms through which these neurons integrate complex input patterns remained unknown. Here we have used 8 detailed morphological reconstructions to develop multicompartmental models of Golgi cells, in which Na, Ca, and K channels were distributed along dendrites, soma, axonal initial segment and axon. The models faithfully reproduced a rich pattern of electrophysiological and pharmacological properties and predicted the operating mechanisms of these neurons. Basal dendrites turned out to be more tightly electrically coupled to the axon initial segment than apical dendrites. During synaptic transmission, parallel fibers caused slow Ca-dependent depolarizations in apical dendrites that boosted the axon initial segment encoder and Na-spike backpropagation into basal dendrites, while inhibitory synapses effectively shunted backpropagating currents. This oriented dendritic processing set up a coincidence detector controlling voltage-dependent NMDA receptor unblock in basal dendrites, which, by regulating local calcium influx, may provide the basis for spike-timing dependent plasticity anticipated by theory.

Author summary

The Golgi cells are the main inhibitory interneurons of the cerebellum granular layer and play a fundamental role in controlling cerebellar processing. However, it was unclear how spikes are processed in the dendrites by specific sets of ionic channels and how they might contribute to integrate synaptic inputs and plasticity. Here we have developed detailed multicompartmental models of Golgi cells that faithfully reproduced a large set of experimental findings and revealed the nature of signal interchange between dendrites and axo-somatic compartments. A main prediction of the models is that synaptic activation of apical dendrites can effectively trigger spike generation in the axonal initial segment followed by rapid spike backpropagation into basal dendrites. Here, incoming mossy fiber inputs and backpropagating spikes regulate the voltage-dependent unblock of NMDA channels and the induction of spike timing-dependent plasticity (STDP). STDP, which was

ModelDB: https://senselab.med.yale.edu/modeldb/ShowModel?model=266806#tabs-1.

Funding: This research was supported by the European Union's Horizon 2020 Framework Programme for Research and Innovation under the Specific Grant Agreement No. 785907 (Human Brain Project SGA2) to ED. This research was also supported by the MNL Project "Local Neuronal Microcircuits" of the Centro Fermi (Rome, Italy) to ED. Model optimizations and simulations were performed on the Piz Daint supercomputer (CSCS – Lugano) with a specific grant (special proposal 03) to ED&SM and using computing resources provided through the PRACE Project 2018184373 to ED&SM. The funders had no role in study design, data collection and analysis, decision to publish, or preparation of the manuscript.

Competing interests: The authors have declared that no competing interests exist.

predicted by theory, may therefore be controlled by contextual information provided by parallel fibers and integrated in apical dendrites, supporting the view that spike timing is fundamental to control synaptic plasticity at the cerebellar input stage.

Introduction

The cerebellar Golgi cell [1–3] is the principal inhibitory interneuron of the cerebellar granular layer [4] and is supposed to play a critical role for spatio-temporal reconfiguration of incoming inputs by regulating neurotransmission and synaptic plasticity along the mossy fiber–granule cell pathway [5–7]. Golgi cells are wired in feed-forward and feed-back loops with granule cells and form a functional syncytium through gap junctions [8]. The excitatory inputs are conveyed by mossy fibers and granule cell ascending axons on the basal dendrites and by parallel fibers on the apical dendrites [9]. The inhibitory inputs come from other Golgi cells [10] and from Lugaro cells [11,12]. The Golgi cells eventually inhibit large fields of granule cells through an extended axonal plexus. Fundamental issues that remain unexplored are how synaptic inputs control Golgi cell spike generation and whether dendritic processing provides the basis for spike-timing dependent plasticity (STDP), which has been predicted by theory [13]. Interestingly, mossy fiber–Golgi cell synapses express NMDA channels (fundamental for synaptic plasticity) at mossy fiber synapses [9] and the dendrites express a diversified set of Ca, Na and K ionic channels [14] that could impact on dendritic computation. A prediction about the possible interactions of these multiple active properties is quite hard and requires a detailed computational analysis of the electrogenic architecture of the neuron and of synaptic integration.

The complement of Golgi cell ionic channels was initially determined with somatic whole-cell recordings using bath-applied pharmacological blockers [15]. In the absence of more detailed information, an initial computational model assumed that Golgi cell intrinsic electroresponsiveness could be generated by active properties concentrated in the soma, while a passive dendritic tree was used to balance the electrotonic load[16,17]. That same model, once reimplemented into a realistic morphology, was used to test electrical transmission through gap junctions in Golgi cell pairs [8]. But since then, the discovery of active dendritic properties [14] and of the complexity of Golgi cell wiring in the local microcircuit [9,10] has changed the perspective. In order to get insight on how this neuron might work based on the interaction of its membrane and synaptic mechanisms, we have developed realistic computational models of Golgi cells based on detailed morphological reconstructions and on the new electrophysiological and immunohistochemical data that have become available about the properties of dendrites and synapses. The new models, further than faithfully reproducing the rich pattern of Golgi cell electrophysiological responses recorded *in vitro* and *in vivo*, provided testable predictions for dendritic processing, synaptic integration and STDP. Interestingly, NMDA receptor-dependent STDP in basal dendrites turned out to be controlled by information provided by parallel fibers and integrated in apical dendrites, suggesting the way spike timing might supervise synaptic plasticity at the cerebellar input stage.

Results

We have reconstructed, optimized and simulated 8 multicompartmental GoC models based on detailed morphologies obtained from mouse cerebellum (Figs 1A and S1). The voltage dependent ionic channels were distributed over the entire neuronal structure, based on indications derived from electrophysiology and immunostaining [14], generating models with active

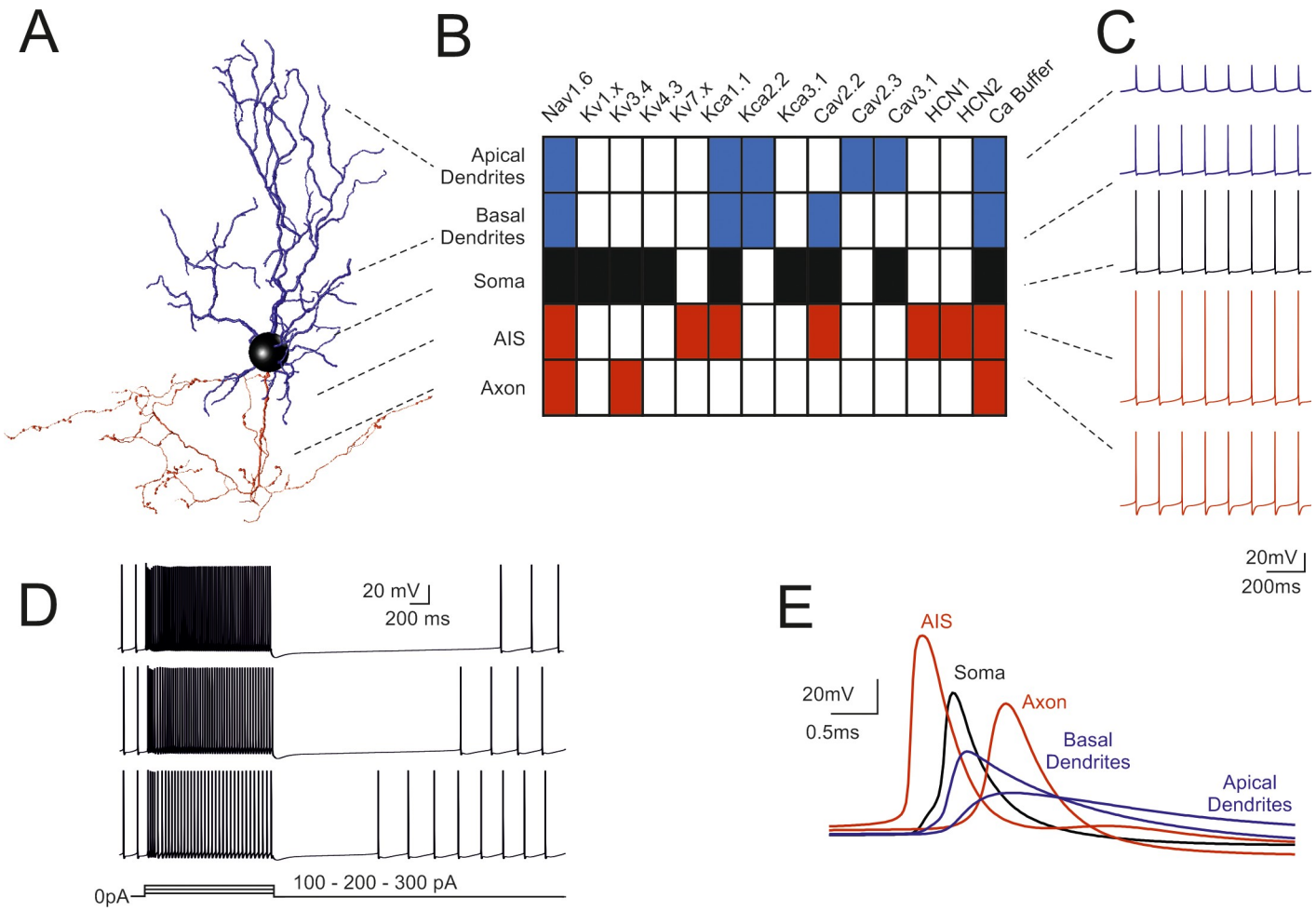

Fig 1. Fundamental electroresponsiveness in a multicompartmental Golgi cell model. (A) 3D morphological reconstruction of a GoC [from [19]] including dendrites (blue), soma (black), axonal initial segment and axon (red). The apical dendrites where distinguished based on their projection into the molecular layer (ML), while basal dendrites remained in the granular layer (GL). (B) Localization of ionic channels in the different model sections according to immunohistochemical, electrophysiological and pharmacological data. (C) Spikes during pacemaking in the different sectors indicated in B. Note the strong spike reduction in apical GoC dendrites but the effective backpropagation into basal dendrites. (D) Responses to 100-200-300 pA step current injections in the model. (E) Spikes (taken from C) on expanded time scale. Note that spikes are generated in the AIS and then propagate with increasing delay to soma, axon, basal and apical dendrites. In this latter, spikelets are severely delayed, reduced and slowed down. When not otherwise specified, examples in the next figures will be taken from this same Golgi cell model.

https://doi.org/10.1371/journal.pcbi.1007937.g001

properties in dendrites, soma, axonal initial segment (AIS) and axon. The ionic channel subtypes, their distribution over the compartments belonging to the same section (Fig 1B), their maximum conductance ranges, as well as the spike features used as template, were the same for the 8 Golgi cell models. The models were tuned through automatic optimization of maximum conductance values based on a genetic algorithm, while targeting an electrophysiological template (see Materials and Methods), and were carefully validated against a wealth of experimental data. All the models were autorhythmic (Fig 2C) and current injection (0.1nA to 0.5nA) increased the firing rate (Fig 2D). During the current steps, spike discharge showed frequency adaptation. At the end of the steps, membrane potential showed a hyperpolarization followed by a pause in spike firing. These properties resembled those observed experimentally [15].

The action potentials were generated in the AIS with forward propagation in the axon and back-propagation in the soma and dendrites (Fig 1E). Axonal invasion took about 1 ms

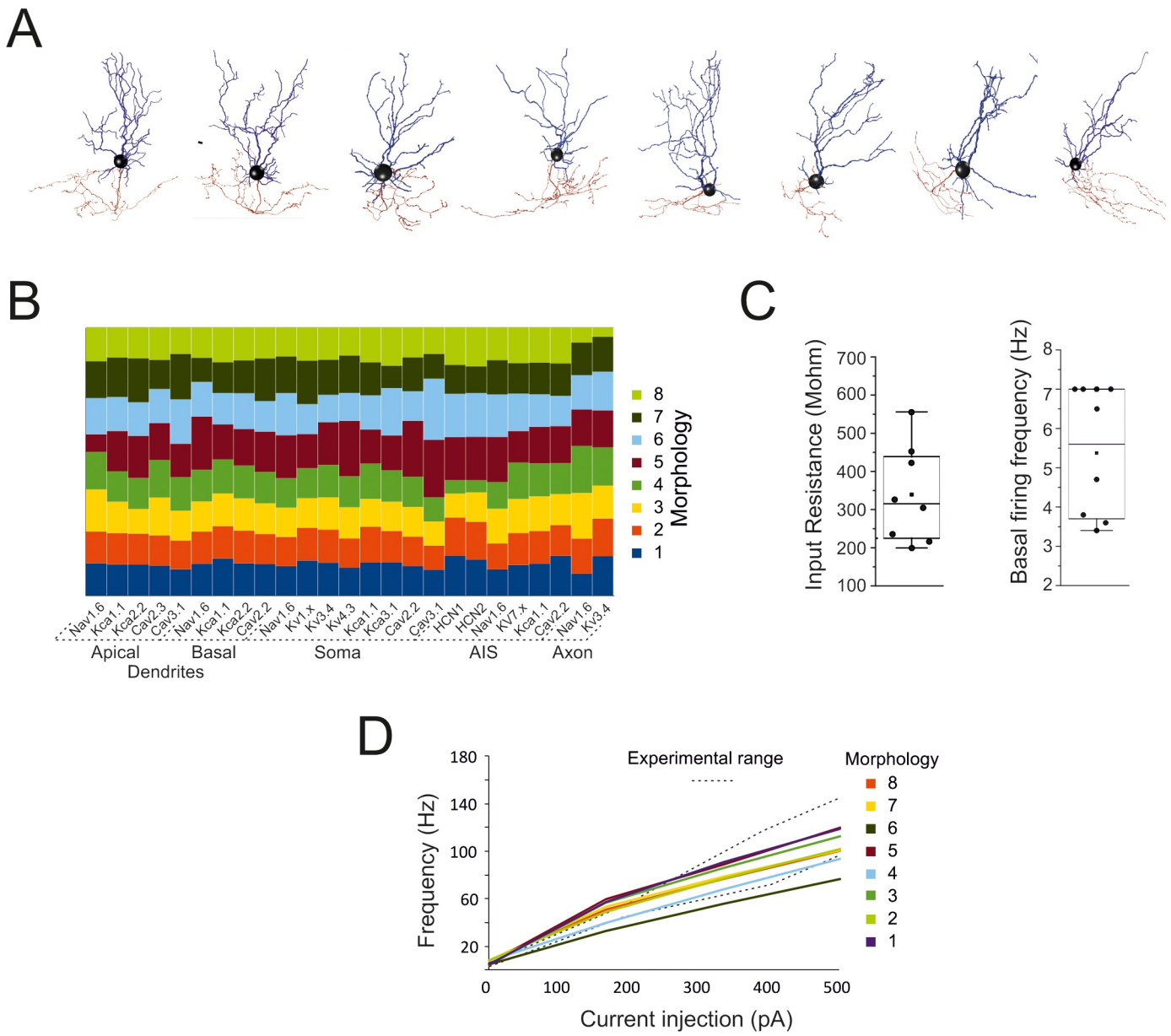

Fig 2. Quantitative aspects of Golgi cell models. (A) The morphologies of the 8 Golgi cells used for modeling. (B) The table shows the balance of maximum ionic channel conductances in the 8 GoC models, demonstrating their similarity. (C) The box-and-whiskers plots show the distribution of input resistance (measured from current transients elicited by 100 ms steps from -70m to– 80 mV in the soma) and basal firing frequency. (D) Frequency-intensity curves for the 8 GoC models compared to the experimental range [dotted lines from [15]]. The same color code is used for the cells in B and D.

https://doi.org/10.1371/journal.pcbi.1007937.g002

according to experimental delay times in the Golgi cell—granule cell circuit [18], while dendritic back-propagation occurred in about 0.5 ms. Backpropagating spikes were 50–80% of AIS size in the basal dendrites but were severely reduced to 10–20% of AIS size in the apical dendrites, as expected from the differential distribution of Na channels anticipated by [14].

Intrinsic model electroresponsiveness with somatic current injection

Following parameter optimization and validation, all the models behaved as typical Golgi cells and showed minor differences in the maximum ionic conductance values (Fig 2A and 2B),

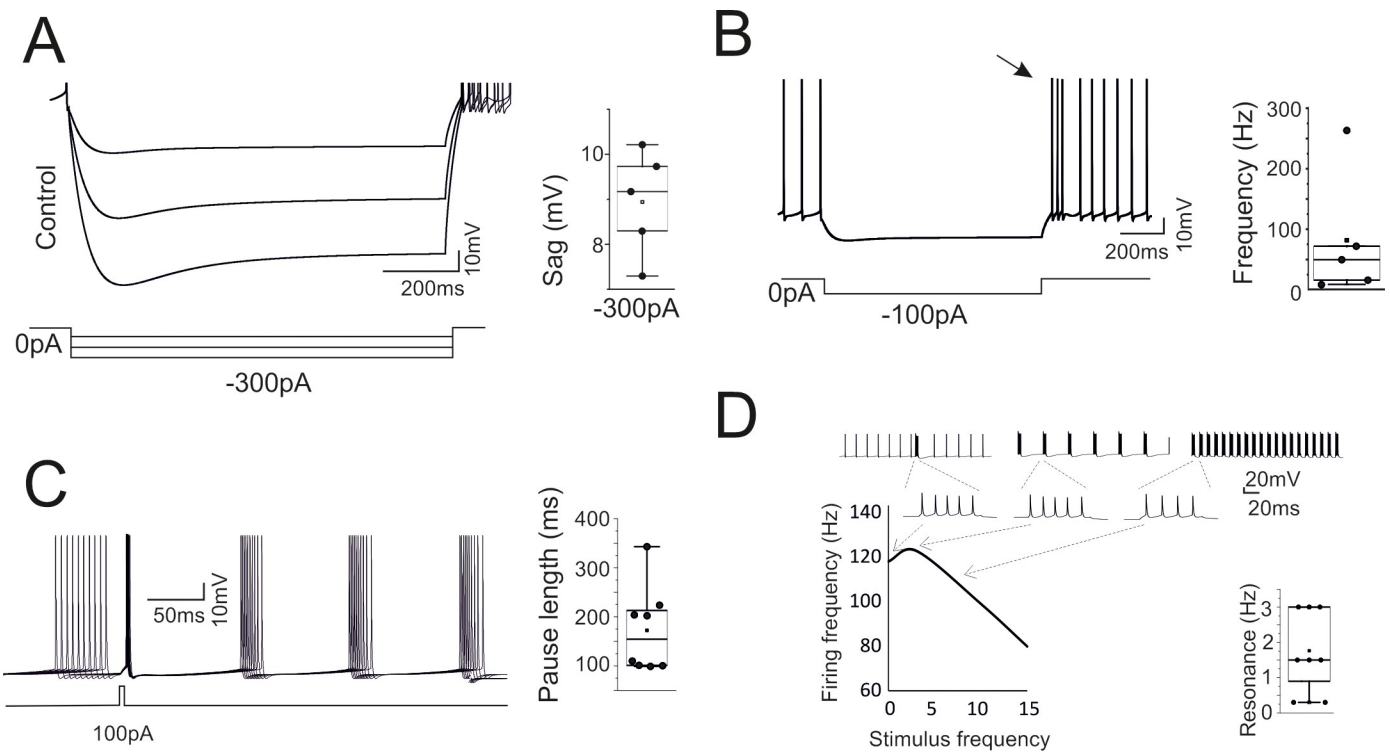

Fig 3. High level model validation: sags, rebounds, phase-reset and resonance. The model was simulated in operating conditions capable of revealing typical GoC behaviors not considered for model construction. (A) Response to hyperpolarizing currents. The model generates sagging hyperpolarization. The box-and-whiskers plot shows sag amplitude in the 8 models. (B) Return to resting activity following hyperpolarizing currents. The model transiently generates a rebound burst (arrow). The box-and-whiskers plot shows burst frequency in the 8 models. (C) Responses following a depolarizing current pulse. The model shows phase-reset. The box-and-whiskers plot shows the pause length in the 8 models. (D) Responses following injection of current steps at different frequencies. The model shows resonance of output spike frequency. The traces illustrate the resonance protocol and an enlargement of the spike bursts used for measuring the output frequency. The box-and-whiskers plot shows resonance frequency in the 8 models.

https://doi.org/10.1371/journal.pcbi.1007937.g003

demonstrating that individual cell morphology did not impact remarkably on physiological properties (S2 Fig).

In the Golgi cell models, the average input resistance was 339.3 ± 128.3 MΩ (n = 8 models) and spontaneous firing frequency was at 5.4±1.7 Hz (n = 8 models) (Fig 2C). The frequency / current relationship was almost linear in a range up to ~100 Hz (Fig 2D).

While the properties reported in Fig 2 were counter checked during the optimization process (the models that did not comply with the reference parameters were eliminated), a more extended set of electroresponsive properties typical of the Golgi cells [15,20] emerged providing an important proof for model validation. A *sag* of 5–8 mV was elicited during negative current injection (Fig 3A). *Rebound bursting* was elicited on return to rest from a hyperpolarized potential (Fig 3B). *Phase-reset* occurred following a brief current pulse injection (Fig 3C). *Resonance* emerged by challenging the model with repetitive current steps (repetition frequency 1–15 Hz), which caused a preferential response at low frequency (1–4 Hz) (Fig 3D). that were previously remapped onto specific ionic channels [16,17]: phase reset was related to calcium entry and the subsequent activation of Kca2.2 channels, the length of the interspike interval was modulated by the H current, rebound bursts were generated by low-threshold Ca channels, resonance depended on Kv7.x. Therefore, the information extracted from the template was sufficient to optimize the ionic conductance balance toward properties beyond those directly assessed during model construction.

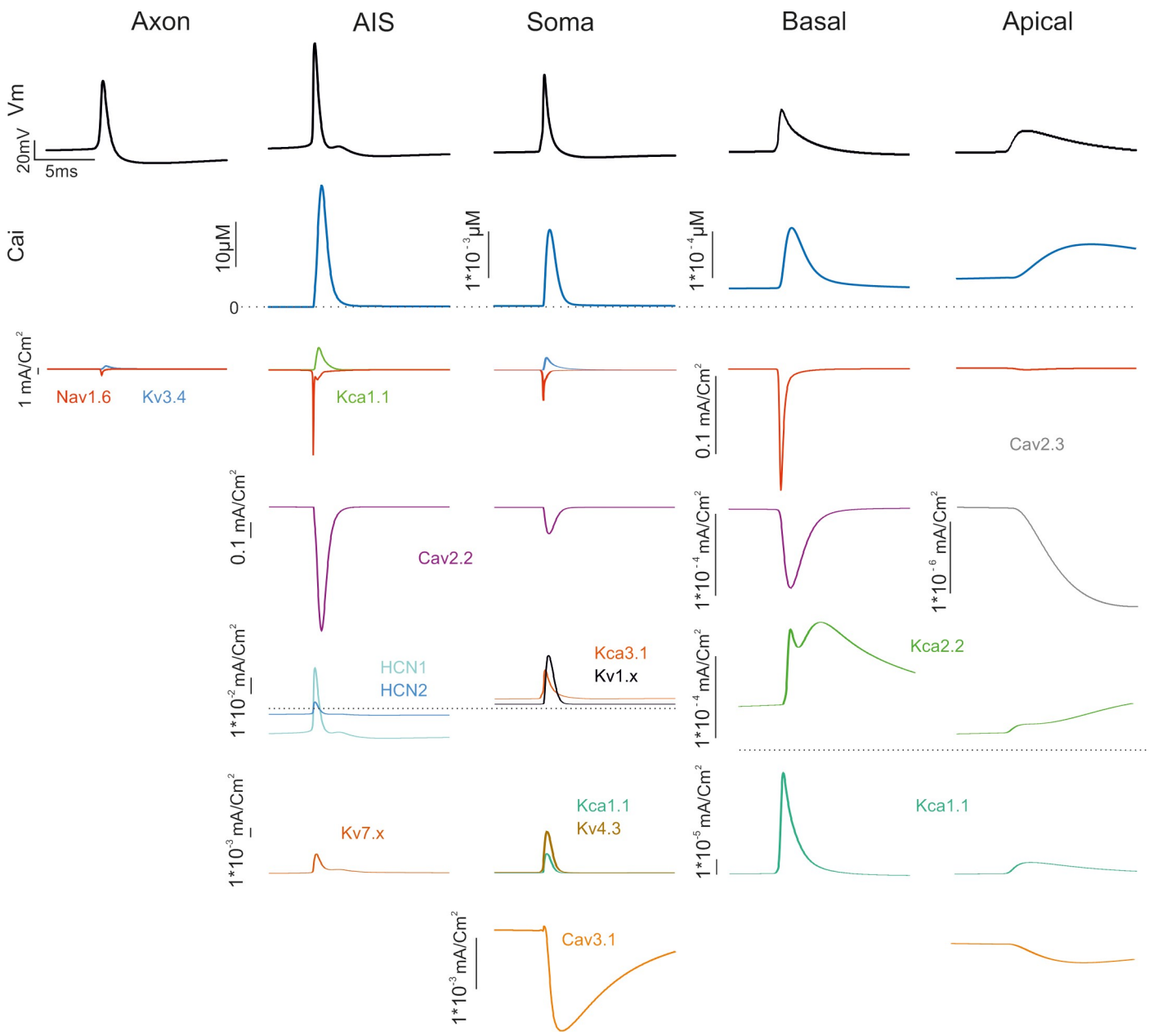

Fig 4. Ionic currents in model sections. The figure shows the ionic currents and calcium concentration changes generated by membrane channels in the GoC model when a spike occurs during autorhythmic firing. Note the localization of channels in different sections and the different calibration scales.

https://doi.org/10.1371/journal.pcbi.1007937.g004

Ionic currents in different model compartments

The ionic currents generated in the different Golgi cell model compartments are illustrated in Fig 4. While the distribution of ionic channels was constrained by immunohistochemistry, electrophysiology and pharmacology, the maximum ionic conductances were the true unknown of the models and were set through automatic parameter optimization. These values eventually determined the ionic current densities shown in Fig 4.

AIS and soma. The AIS, in addition to sodium channels (Nav1.6), also hosted high-threshold calcium channels, potassium channels and H channels (Cav2.2, Kca1.1, HCN1/ HCN2,

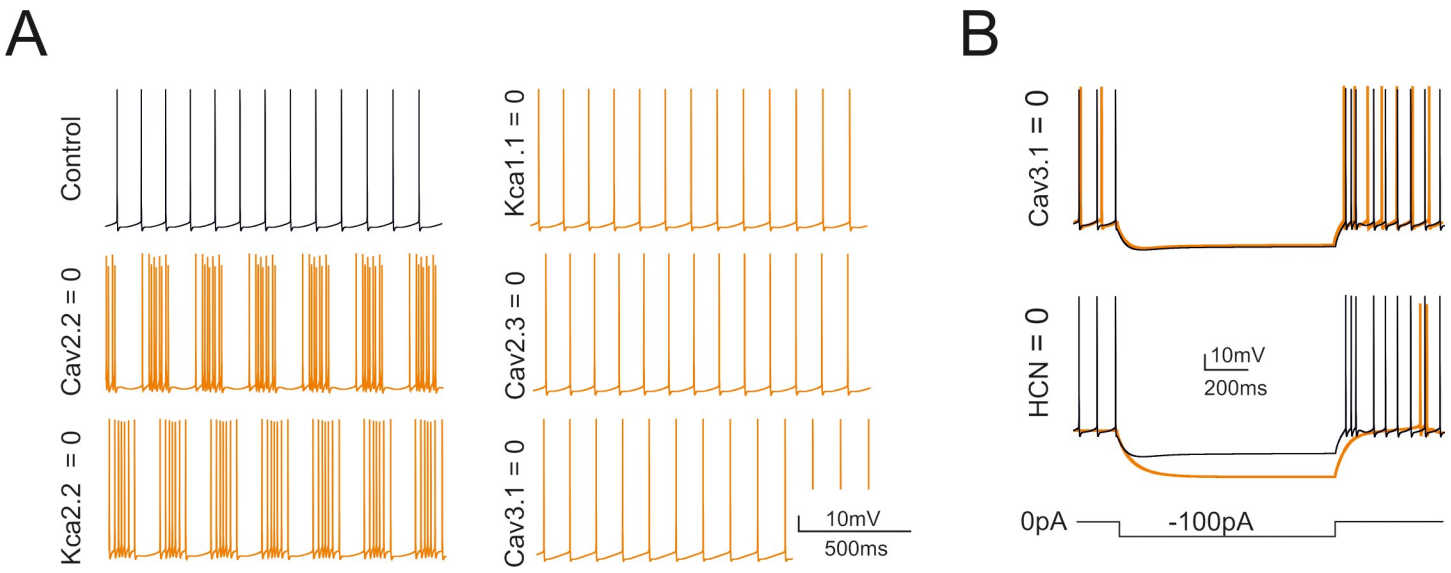

Fig 5. Selective switch-off of ionic mechanisms. Counter-testing of the GoC model obtained by switch-off of ionic channels in specific model sections. (A) Effect on basal firing of the switch-off of Cav2.2, Kca2.2, Kca1.1, Cav2.3, Cav3.1. These simulations imitate the experiments on pharmacological block reported in [14]. (B) Effect on the responses to negative currents steps (during the step and in the rebound phase) of the switch-off of HCN (HCN1 and HCN2) and Cav3.1.

https://doi.org/10.1371/journal.pcbi.1007937.g005

Kv7.x). The soma hosted sodium channels (Nav1.6), high-threshold and low-threshold calcium channels (Cav2.2, Cav3.1) and various potassium channels (Kca1.x, Kca3.1, Kv3.4). The AIS Na current proved critical for action potential generation [21] and had a 3 times higher density compared to soma (13.5 mA/cm^2 vs. 4.5 mA/cm^2). The Cav2.2 channels were also expressed in AIS and caused the intracellular calcium concentration $[Ca^{2+}]_i$ to reach levels 3 times higher than in the soma. This peculiar phenomenon was also observed in Cartwheel neurons of the Cochlear Nucleus and in cerebral cortex L5 Pyramidal cells [22,23]. The main effect of the calcium current and of the associated $[Ca^{2+}]_i$ increase was to activate Kca1.1 and Kca3.1 and to regulate action potential generation along with the voltage-dependent K current Kv3.4. HCN1 and HCN2 increased the action potential threshold and regulated the pacemaker cycle, while Kv7.x was critical for resonance as anticipated by [16,17].

Dendrites. The basal and apical dendrites hosted, in addition to a low density of sodium channels (Nav1.6), a repertoire of calcium channels (Cav2.2, Cav2.3, Cav3.1) and calcium-dependent potassium channels (Kca2.2). These currents sustained spike backpropagation, which was much more effective in the basal than apical dendrites.

Selective switch-off of ionic currents in the model

The impact of ionic channels on spontaneous firing was evaluated by selective switch-off imitating pharmacological blockade [14,15] (Fig 5). The switch-off of the main calcium current (Cav2.2) uncovered oscillatory bursting at 4-5Hz. A similar oscillatory bursting was seen with the switch-off of Kca2.2 in apical and basal dendrites, indicating that the main effect of Cav2.2 was to control Kca2.2. The switch-off of Cav2.3 had no visible impact on spontaneous firing. The switch-off of Kca1.1 and Cav3.1 caused just a slight increase in spontaneous firing frequency. As a whole, during spontaneous activity, the apical dendrites ionic channels showed little involvement. The switch-off of HCN1 and HCN2 abolished the sag and reduced spontaneous firing frequency to 2.2 ±2.1 Hz (n = 8). The switch-off of Cav3.1 in the apical and the somatic sections abolished rebound bursts. All these tests were in good matching with

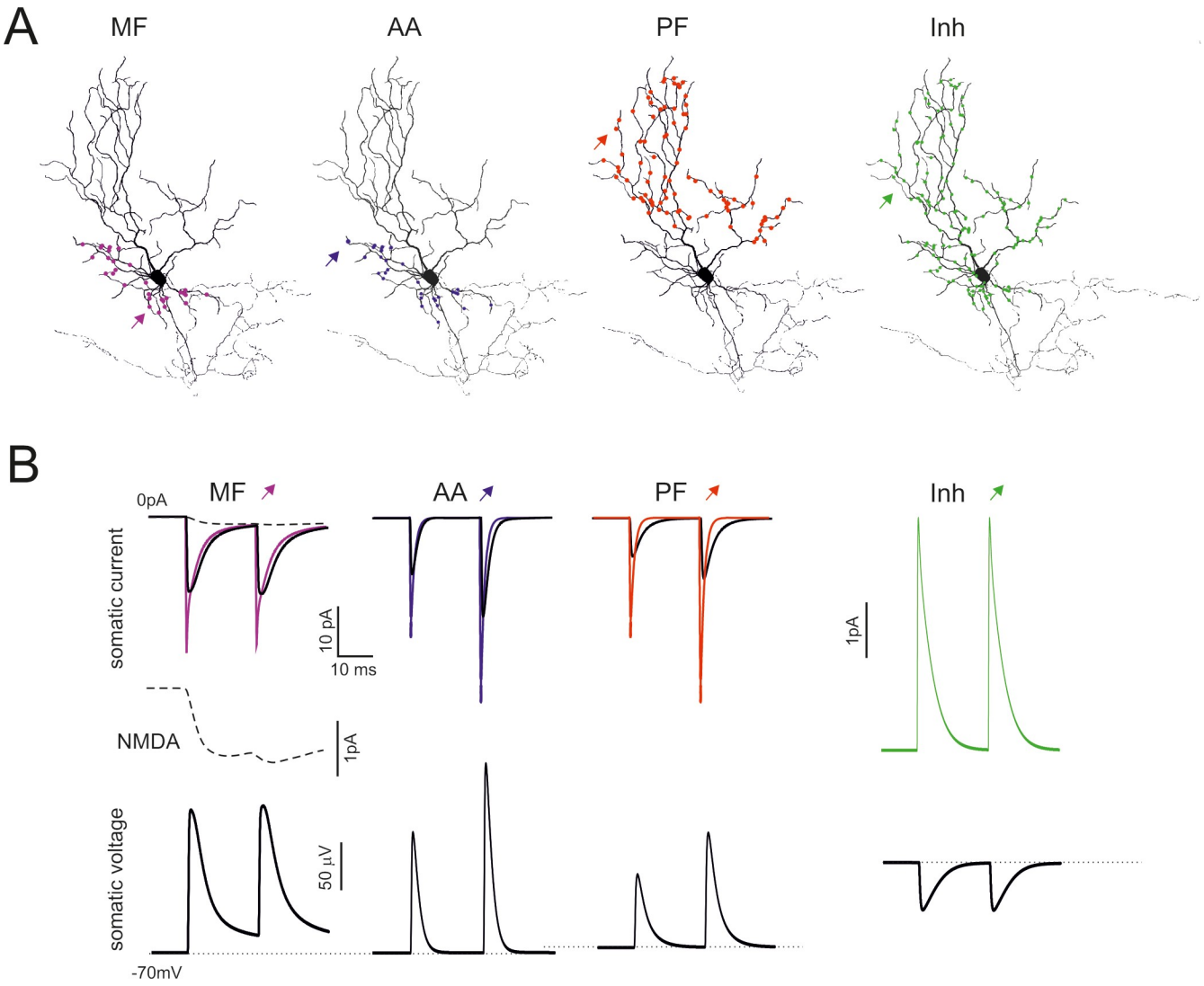

Fig 6. Model responses to synaptic inputs. (A) The figure shows the localization of mossy fibers (MF), ascending axon (AA), parallel fiber (PF), and inhibitory (Inh) synapses. (B) Synaptic currents generated by single MF, AA, PF and Inh synapses. The thin line is the current generated at the synaptic site, the thin line is the current recorded in the soma. The dashed line is the NMDA current. The corresponding EPSPs and IPSPs are reported at the bottom. In all cases the responses are elicited by a stimulus pair at 50 Hz.

https://doi.org/10.1371/journal.pcbi.1007937.g006

pharmacological experiments [14,15] and provided a strong support to model validation by showing that the ionic maximum conductances set through automatic optimization were mechanistically related to the main functional properties of the Golgi cell.

Synaptic properties of the Golgi cell model

The implications of dendritic processing were analyzed by using realistic representations of synaptic transmission, including presynaptic release dynamics of vesicle cycling, neurotransmitter diffusion and postsynaptic receptors activation (see [24–28]. The models were endowed with parallel fiber, ascending axon and mossy fiber synapses using information taken from literature [9] (Fig 6A). The parallel fiber on apical dendrites and ascending axon on apical and basal dendrites were facilitating (paired pulse ratio, PPR>1) and were endowed with AMPA

receptors. The mossy fiber on the basal dendrites, at least 20μm away from the soma, were neither facilitating nor depressing (paired pulse ratio, PPR = 1) and were endowed with AMPA receptors and NMDA NR2B receptors. The basal dendrites received GABA-A receptor-mediated inputs (Fig 6A). The only part of the neuron devoid of synapses was the dendritic trunk hiding in the PC layer.

Unitary EPSCs at their generation site had fast kinetics but the EPSCs were reduced in amplitude and slowed down when seen from the soma, as expected from electrotonic decay along the dendrites (Fig 6B). The EPSCs generated on apical dendrites were more heavily filtered than those generated on basal dendrites. Moreover, mossy fiber EPSCs had a small but sizeable NMDA current component. In aggregate, the simulations confirmed the interpretation of experimental EPSC properties [9]. Unitary IPSCs were also similar to those reported experimentally [10]. The unitary EPSCs and IPSCs had small size (10 pA range at -70 mV) and generated comparatively small voltage deflections with PPR resembling that of the EPSCs and IPSCs (Fig 6B). The ascending axon EPSPs were faster than parallel fiber EPSPs but slower that mossy fiber EPSP, whose kinetics were protracted by the NMDA current.

The efficiency of synaptic activation

While the picture shown in Fig 7B is a direct reflection of the known EPSC properties and dendritic filtering, the synaptic response is expected to change when the number of synapses increases and EPSPs grow enough to engage dendritic voltage-dependent mechanisms (Fig 8A). In order to predict the efficiency of spatial integration over the different input channels, the model was stimulated with an increasing number of synchronous synaptic inputs. The mossy fiber, ascending axon and parallel fiber inputs required the simultaneous activation of 2–3 synapses to generate a spike, supporting the ability of the GoC models to integrate synaptic inputs with high efficiency.

When the model was stimulated with a short burst (5 spikes@100Hz) delivered either through the mossy fibers (20 synapses), the ascending axon (20 synapses), the parallel fibers (89 synapses), all the three excitatory inputs generated a short spike burst followed by a pause that effectively reset the pacemaker cycle (cf. the PSTHs in Figs 7B and 3C) (S1–S3 Videos). Synaptic inhibition delivered in correspondence with the excitatory burst (20 synapses) reduced the number of emitted spikes but did not impact remarkably on the pause length (Fig 7C). The effect of inhibition on the number of emitted spikes and of the subsequent pause depended on the number of excitatory synapse and was poorly sensitive to the relative excitation/inhibition phase in the ±10 ms range (Fig 7D). These response patterns resembled those observed *in vivo* following punctuate facial stimulation [29].

Active dendritic currents during synaptic transmission

The results reported above suggest that dendritic excitation in Golgi cells is rather complex. First, given the differential density of Na channels, the basal dendrites show a more efficient spike backpropagation than the apical dendrites (Fig 1C and 1D). Secondly, Ca channels are localized differentially (Fig 1B), with high-threshold Ca channels (Cav2.2) located in basal dendrites (as well as in soma and initial segment) and low-threshold Ca channels (Cav3.1) located in distal dendrites (as well as in soma). We thought these factors could reverberate into an asymmetric dendritic excitation during synaptic transmission.

Fig 8 illustrates the underlying ionic mechanisms and Ca transients. Local spikes in basal dendrites were associated with rapid calcium transients, which were sustained by Cav2.2 and traversed the μM range. Excitation propagating to apical dendrites was slowly integrated by Cav3.1 activation causing Ca spikelets raiding a prolonged calcium wave. The slow local

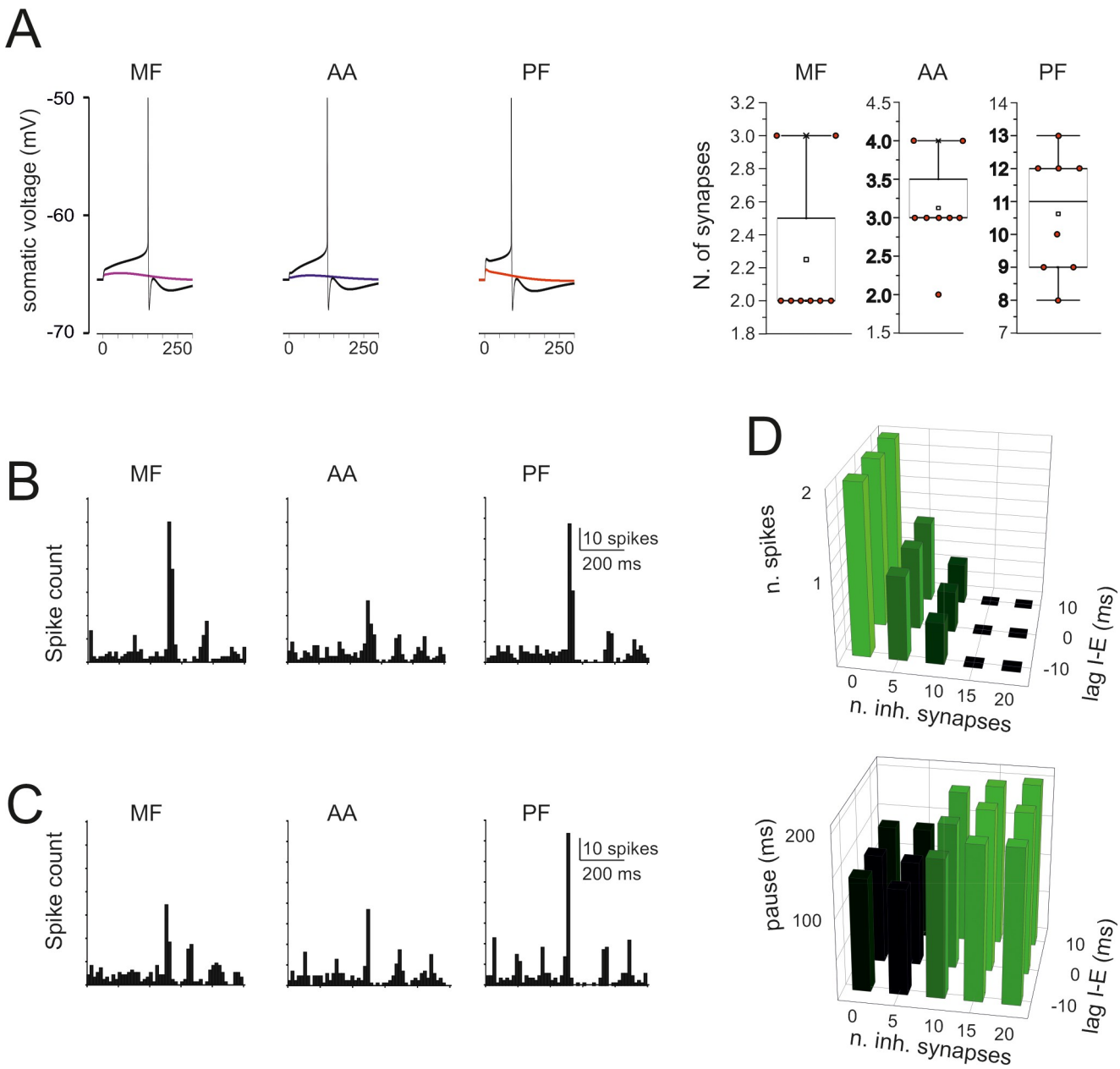

Fig 7. Simulations of synaptic excitation and inhibition. (A) The traces show spikes elicited by a single stimulus on 2 MF, 3 AA, and 12 PFs. The number of synapses that need to the activated simultaneously in order to elicit a spike is shown in the box-and-whiskers plots, which report the effect of stimuli delivered after switch-off of pacemaking with a small negative current. (B) PSTH of responses elicited by a short train (5 impulses @100 Hz) to 20 MF, 20 AA, and 89 PF synapses. Note that the response bursts are followed by a pause (corresponding to phase-reset). (C) PSTH of responses elicited by a short train (5 impulses @100 Hz) to 20 MF, 20 AA, and 89 PF synapses plus 20 inhibitory synapses activated 10 ms after the excitatory input. Note that the decrease of response bursts compared to B. (D) Number of spikes and pause length as a function of the number of inhibitory synapse and of the lag of inhibition with respect to excitation.

https://doi.org/10.1371/journal.pcbi.1007937.g007

depolarization in apical dendrites was associated with a massive calcium wave sustained by Cav3.1 and traversing the μM range. The major repolarizing role was sustained by small-K channels (KCa2.2) in apical dendrites, which outperformed big-K channels (KCa1.1) by almost one order of magnitude. These simulations support the conclusion that dendritic processing in Golgi cells is markedly asymmetric.

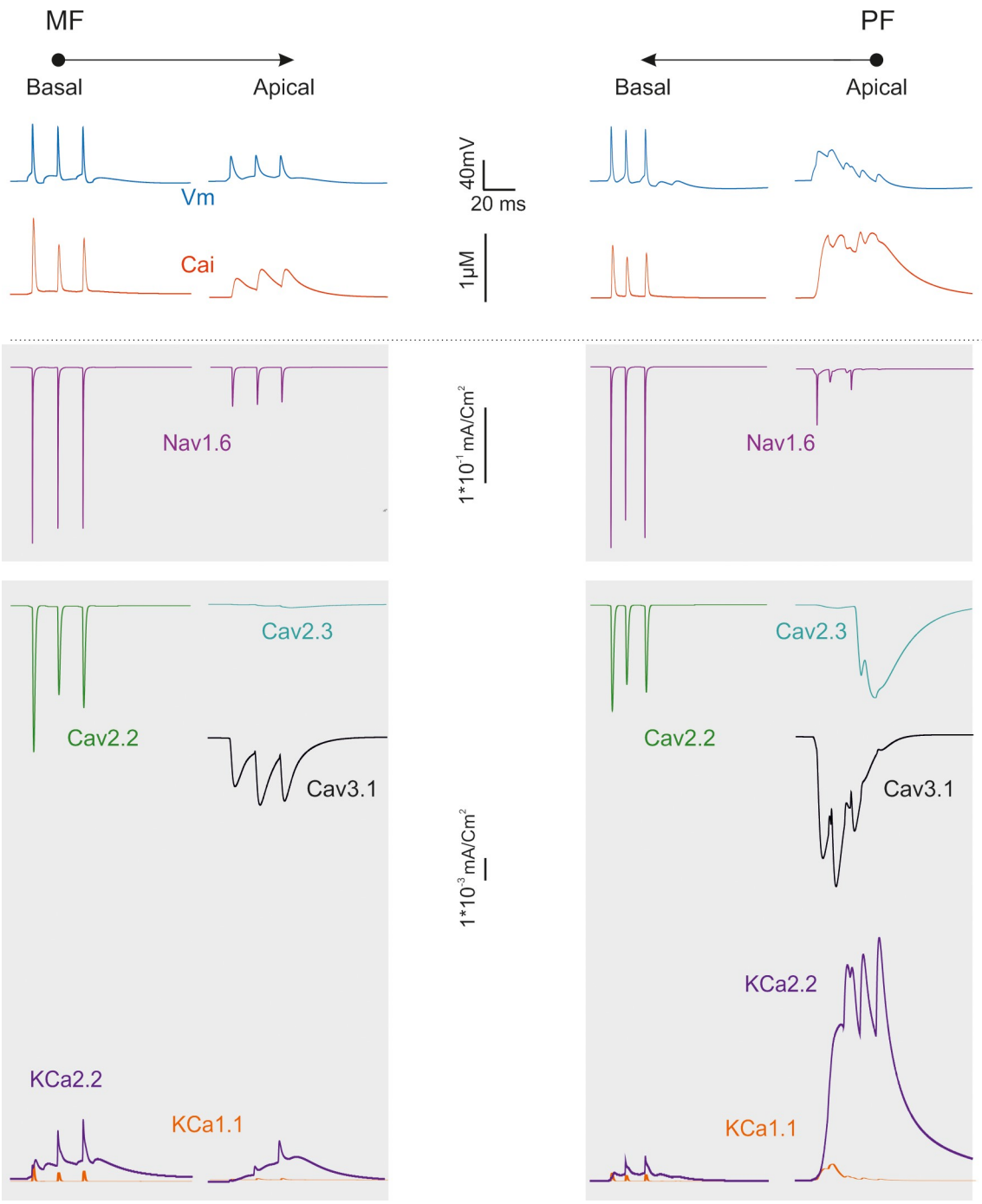

Fig 8. Ionic current in the dendrites during synaptic transmission. The traces show the ionic currents and intracellular calcium concentration changes elicited by activation of a short bursts of synaptic activity in either MFs in basal dendrites or PFs in apical dendrites.

https://doi.org/10.1371/journal.pcbi.1007937.g008

Prediction of coincidence detection and STDP between parallel fiber and mossy fiber activity

Golgi cell dendritic processing would be much enriched by considering the interaction of inputs occurring on basal and apical dendrites (an analogous case has been investigated in

pyramidal neurons; [30,31]. Given the complexity of the synaptic input-output (I/O) space (e.g. see S4 Fig), the interaction between basal and apical dendrites is illustrated for the case of short bursts (5 spikes@100Hz) delivered either through mossy fibers (20 synapses), parallel fibers (89 synapses) or both (Fig 9A). Mossy fiber stimulation on basal dendrites determined rapid synaptic currents that were transmitted to AIS. AIS generated spikes, which travelled back to the basal dendrites and partially to the apical dendrites. Parallel fiber stimulation on apical dendrites activated slow local currents that were transmitted to AIS generating spikes, which travelled back to the basal dendrites and at a much lesser extent to the apical dendrites. Joint mossy fiber and parallel fiber stimulation improved AIS activation generating again a robust backpropagation into basal dendrites. Finally, inhibition severely impaired both spike generation and dendritic backpropagation.

The electrogenic architecture of GoCs revealed by simulations suggested that dendritic processing could implement a coincidence detector driving spike-timing dependent plasticity (STDP) [32,33]. Fig 9B shows the effect of phase-correlated parallel fiber and mossy fiber inputs. When a parallel fiber input precedes a mossy fiber input, this latter falls in the AHP region of the backpropagating spike. The NMDA channels do not unblock (Fig 9C) and the associated Ca influx is small. This would result in LTD. When a parallel fiber input follows a mossy fiber input, this latter intercepts the upstroke of the backpropagating spike. NMDA channels unblock (Fig 9C) raising the associated Ca influx considerably. This would result in LTP. Activation of inhibitory synapses and reduced the burst and its backpropagation, thereby effectively preventing NMDA channel unblock and LTP. A schematic of the possible mechanisms involved and a prediction of STDP with different synaptic input patterns is shown in S4 Fig.

Discussion

The simulation of multicompartmental models of cerebellar Golgi cells showed an asymmetric communication between cell compartments, with apical dendrites being favored for integration of multiple synaptic inputs and basal dendrites for rapid spike back-propagation and NMDA receptor voltage-dependent regulation. The electrogenic architecture of Golgi cells therefore sets up a cellular coincidence detector of activities conveyed by mossy fibers and parallel fibers, with important reflections on the way Golgi cells perform local computations and regulate STDP.

The multicompartmental models used here allowed to integrate complex data sets and to predict electroresponsive dynamics in functional conditions that would be hard to assess experimentally. The Golgi cell models were parameterized using objective optimization routines targeting cell firing as a template and yielding the maximum conductance of voltage-dependent ionic channels in the soma, dendrites, AIS and axon [14]. The models were validated toward high-level electroresponsive properties including rebound sags and bursts, phase reset and resonance [14,15,20]. Interestingly, all the 8 optimized models reproduced response patterns consistent with experimental Golgi cell activity with a similar ionic conductance balance (cf. Fig 1D) that can be taken as a canonical property of these neurons. But then an obvious question arises: why previous models, with simplified morphology, passive dendrites and a limited set of ionic mechanisms collapsed into the soma [8,16,17,35] were also able to capture the same response patterns? Simpler models already predicted that phase reset was due to calcium entry and the subsequent activation of Ca channels, that the length of the interspike interval was modulated by HCN1 channels, that rebound bursts were generated by low-threshold Ca channels, and that resonance depended on an M-like current. The answer is that all these ionic channels are located in the AIS or in its proximity and do not engage specific

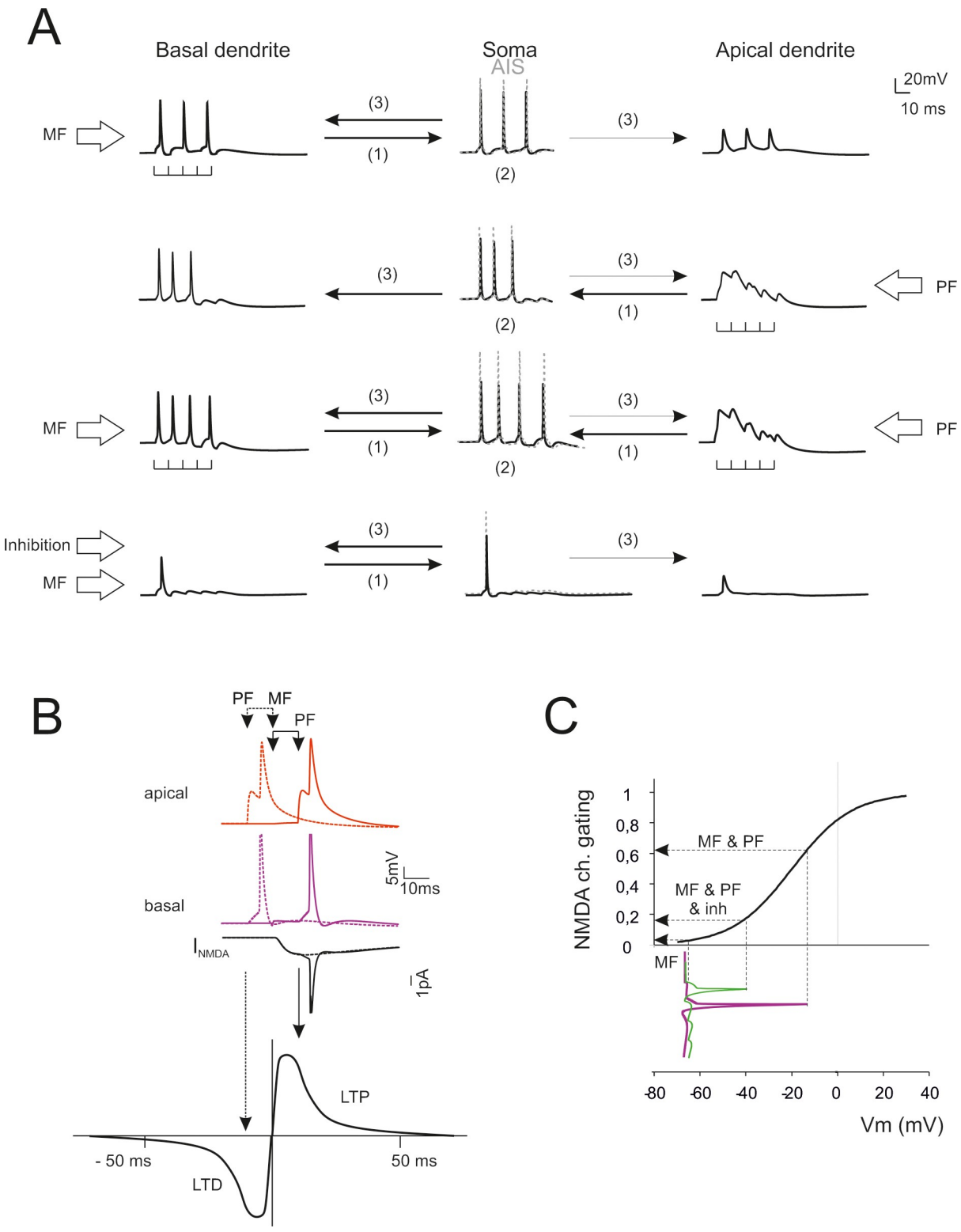

Fig 9. Predictions of dendritic computation and STDP. (A) Dendrite–AIS interplay during synaptic transmission. Stimulation of basal dendrites boosts the AIS encoder that sends backpropagating spikes in basal dendrites (only small spikelets are transmitted to the apical dendrites). Stimulation of apical dendrites generates a slow local response boosting the AIS encoder that sends backpropagating spikes in basal dendrites. Conjoint stimulation of apical and basal dendrites reinforces AIS encoding and spike backpropagation in basal dendrites. Activation of inhibitory synapses severely impairs both spike generation and backpropagation. (B) STDP at mossy fiber inputs. Backpropagating spikes

are elicited by PF stimulation either ~10 ms before or ~10 ms after a single synapse activation in the MFs. The NMDA receptor-dependent current (I_{NMDA}) generated at the MF synapse is shown in the two cases. The bottom plot shows a theoretical STDP curve (from [34]) showing modest I_{NMDA} changes leading into the LTD region and large I_{NMDA} changes leading into the LTP region. (C) The NMDA receptors operate as coincidence detectors of mossy fiber synaptic transmission and depolarization caused by spike backpropagation. The NMDA channel gating curve (corresponding to voltage-dependent Mg unblock) is intercepted in different points depending on whether spike backpropagation is present (MF & PF), reduced by inhibition (MF & PF & inh), or absent (MF).

https://doi.org/10.1371/journal.pcbi.1007937.g009

dendritic interactions. As said, the importance of ionic channels distribution emerged during dendritic synaptic integration.

The electrogenic architecture of Golgi cells

As in other central neurons, like Purkinje cells [28,36], inferior olivary cells [37], pyramidal neurons [30,31,38]], in Golgi cells the dendritic calcium channels played a fundamental role. A variety of Ca channels were located in the dendrites [14] and AIS [23,39]. The models showed that, in basal dendrites, Cav2.2 channel activation followed the action potential trajectory generating rapid Ca transients. In the apical dendrites, Cav3.1 channels boosted slow Ca spikes that were enhanced by Cav2.3 channels. It should be noted that the Cav2.2 channels in basal dendrites enhanced pacemaking while the Cav3.1 and Cav2.3 channels of the apical dendrites did not affect it substantially. Moreover, the Cav3.1 channels sustained post-inhibitory rebound bursts. Other Ca channels (Cav2.1, Cav1.x) were not introduced but they may conceivably amplify and modify the local response. Recently, dendritic Ca spikes have been measured in Golgi cells [40] following mossy fiber stimulation and have been related to activation of Cav3.1 and Cav1.x channels and to the induction of long-term synaptic plasticity. The Kca2.2 channels had also fundamental roles: in basal dendrites they caused phase-reset, dumped basal firing frequency and prevented rhythmic low-frequency bursting, while in apical dendrites they limited calcium spike duration. The Kca1.1 channels in soma, dendrites and AIS enhanced spike after-hyperpolarization. In general, the electrogenic architecture of the Golgi cell was such that the basal dendrites were more rapidly interacting with the AIS and the firing mechanism than the apical dendrites, which conveyed to AIS slow currents controlling spike burst generation.

A critical role was played by Nav1.6 channels, which were located at decreasing density in AIS > axon > soma > basal dendrites >> apical dendrites. Due to this differential distribution, fast Na spikes were generated in the AIS [21] and propagated down along the axon. While uncertainty remains about Na channel density in the axon, the assumption of homogeneous channel distribution yields transmission delays compatible with feedback inhibition measured in the granule cell–Golgi cell loop [18]. The spikes also invaded the soma and efficiently backpropagated in basal dendrites but much less so in apical dendrites, which showed heavily filtered spikelets in their terminal part.

A relevant set of ionic channels was located in the AIS, presumably to increase current density and improve control over the firing cycle. These channels controlled high level features of neuron discharge: the HCN channels regulated pacemaker frequency and sags, the M-channels regulated low-frequency resonance, and the LVA channels enhanced burst generation (see [16,17]. Surprisingly the model predicted high local Ca raise in AIS during spikes, similar to Cartwheel neurons of the Cochlear Nucleus and in cerebral cortex L5 Pyramidal cells [22,23]. This effect, which promoted local Kca1.1 and Kca2.2 channel activation, remains to be demonstrated experimentally.

The synaptic architecture of Golgi cells

A recent estimate of the number of synaptic inputs impinging on Golgi cell dendrites yielded about 400 ascending axon synapse, 4000 parallel fiber synapses, and 40 mossy fiber synapse

per Golgi cell [9]. Here we have partially explored the synaptic input space in order to generate EPSPs and spikes in Golgi cells and investigate the principles of neurotransmission in this neuron. Short-term facilitation at ascending axon and parallel fiber synapses make the Golgi cell poorly sensitive to sparse low-frequency spikes while responding promptly to spike bursts at more than 10 Hz. This high-pass filter at the granule cell—Golgi cell input would prevent, through Golgi cell—granule cell recurrent inhibition, circuit run-away with strong activity in granule cells. Conversely, the mossy fiber synapses, which do not have apparent facilitation or depression during bursts, would allow reliable transmission at all frequencies providing the basis for a linear input-output transformation. Finally, Golgi cell resonance would improve synaptic input tracking in the theta-band, supporting plasticity mechanisms operating on this frequency band.

The effect of synaptic inhibition (illustrated in Fig 7) is clearly to reduce or "dump" the Golgi cell response burst (with an evident effect when inhibition engages more than ~10 synapses). The impact of inhibition on NMDA receptor-dependent long-term synaptic plasticity is illustrated in Fig 9C. In principle, modulating the burst through inhibition would allow to visit a relevant portion of the STDP curve and to modify plasticity accordingly.

Predictions of dendritic integration

The Golgi cell models provided testable predictions about the interplay of basal and apical dendrites under various patterns of excitation and inhibition [8–10].

First, simulations showed how the dendrites transferred synaptic currents generated by mossy fibers, granule cell ascending axons and parallel fibers. Dendritic filtering reduced and slowed down the AMPA EPSCs on their way to the soma, more effectively in apical than basal dendrites. The NMDA current protracted the time course and enhanced temporal summation at mossy fiber synapses. These simulations confirmed the interpretation of synaptic currents recorded in patch-clamp experiments *in vitro* [9].

Secondly, simulations predicted anew the somatic voltage changes caused by the activation of specific synaptic pathways. All the excitatory synapses showed high efficacy, with just a few active contacts capable of driving a spike, but the mossy fiber and ascending axon synapses proved ~5 times more effective that parallel fiber synapses. Repetitive transmission induced spike bursts followed by phase reset, generating a burst-pause pattern similar to that observed *in vivo* [29]. The inhibitory synapses were strategically placed to shunt currents travelling between the distal part of dendrites and soma and effectively reduced AIS activation as well as backpropagating spikes.

Thirdly, simulations revealed a marked asymmetry in dendritic integration. During repetitive synaptic activation, the basal dendrites showed rapid spike bursts travelling back from the AIS, while the apical dendrites generated slow local depolarizations poorly affected by AIS activity.

The input-output hyperspace was governed by the interaction of basal and apical dendrites (S4 Fig) in a way that resembles cortical pyramidal neurons. The analogy could be extended to dendritic control mechanisms, with the soma and basal dendrites processing Na spikes and apical dendrites processing Ca spikes. It is therefore possible that Golgi cells of cerebellum share common plasticity rules and computational principles with pyramidal neurons [30,31].

Implications for Golgi cell computation and plasticity

STDP is a form of synaptic plasticity depending on the temporal correlation of two neural events, one leading to synaptic activation of NMDA receptors and the other to depolarizing phenomena (e.g. spike bursts) regulating NMDA channels unblock [30,33,41–43] (S5 Fig).

Indeed, model simulations showed that apical dendrites can regulate the number of AIS spikes that then backpropagate into basal dendrites with consequent regulation of NMDA channel unblock (when the mossy fiber synapses are also active). The availability of NMDA currents, generated in basal dendrites of the Golgi cell model with different synaptic input patterns, allowed to simulate the possible mechanisms of STDP induction in Golgi cells (S5 Fig). The Shouval-Bear-Cooper model of plasticity [42,43] predicted that reliable STDP would occur with an inversion point between LTP and LTD at 0.75 μm $[Ca^{2+}]_i$ and a rate of change of 10. With these parameters, STDP magnitude ranges up to ±50% and increases with the number of active parallel fibers, i.e. with the depolarization conveyed from apical to basal dendrites. The time window of STDP extends over ±100 ms, thereby matching the period of Golgi cell pacing in the theta-band.

In this way, the apical dendrites could integrate multimodal information coming from parallel fibers and then influence the coincidence of spikes with specific synaptic inputs arriving on the basal dendrites. And since many Golgi cells can pulsate together due to gap-junctions and reciprocal inhibition, spike timing would extend over the interneuron network. This property would be important for mossy fiber–Golgi cell STDP, which has been hypothesized [13] to enable the acquisition of incoming mossy fiber patterns in an oscillating network of Golgi cell interneurons. It is worth noticing that the Golgi cells pacemaker oscillation occurs in the theta band, which is the most efficient in generating STDP at the neighboring mossy fiber–granule cell synapses [34] and that granule cells NMDA receptor unblock could be critically controlled by Golgi cells regulating spatiotemporal network coding [7]. Therefore, the Golgi cell electrogenic architecture may play a central role in controlling granular layer network functioning and plasticity as a whole.

Conclusions

The present simulations, beyond faithfully reproducing the rich pattern of Golgi cell electrophysiological properties recorded *in vitro* and *in vivo*, suggest that Golgi cells operate as oriented coincidence detectors of parallel fiber and mossy fiber activity. The strong coupling of basal dendrites to the AIS encoder makes them easy to invade by backpropagating spikes regulating NMDA channel unblock and STDP induction at the mossy fiber inputs. In turn, apical dendrites can integrate time-dispersed parallel fiber inputs and influence the AIS encoder controlling spike generation. These properties resemble to some extent those reported in pyramidal cells, which also express differentiated ionic mechanisms in their basal and apical dendrites. Oriented dendritic processing could therefore set up a cellular coincidence detector and explain a critical aspect of the learning mechanisms in the cerebellar granular layer. This prediction waits for electrophysiological confirmation using selective optogenetic stimulation of the different synaptic pathways impinging onto the Golgi cells.

Materials and methods

Model construction

In this work we have reconstructed and simulated active multicompartmental models of cerebellar Golgi Cells (GoCs) in NEURON [44,45]. The models were based on 8 mouse GoC detailed morphologies. The voltage-dependent ionic channels were distributed according to immunohistochemical, electrophysiological and pharmacological data [8,14]. The gating properties were obtained from previous works [16,17,46–48] taking care of matching as much as possible the GoC genotype. The synaptic distribution and receptor gating properties were also precisely matched to experimental determinations [9,10]. The models were optimized with BluePyOpt [49,50] against features extracted from templates derived from experimental

recordings [15]. This is the first family of GoC models accounting for active excitable properties in the axonal initial segment (AIS), axon, dendrites and soma and for selective activation of different receptor types at distinct synaptic locations.

Morphology. Detailed morphologies of 8 GoCs (Neurolucida reconstructions taken from sagittal slice of male and female P23—P29 mice; [19]) were downloaded from NeuroMorpho.org and imported in the NEURON simulator. Four morphologies showed the axon stemming from the soma and four from a basal dendrite. This morphological characteristic is rather common in the brain [51] and was reported also in cerebellar granule cells [52] and in the inferior olivary nucleus. Each morphology was segmented into compartments and the dendrites, axons, soma and axon initial segment (AIS) were identified based on their location and geometrical properties. The distinction between basal and apical dendrites was performed based on their proximity to the soma and Purkinje cell layer [19]. The dendrites contained in the granular layer were classified as basal dendrites, whereas the branches projecting to and located in the molecular layer where classified as apical dendrites. The geometrical properties of model compartments are reported in Supporting Information (S1 Table). It should be noted that the available Golgi cell reconstructions have rather complete dendritic trees but are usually missing part of the axonal plexus [53].

Passive properties. The passive properties of the GoC models were set to match passive current transients and spike shape using the following parameters. Axial resistance was set to the standard value of $R_a = 122\ \Omega{\cdot}cm$ [28] for all the sections. Membrane capacitance was set to the standard value $C_m = 1\mu F/cm^2$ in all compartments except in dendrites, were it was set to $C_m = 2.5\ \mu F/cm^2$ to match spike amplitude. Leakage conductance was set to $G_L = 3{\cdot}10^{-5}\ S/cm^2$ in all compartments except in the axon, where it was set at $G_L = 1{\cdot}10^{-6}\ S/cm^2$ according to recent measurements [54,55]. The reversal potentials were set to +60 mV sodium channels, -80 mV for potassium channels, -20 mV for HCN channels, -70 mV for Cl channels [16,17]. The reversal potential for leakage was adjusted to -55 mV in order to guarantee proper basal firing frequency. The resulting input resistance, calculated with a 10 mV negative step from -70mV, was 339.3 ± 128.3MΩ in agreement with experimental determinations (Forti et al., 2006).

Membrane mechanisms. The GoC models, in the absence of more specific information, were endowed with ionic mechanism that were previously validated and used in GrC models [28,55], PC models [27,46,47,56] and Golgi cell models [8,16,17] (see Table 1).

Nav1.6 –The sub-type of GoC sodium channels was determined experimentally [58] but only recently their distribution on the dendritic tree was suggested by electrophysiological experiments [14]. The gating mechanism was taken from [47]. The maximum conductance values were set according to literature, with AIS [8] > soma > basal dendrite > apical dendrite > axon [14].

Kv1.x - The low threshold Kv1.x channels (summarizing properties of Kv1.1 and Kv1.2), in accordance with experiments [62], were placed on the somatic compartment. The gating mechanism was taken from [47].

Kv3.4 –This ionic channel with delayed rectifier properties was restricted to the somatic compartment [63]. The gating mechanism was taken from [47].

Kv4.3 –This ionic channel with A-type properties was placed in the soma. The gating mechanism was taken from a previous GoC model [16,17].

Cav2.2 and Cav2.3 –The high-threshold calcium channels were recently suggested to have distinct locations [14]. Accordingly, the N-type calcium channels (Cav2.2) were placed in basal dendrites. Localization in the soma and AIS was inferred from immunolocalization data [64]. The R-type calcium channels (Cav2.3) were placed in the distal dendrites. The gating mechanism of Cav2.2 was taken from a previous GrC model [48], that of Cav2.3 from [61].

Table 1. Ionic mechanisms in the GoC model. The table shows the main properties of ionic channels used in the Golgi cell models. For each ionic channel type, the columns specify the maximum ionic conductance $G_{i\text{-}max}$ (value of the model in Fig 1 along with the range of parameters in the 8 models), ionic channels reversal potential E_{rev}, the type of ionic channel mathematical representation and the reference from which the ionic channel gating equations have been taken, Markovian or Hodgkin-Huxley (HH).

Type	*Location*	$G_{i\text{-}max}$ *(S/cm²)*	E_{rev} *(mV)*	*Type of ionic Channel model*	*Reference*
Na CHANNEL					
Nav1.6	Apical Dendrites	0.0049 (0.0024–0.0068)	60	Markovian	[47,57,58]
	Basal Dendrites	0.008 (0.006–0.00135)			
	Soma	0.149 (0.143–0.24)			
	AIS	0.172 (0.17–0.2)			
	Axon	0.011 (0.0072–0.025)			
K CHANNEL					
Kv1.x	Soma	0.005 (0.004–0.007)	-80	HH	[47]
Kv3.4	Soma	0.149 (0.11–0.195)	-80	HH	[57,58]
	Axon	0.0091 (0.0021–0.010)			
Kv4.3	Soma	0.004 (0.0035–0.0085)	-80	HH	[59]
Kv7.x	AIS	0.0002 (0.00022–0.0003)	-80	HH	[16,17,48]
Ca DEPENDENT K CHANNELS					
Kca1.1	Apical Dendrites	0.01 (0.008–0.014)		Markovian	[46]
	Basal Dendrites	0.012 (0.009–0.014)			
	Soma	0.017 (0.0145–0.019)			
	AIS	0.1 (0.09–0.12)			
Kca2.2	Apical Dendrites	0.0024 (0.0018–0.0045)	-80	Markovian	[16,17]
	Basal Dendrites	0.016 (0.015–0.019)			
Kca3.1	Soma	0.0101 (0.09–0.15)	-80	HH	[60]
CA CHANNEL					
Cav2.2	Basal Dendrites	0.0013 (0.00125–0.0019)	137.5	HH	[48]
	Soma	0.0087 (0.0078–0.0165)			
	AIS	0.0059 (0.0045–0.0075)			
Cav2.3	Apical Dendrites	0.0012 (0.0012–0.0017)	137.5	HH	[61]
Cav3.1	Apical Dendrites	3.69e-5 (3.6e-5–7.5e-5)	137.5	HH	[46]
	Soma	3.40e-5 (3e-5–9.5e-5)			

(*Continued*)

Table 1. (Continued)

Type	*Location*	$G_{i\text{-}max}$ *(S/cm²)*	E_{rev} *(mV)*	*Type of ionic Channel model*	*Reference*
MIXED CATIONIC CHANNEL					
HCN1	AIS	0.00033 (0.0001–0.00038	-20	HH	[16,17]
HCN2	AIS	0.0003 (0.0003–0.00035	-20	HH	[16,17]
CALCIUM BUFFER (mM)–PUMPS DENSITY		**mol/cm2**			
Ca Buffer	Apical Dendrites	5*10–9		Markovian	[46]
	Basal Dendrites	2*10–9			
	Soma	1*10–7			
	AIS	1*10–8			
	Axon	1*10–8			

https://doi.org/10.1371/journal.pcbi.1007937.t001

Cav3.1 –The presence of low threshold T-type calcium channels (Cav3.1) on the soma was reported by immunohistochemistry [65] and on the apical dendrites was suggested by electrophysiology [14]. Accordingly, we placed Cav3.1 in these locations. The gating mechanism was taken from [46].

KCa1.1, KCa2.2 and KCa3.1 –The big-k calcium-dependent potassium channel (Kca1.1), which can cluster with Cav2.x channels, was placed on the dendritic, somatic and AIS compartments based on immunohistochemical and electrophysiological data [66]. The gating mechanism was taken from [46]. The small-k calcium-dependent potassium channel (KCa2.2) was placed in the dendrites on the basis of electrophysiological recordings showing its importance in limiting calcium-dependent bursting [15] and based on the fact that KCa2.2 doesn't normally coexist with either KCa3.1 or Cav3.1 (see below and the section on results). The gating mechanism was taken from a previous GoC model [16,17], with the caveat that this channel model describes more closely KCa2.2 (SK2) than KCa2.3 (SK3) typical of Golgi cells [67,68]. The middle conductance calcium-dependent potassium channel (KCa3.1) was placed in the soma [69]. The gating mechanism was taken from mitral cells of the olfactory bulb [60].

HCN1 and HCN2 –The H-channels, which were identified electrophysiologically in GoCs [15], have been located in the AIS (Vervaeke, 2012). The gating mechanism was taken from a previous GoC model [16,17].

Kv7.x –The M-current was identified electrophysiologically [15] and was assumed to correspond to Kv7.xchannels [15,64]. Based on anchoring of Kv7.x to Ankyrin-G [70,71], the channels were placed in the AIS using gating mechanisms developed for the GrC [48].

Calcium dynamics–The calcium buffer was taken from a PC model [27,46,56] and modified to contain Parvalbumin [72] and Calmodulin [73], the typical calcium binding proteins of the Golgi cell. The calcium pumps density was increased with respect to default to stabilize spike generation over 2 sec simulations. The density of calcium pumps was set to $2{\cdot}10^{-9}$ mol/cm^2 for the apical dendrites, $5{\cdot}10^{-9}$ mol/cm^2 for the basal dendrites, $1{\cdot}10^{-7}$ mol/cm^2 for the soma and $1{\cdot}10^{-8}$ mol/cm^2 for the AIS.

Synaptic mechanisms. Golgi cells receive synapses from different excitatory pathways (parallel fiber and ascending axon from granule cells, mossy fibers from various brain regions including the DCN; [74]) and from inhibitory neurons. Excitatory synapses have been recently characterized in detail [9]. The parallel fiber synapses were distributed on the apical dendrites, one per compartment. The ascending axon synapses were placed on the basal dendrites, one per section at some distance from the mossy fiber synapses [9]. The mossy fiber synapses were placed on the basal dendrites using sections which were, at least, 20micron away from the soma [75]. The inhibitory synapses on GoCs are still an open issue but recent evidence reports

them both on the apical and basal dendrites [12]. The apical dendrites reportedly receive a low amount of inhibition from molecular layer interneurons and Lugaro cells, while the basal dendrites receive inhibition from other GoCs and the deep cerebellar nuclei (DCN) [76]

The synapses were modelled using dynamic mechanisms for presynaptic neurotransmitter release [24,26], in which key parameters area the recovery and facilitation time constant (τ_{REC} and τ_{FAC}) and release probability (p), and specific kinetic schemes for AMPA, NMDA and GABA receptors. AMPA receptors were placed at mossy fiber and ascending axon synapses on the basal dendrites and at parallel fiber synapses on apical dendrites, NMDA receptors were placed only at mossy fiber synapses on basal dendrites, GABA receptors were placed at Golgi cell inhibitory synapses on both dendrites. Glycinergic synapses [11] and extrasynaptic NMDA receptors [77] were not taken into consideration since their activation would require mechanisms that were not investigated in the present model. The ionic reversal potential was set to 0 mV for AMPA and NMDA receptors and to -70 mV for GABA receptors.

The AMPA receptor kinetic scheme for the parallel fiber and ascending axon synapses was the same as in PCs [27]. The synapses were configured with the following parameters: $p = 0.4$, $\tau_{REC} = 35.1$ ms, $\tau_{FAC} = 55$ ms, and AMPA $G_{max} = 1200$ pS. This allowed to obtain short-term facilitation with AMPA-EPSCs of ~25pA (at -70 mV) [9] matching EPSCs kinetics recorded from the soma.

The AMPA and NMDA receptor kinetic scheme for the mossy fiber synapses were taken from a granule cell model [55]. The NMDA receptor was modified from the original work with a new kinetic scheme built to reproduce the NR2B subunit-containing receptors [78]. About 10% of the 5.5pA maximum current was converted into calcium influx. The synapses were configured with the following parameters: $p = 0.43$, $\tau_{REC} = 5$ ms, $\tau_{FAC)} = 8$ ms, AMPA $G_{max} = 1200$pS and NMDA $G_{max} = 10000$ pS. The simulated EPSC was characterized by a fast AMPA peak (~25pA at -70 mV) followed by a slow NMDA receptor-dependent component and showed temporal summation during repetitive stimulation [9] matching the EPSCs kinetics experimentally recorded from the soma.

The GABA-A receptor kinetic scheme for the inhibitory synapses was taken from recent work that has identify α3β3γ2 GABA subunit containing receptors in the apical and basal dendrites [12,79]. The synapses were configured with the following parameters: $p = 0.5$, $\tau_{REC} = 15$ ms, $\tau_{FAC} = 4$ ms, reversal potential = -70 mV and GABA $G_{max} = 2600$pS. The simulated IPSC peak (~3.5 pA at -80 mV) matched the EPSCs kinetics experimentally recorded from the soma [10].

Model optimization

The optimization workflow has been adapted from the one used for the GrC model [28,55]. We used a genetic algorithm to optimize the maximum ionic conductances (the free parameters in the model) for the ionic channels located in all compartments belonging to the same section (apical and basal dendrites, soma, AIS and axon). Optimization occurred against *features* extracted from data reported in [15], which provides highly controlled and reliable whole-cell patch clam recordings of GoC discharge at rest and during current injection. The features used were: action potential width, ISI coefficient of variation (ISI_CV), AHP depth, Action potential height, mean firing frequency, spike count.

The simulations were performed with BluePyopt, using NEURON 7.7 and Python 2.7.15 with fixed time step (0.025ms) [45]. The temperature was set at 32˚ as in slice recordings [15] and all ionic current kinetics were normalized to this value using Q_{10} corrections [28,55]. The stimulation protocol included three positive current injections (0.2, 0.4, 0.6 nA) lasting for 2s.

The optimizations used a population size of 576 individuals and were repeated for 10 generations. The optimizations (running on the Piz Daint—CSCS supercomputer) required 16

nodes (36 cores each) with a computational time ranging from 2:30 to 4:30 hours, depending on the complexity of each morphology.

Model validation

Model validation consisted in a series of steps, automatically performed with custom-made Python protocols.

The first validation step involved the simulation of each individual of the last generation to assess two fundamental properties: (1) the presence of spontaneous firing and (2) the ability of the models to generate the correct I/O relationship. The first validation criterion required a basal frequency between 2 and 15Hz and an ISI_CV < 0.3 (see Fig 1). The second validation criterion required that the average frequency during the same current steps used for optimization (0.4 nA and 0.6 nA) fell within the experimental range (see Fig 2).

The second validation step assessed the depth of the sag. Each individual was injected with a negative current step (-0.2 nA) lasting for 1000 ms (Fig 3). Validation required that the sag depth fell between 4.4 mV and 10mV [8,15–17]. In order to do so, a specific optimization was run and the successful models were passed to the third validation step. After the firsts and second validation step, the success rate for the eight morphologies was 32 ± 27.1%.

The third validation step assessed the compatibility of the model with experimental pharmacological blockade of Cav2.2, Kca1.1 and Kca2.2 ionic channels [14]. The channels conductance was reduced up to 90%. Models capable of generating bursts, with Cav2.2 partially blocked, were taken in consideration for their response to reductions of Kca2.2 and Kca1.1 conductance. After the third validation step, the valid models were just 10–20% of the initial population.

In aggregate, each model shown in the paper was selected from a large set of possible models (1152). About 60% of the models were discarded because they did not match the typical features of a Golgi cell (i.e. did not show spontaneous firing, an appropriate Input-Output relationship or a sag). Among the models surviving triage, only a part (about 10% of the total) showed correct sensitivity to ionic channel blockers. Out of these ~100 models, one was randomly chosen and shown in the paper. The model parameter space is illustrated in S3 Fig.

Data analysis

The optimizations results, validations and single simulations where analyzed with custom Python scripts and, for specific cases, with MATLAB 2018a/b provided by the University of Pavia. The morphologies were plotted with Vaa3D [80]. The data used to plot the graphs can be found in S1 Data.

Supporting information

S1 Table. Dimension and number of compartments in the Golgi cell model. The table shows parameters of compartments used in the 8 Golgi cell models taken from NeuroMorpho [19].
(XLSX)

S1 Data. Source data for the graphs. The table contains the source data used to plot the graphs for the main text figures.
(XLSX)

S1 Fig. Electroresponsiveness of the 8 Golgi cell models. The GoC experimental template is shown to the top along with the step current injection protocol used to elicit the electrical response [15]. The same stimulation protocol was applied to the 8 Golgi cell models. For each model the panels show the morphological reconstruction and the electrical response. Note the

similarity among the models and between them and the experimental case.
(TIF)

S2 Fig. Variability of ionic conductances in Golgi cell models. The table shows the maximum ionic channel conductances of 5 randomly chosen individuals for each of the 8 GoC models. The 40 individuals (all validated according to the criteria explained in Materials and Methods) show that the model optimization algorithms thoroughly explored the parameter space providing diverse ionic conductance patterns. In other words, there are different combinations of conductance values that allow to achieve a spike discharge compatible with the experimental templates.
(TIF)

S3 Fig. Schematics of Golgi cell connectivity. The figure illustrates the connectivity of GoCs with MFs and GrCs. Inside the glomerulus, a Golgi cell basal dendrite receives excitatory inputs from a MF terminal, while the Golgi cell axon inhibits granule cell dendrites. The granule cells excite the Golgi cell dendrites thought the AAs and PFs. The PF activate only AMPA receptors, while the AA and MF activate both AMPA and NMDA—NR2B-containing receptors. Reciprocal inhibition occurs between the GoC axons and dendrites. Golgi cell; GrC, granule cell; AA, ascending axon; PF, parallel fiber; MF, mossy fiber.
(TIF)

S4 Fig. The synaptic input-output space of a Golgi cell model. The synaptic input-output (I/O) space of the Golgi cell model was computed from the response to combined activation of basal and apical dendrites through the corresponding input pathways. The simulations have been repeated using a short train of 5spikes@100Hz on both mossy fibers and parallel fibers and the corresponding output frequency is color-codeded. The stars indicate 4 points in the I/O plane that were used to compute STDP, as shown in S5 Fig.
(TIF)

S5 Fig. Simulation of STDP in the Golgi cell model. (A) Schematics of the STDP model applied to Golgi cells [42,43]. The coincidence of MF and PF activity regulates NMDA-R activation and channel unblock causing Ca^{2+} entry and a change in Ca^{2+} concentration, $\Delta[Ca^{2+}]_i$. This, in turn, is transformed into STDP by sigmoidal transfer functions accounting for the molecular mechanisms of Ca-dependent plasticity. **(B)** Based on the I/O plots of S4 Fig, our simulations used 11 mossy fiber synapse and an increasing number of parallel fiber synapses (11, 31, 61, 81), both stimulated with a 5spikes@100Hz burst. The $\Delta[Ca^{2+}]_{i.}$ generated by NMDA channels in the corresponding dendritic compartment reflects local Ca regulation, including removal due to diffusion and extrusion but not amplification by local calcium stores. This amplification, e.g. in the neighboring granule cell dendrites, is of about 3 times [81]. Therefore, the $\Delta[Ca^{2+}]_{i.}$ caused by NMDA channel opening was multiplied by 3 times bringing $\Delta[Ca^{2+}]_{i.}$ around the STDP transition point (~0.75 μM). With a rate of change of 10, the model yields a classical STDP curve for the Golgi cell with a gain that depends on the amount of depolarization conveyed by the parallel fibers acting on apical dendrites. **(C)** Dependence of STDP magnitude on the number of active parallel fibers. The gain tends to plateau around ±40%.
(TIF)

S1 Video. Golgi cell model activation by a mossy fiber burst. The same GoC model shown in Fig 1 is activated with a burst (5 spikes@100Hz) delivered through the mossy fibers (20 synapses). The model generates a short spike burst followed by a pause that effectively reset the pacemaker cycle. Membrane potential is represented in color code (scale at the top left) on the

model morphology. The plots show membrane potential traces taken in the soma, basal dendrite and apical dendrite.
(MP4)

S2 Video. Golgi cell model activation by an ascending axon burst. The same GoC model shown in Fig 1 is activated with a burst (5 spikes@100Hz) delivered through the ascending axons (20 synapses). The model generates a short spike burst followed by a pause that effectively reset the pacemaker cycle. Membrane potential is represented in color code (scale at the top left) on the model morphology. The plots show membrane potential traces taken in the soma, basal dendrite and apical dendrite.
(MP4)

S3 Video. Golgi cell model activation by a parallel fiber burst. The same GoC model shown in Fig 1 is activated with a burst (5 spikes@100Hz) delivered through the parallel fibers (89 synapses). The model generates a short spike burst followed by a pause that effectively reset the pacemaker cycle. Membrane potential is represented in color code (scale at the top left) on the model morphology. The plots show membrane potential traces taken in the soma, basal dendrite and apical dendrite.
(MP4)

Acknowledgments

Special thanks to the HBP Neuroinformatics Platform, HBP Brain Simulation Platform, HBP HPAC Platform for providing access to informatic infrastructures and supercomputing resources.

Author Contributions

Conceptualization: Egidio D'Angelo.

Formal analysis: Egidio D'Angelo.

Funding acquisition: Egidio D'Angelo.

Investigation: Stefano Masoli, Alessandra Ottaviani.

Methodology: Stefano Masoli, Stefano Casali.

Project administration: Egidio D'Angelo.

Software: Stefano Masoli, Alessandra Ottaviani, Stefano Casali.

Supervision: Egidio D'Angelo.

Validation: Stefano Masoli, Alessandra Ottaviani.

Visualization: Stefano Masoli, Alessandra Ottaviani, Egidio D'Angelo.

Writing – original draft: Stefano Masoli.

Writing – review & editing: Egidio D'Angelo.

References

1. Bentivoglio M, Cotrufo T, Ferrari S, Tesoriero C, Mariotto S, Bertini G, et al. The original histological slides of camillo golgi and his discoveries on neuronal structure. Front Neuroanat. 2019; 13: 1–13. https://doi.org/10.3389/fnana.2019.00001 PMID: 30760983
2. Golgi C. The neuron doctrine—theory and facts. 1906.

3. Galliano E, Mazzarello P, D'Angelo E. Discovery and rediscoveries of Golgi cells. J Physiol. 2010; 588: 3639–3655. https://doi.org/10.1113/jphysiol.2010.189605 PMID: 20581044
4. Eccles JC, Llinás RR, Sasaki K. Golgi Cell Inhibition in the Cerebellar Cortex. Nature. 1964; 204: 1265–1266. https://doi.org/10.1038/2041265a0 PMID: 14254404
5. D'Angelo E, De Zeeuw CI. Timing and plasticity in the cerebellum: focus on the granular layer. Trends Neurosci. 2009; 32: 30–40. https://doi.org/10.1016/j.tins.2008.09.007 PMID: 18977038
6. D'Angelo E. The critical role of Golgi cells in regulating spatio-temporal integration and plasticity at the cerebellum input stage. Front Neurosci. 2009; 2: 35–46. https://doi.org/10.3389/neuro.01.008.2008 PMID: 18982105
7. Sudhakar SK, Hong S, Raikov I, Publio R, Lang C, Close T, et al. Spatiotemporal network coding of physiological mossy fiber inputs by the cerebellar granular layer. PLoS Computational Biology. 2017. https://doi.org/10.1371/journal.pcbi.1005754 PMID: 28934196
8. Vervaeke K, Lorincz A, Nusser Z, Silver RA. Gap junctions compensate for sublinear dendritic integration in an inhibitory network. Science (80-). 2012; 335: 1624–1628. https://doi.org/10.1126/science.1215101 PMID: 22403180
9. Cesana E, Pietrajtis K, Bidoret C, Isope P, D'Angelo E, Dieudonné S, et al. Granule cell ascending axon excitatory synapses onto Golgi cells implement a potent feedback circuit in the cerebellar granular layer. J Neurosci. 2013; 33: 12430–46. https://doi.org/10.1523/JNEUROSCI.4897-11.2013 PMID: 23884948
10. Hull C, Regehr WG. Identification of an Inhibitory Circuit that Regulates Cerebellar Golgi Cell Activity. Neuron. 2012; 73: 149–158. https://doi.org/10.1016/j.neuron.2011.10.030 PMID: 22243753
11. Dieudonne S. Glycinergic synaptic currents in Golgi cells of the rat cerebellum. Proc Natl Acad Sci. 1995; 92: 1441–1445. https://doi.org/10.1073/pnas.92.5.1441 PMID: 7877998
12. Eyre MD, Nusser Z. Only a Minority of the Inhibitory Inputs to Cerebellar Golgi Cells Originates from Local GABAergic Cells. eNeuro. 2016; 3: 1–14. https://doi.org/10.1523/ENEURO.0055-16.2016 PMID: 27257627
13. Garrido JA, Luque NR, Tolu S, D'Angelo E. Oscillation-Driven Spike-Timing Dependent Plasticity Allows Multiple Overlapping Pattern Recognition in Inhibitory Interneuron Networks. Int J Neural Syst. 2016; 26: 1650020. https://doi.org/10.1142/S0129065716500209 PMID: 27079422
14. Rudolph S, Hull C, Regehr WG. Active Dendrites and Differential Distribution of Calcium Channels Enable Functional Compartmentalization of Golgi Cells. J Neurosci. 2015; 35: 15492–15504. https://doi.org/10.1523/JNEUROSCI.3132-15.2015 PMID: 26609148
15. Forti L, Cesana E, Mapelli J, D'Angelo E. Ionic mechanisms of autorhythmic firing in rat cerebellar Golgi cells. J Physiol. 2006; 574: 711–29. https://doi.org/10.1113/jphysiol.2006.110858 PMID: 16690702
16. Solinas S, Forti L, Cesana E, Mapelli J, De Schutter E, D'Angelo E, et al. Fast-reset of pacemaking and theta-frequency resonance patterns in cerebellar golgi cells: simulations of their impact in vivo. Front Cell Neurosci. 2007; 1: 4. https://doi.org/10.3389/neuro.03.004.2007 PMID: 18946522
17. Solinas SMG, Forti L, Cesana E, Mapelli J, De Schutter E, D'Angelo E. Computational reconstruction of pacemaking and intrinsic electroresponsiveness in cerebellar Golgi cells. Front Cell Neurosci. 2007; 1:2: 2. https://doi.org/10.3389/neuro.03.002.2007 PMID: 18946520
18. Armano S, Rossi P, Taglietti V, D'Angelo E. Long-term potentiation of intrinsic excitability at the mossy fibergranule cell synapse of rat cerebellum. J Neurosci. 2000; 20: 5208–5216. https://doi.org/10.1523/JNEUROSCI.20-14-05208.2000 PMID: 10884304
19. Szoboszlay M, Lőrincz A, Lanore F, Vervaeke K, Silver RA, Nusser Z. Functional Properties of Dendritic Gap Junctions in Cerebellar Golgi Cells. Neuron. 2016; 90: 1043–1056. https://doi.org/10.1016/j.neuron.2016.03.029 PMID: 27133465
20. Dieudonné S. Submillisecond kinetics and low efficacy of parallel fibre-Golgi cell synaptic currents in the rat cerebellum. J Physiol. 1998; 510: 845–866. https://doi.org/10.1111/j.1469-7793.1998.845bj.x PMID: 9660898
21. Lorincz A, Nusser Z. Cell-type-dependent molecular composition of the axon initial segment. J Neurosci. 2008; 28: 14329–40. https://doi.org/10.1523/JNEUROSCI.4833-08.2008 PMID: 19118165
22. Bender KJ, Trussell LO. Axon initial segment Ca2+ channels influence action potential generation and timing. Neuron. 2009; 61: 259–271. https://doi.org/10.1016/j.neuron.2008.12.004 PMID: 19186168
23. Yu Y, Maureira C, Liu X, McCormick D. P/Q and N channels control baseline and spike-triggered calcium levels in neocortical axons and synaptic boutons. J Neurosci. 2010; 30: 11858–11869. https://doi.org/10.1523/JNEUROSCI.2651-10.2010 PMID: 20810905
24. Tsodyks M, Pawelzik K, Markram H. Neural networks with dynamic synapses. Neural Comput. 1998; 10: 821–835. https://doi.org/10.1162/089976698300017502 PMID: 9573407

25. Mapelli L, Rossi P, Nieus T, D'Angelo E. Tonic activation of GABAB receptors reduces release probability at inhibitory connections in the cerebellar glomerulus. J Neurophysiol. 2009; 101: 3089–3099. https://doi.org/10.1152/jn.91190.2008 PMID: 19339456

26. Nieus T, Sola E, Mapelli J, Saftenku E, Rossi P, D'Angelo E. LTP regulates burst initiation and frequency at mossy fiber-granule cell synapses of rat cerebellum: experimental observations and theoretical predictions. J Neurophysiol. 2005; 95: 686–699. https://doi.org/10.1152/jn.00696.2005 PMID: 16207782

27. Masoli S, D'Angelo E. Synaptic Activation of a Detailed Purkinje Cell Model Predicts Voltage-Dependent Control of Burst-Pause Responses in Active Dendrites. Front Cell Neurosci. 2017; 11: 1–18. https://doi.org/10.3389/fncel.2017.00001 PMID: 28154525

28. Masoli S, Rizza MF, Sgritta M, Van Geit W, Schürmann F, D'Angelo E. Single Neuron Optimization as a Basis for Accurate Biophysical Modeling: The Case of Cerebellar Granule Cells. Front Cell Neurosci. 2017; 11: 1–14. https://doi.org/10.3389/fncel.2017.00001 PMID: 28154525

29. Vos BP, Volny-Luraghi A, Maex R, Schutter E De. Precise spike timing of tactile-evoked cerebellar golgi cell responses: a reflection of combined mossy fiber and parallel fiber activation? Progress in Brain Research. 2000. pp. 95–106. https://doi.org/10.1016/S0079-6123(00)24010-7

30. Ilan LB, Gidon A, Segev I. Interregional synaptic competition in neurons with multiple STDP-inducing signals. J Neurophysiol. 2011; 105: 989–998. https://doi.org/10.1152/jn.00612.2010 PMID: 21123659

31. Shai AS, Anastassiou CA, Larkum ME, Koch C. Physiology of Layer 5 Pyramidal Neurons in Mouse Primary Visual Cortex: Coincidence Detection through Bursting. PLoS Comput Biol. 2015; 11: 1–18. https://doi.org/10.1371/journal.pcbi.1004090 PMID: 25768881

32. Bi GQ, Poo MM. Synaptic modifications in cultured hippocampal neurons: Dependence on spike timing, synaptic strength, and postsynaptic cell type. J Neurosci. 1998; 18: 10464–10472. https://doi.org/10.1523/JNEUROSCI.18-24-10464.1998 PMID: 9852584

33. Ebner C, Clopath C, Jedlicka P, Cuntz H. Unifying Long-Term Plasticity Rules for Excitatory Synapses by Modeling Dendrites of Cortical Pyramidal Neurons. Cell Rep. 2019; 29: 4295–4307.e6. https://doi.org/10.1016/j.celrep.2019.11.068 PMID: 31875541

34. Sgritta M, Locatelli F, Soda T, Prestori F, D'Angelo EU. Hebbian Spike-Timing Dependent Plasticity at the Cerebellar Input Stage. J Neurosci. 2017; 37: 2809–2823. https://doi.org/10.1523/JNEUROSCI.2079-16.2016 PMID: 28188217

35. Geminiani A, Casellato C, Locatelli F, Prestori F, Pedrocchi A, D'Angelo E. Complex Dynamics in Simplified Neuronal Models: Reproducing Golgi Cell Electroresponsiveness. Front Neuroinform. 2018;12. https://doi.org/10.3389/fninf.2018.00012 PMID: 29615887

36. Llinás R, Sugimori M, Lin JW, Cherksey B. Blocking and isolation of a calcium channel from neurons in mammals and cephalopods utilizing a toxin fraction (FTX) from funnel-web spider poison. Proc Natl Acad Sci U S A. 1989; 86: 1689–93. https://doi.org/10.1073/pnas.86.5.1689 PMID: 2537980

37. Schweighofer N, Doya K, Kawato M. Electrophysiological properties of inferior olive neurons: A compartmental model. J Neurophysiol. 1999; 82: 804–817. https://doi.org/10.1152/jn.1999.82.2.804 PMID: 10444678

38. Gidon A, Zolnik TA, Fidzinski P, Bolduan F, Papoutsi A, Poirazi P, et al. Dendritic action potentials and computation in human layer 2/3 cortical neurons. Science (80-). 2020; 367: 83–87. https://doi.org/10.1126/science.aax6239 PMID: 31896716

39. Abiraman K, Anastasios VT, Lykotrafitis G. KCa2 channel localization and regulation in the axon initial segment. FASEB J. 2018; 32: 1794–1805. https://doi.org/10.1096/fj.201700605R PMID: 29180442

40. Locatelli F, Soda T, Montagna I, Tritto S, Botta L, Prestori F, et al. Calcium channel-dependent induction of long-term synaptic plasticity at excitatory Golgi cell synapses of cerebellum. bioRxiv Neurosci. 2019;720270.

41. Markram H, Gerstner W, Sjöström PJ. Spike-timing-dependent plasticity: A comprehensive overview. Front Synaptic Neurosci. 2012; 4: 2010–2012. https://doi.org/10.3389/fnsyn.2012.00002 PMID: 22807913

42. Shouval HZ, Bear MF, Cooper LN. A unified model of NMDA receptor-dependent bidirectional synaptic plasticity. Proc Natl Acad Sci U S A. 2002; 99: 10831–10836. https://doi.org/10.1073/pnas.152343099 PMID: 12136127

43. Shouval HZ, Wang SSH, Wittenberg GM. Spike timing dependent plasticity: A consequence of more fundamental learning rules. Front Comput Neurosci. 2010; 4: 1–13. https://doi.org/10.3389/neuro.10.001.2010 PMID: 20422044

44. Hines ML, Davison AP, Muller E. NEURON and Python. Front Neuroinform. 2009; 3: 1. https://doi.org/10.3389/neuro.11.001.2009 PMID: 19198661

45. Hines M, Carnevale NT. Neuron: A Tool for Neuroscientists. Neurosci. 2001; 7: 123–135. https://doi.org/10.1177/107385840100700207 PMID: 11496923

46. Anwar H, Hong S, De Schutter E. Controlling Ca 2+-activated K + channels with models of Ca 2+ buffering in purkinje cells. Cerebellum. 2012; 11: 681–693. https://doi.org/10.1007/s12311-010-0224-3 PMID: 20981513

47. Akemann W, Knöpfel T. Interaction of Kv3 potassium channels and resurgent sodium current influences the rate of spontaneous firing of Purkinje neurons. J Neurosci. 2006; 26: 4602–12. https://doi.org/10.1523/JNEUROSCI.5204-05.2006 PMID: 16641240

48. D'Angelo E, Nieus T, Maffei A, Armano S, Rossi P, Taglietti V, et al. Theta-frequency bursting and resonance in cerebellar granule cells: experimental evidence and modeling of a slow k+-dependent mechanism. J Neurosci. 2001; 21: 759–70. 21/3/759 [pii] https://doi.org/10.1523/JNEUROSCI.21-03-00759.2001 PMID: 11157062

49. Van Geit W, Gevaert M, Chindemi G, Rössert C, Courcol J-D, Muller EB, et al. BluePyOpt: Leveraging Open Source Software and Cloud Infrastructure to Optimise Model Parameters in Neuroscience. Front Neuroinform. 2016; 10: 1–30. https://doi.org/10.3389/fninf.2016.00001 PMID: 26834620

50. Van Geit W. Blue Brain Project (2015). eFEL.Available online at: https://github.com/BlueBrain/eFEL (Accessed February 16, 2016). 2015. https://doi.org/10.5281/zenodo.30074

51. Thome C, Kelly T, Yanez A, Schultz C, Engelhardt M, Cambridge SB, et al. Axon-carrying dendrites convey privileged synaptic input in hippocampal neurons. Neuron. 2014; 83: 1418–1430. https://doi.org/10.1016/j.neuron.2014.08.013 PMID: 25199704

52. Triarhou LC, Bourne JA, Manger P. Axons emanating from dendrites: phylogenetic repercussions with Cajalian hues. 2014. https://doi.org/10.3389/fnana.2014.00133 PMID: 25477788

53. Tabuchi S, Gilmer JI, Purba K, Person AL. Pathway-Specific Drive of Cerebellar Golgi Cells Reveals Integrative Rules of Cortical Inhibition. J Neurosci. 2019; 39: 1169–1181. https://doi.org/10.1523/JNEUROSCI.1448-18.2018 PMID: 30587539

54. Dover K, Marra C, Solinas S, Popovic M, Subramaniyam S, Zecevic D, et al. FHF-independent conduction of action potentials along the leak-resistant cerebellar granule cell axon. Nat Commun. 2016; 7: 12895. https://doi.org/10.1038/ncomms12895 PMID: 27666389

55. Masoli S, Tognolina M, Laforenza U, Moccia F, D'Angelo E. Parameter tuning differentiates granule cell subtypes enriching transmission properties at the cerebellum input stage. Commun Biol. 2020; 3: 222. https://doi.org/10.1038/s42003-020-0953-x PMID: 32385389

56. Masoli S, Solinas S, D'Angelo E. Action potential processing in a detailed Purkinje cell model reveals a critical role for axonal compartmentalization. Front Cell Neurosci. 2015; 9: 1–22. https://doi.org/10.3389/fncel.2015.00001 PMID: 25667569

57. Raman IM, Bean BP. Inactivation and recovery of sodium currents in cerebellar Purkinje neurons: evidence for two mechanisms. Biophys J. 2001; 80: 729–737. https://doi.org/10.1016/S0006-3495(01)76052-3 PMID: 11159440

58. Khaliq ZM, Gouwens NW, Raman IM. The contribution of resurgent sodium current to high-frequency firing in Purkinje neurons: an experimental and modeling study. J Neurosci. 2003; 23: 4899–4912. https://doi.org/10.1523/JNEUROSCI.23-12-04899.2003 PMID: 12832512

59. Diwakar S, Magistretti J, Goldfarb M, Naldi G, D'Angelo E. Axonal Na+ channels ensure fast spike activation and back-propagation in cerebellar granule cells. J Neurophysiol. 2009; 101: 519–532. https://doi.org/10.1152/jn.90382.2008 PMID: 19073816

60. Rubin DB, Cleland T a. Dynamical mechanisms of odor processing in olfactory bulb mitral cells. J Neurophysiol. 2006; 96: 555–68. https://doi.org/10.1152/jn.00264.2006 PMID: 16707721

61. Sterratt DC, Groen MR, Meredith RM, van Ooyen A. Spine calcium transients induced by synaptically-evoked action potentials can predict synapse location and establish synaptic democracy. PLoS Comput Biol. 2012;8. https://doi.org/10.1371/journal.pcbi.1002545 PMID: 22719238

62. McNamara NMC. Ultrastructural Localization of a Voltage-gated K+ Channel a Subunit (Kv 1.2) in the Rat Cerebellum. Eur J Neurosci. 1996; 8: 688–699. https://doi.org/10.1111/j.1460-9568.1996.tb01254.x PMID: 9081620

63. Martina M, Yao GL, Bean BP. Properties and functional role of voltage-dependent potassium channels in dendrites of rat cerebellar Purkinje neurons. J Neurosci. 2003; 23: 5698–707. https://doi.org/10.1523/JNEUROSCI.23-13-05698.2003 PMID: 12843273

64. Leterrier C. The Axon Initial Segment, 50 Years Later: A Nexus for Neuronal Organization and Function. Current Topics in Membranes. Elsevier Ltd; 2016. https://doi.org/10.1016/bs.ctm.2015.10.005 PMID: 26781833

65. Molineux ML, McRory JE, McKay BE, Hamid J, Mehaffey WH, Rehak R, et al. Specific T-type calcium channel isoforms are associated with distinct burst phenotypes in deep cerebellar nuclear neurons.

Proc Natl Acad Sci U S A. 2006; 103: 5555–5560. https://doi.org/10.1073/pnas.0601261103 PMID: 16567615

66. Cheron G, Sausbier M, Sausbier U, Neuhuber W, Ruth P, Dan B, et al. BK Channels Control Cerebellar Purkinje and Golgi Cell Rhythmicity In Vivo. PLoS One. 2009; 4: e7991. https://doi.org/10.1371/journal.pone.0007991 PMID: 19956720

67. Gymnopoulos M, Cingolani LA, Pedarzani P, Stocker M. Developmental mapping of small-conductance calcium-activated potassium channel expression in the rat nervous system. J Comp Neurol. 2014; 522: 1072–1101. https://doi.org/10.1002/cne.23466 PMID: 24096910

68. Stocker M, Pedarzani P. Differential distribution of three Ca(2+)-activated K(+) channel subunits, SK1, SK2, and SK3, in the adult rat central nervous system. Mol Cell Neurosci. 2000; 15: 476–493. https://doi.org/10.1006/mcne.2000.0842 PMID: 10833304

69. Turner RW, Kruskic M, Teves M, Scheidl-Yee T, Hameed S, Zamponi GW. Neuronal expression of the intermediate conductance calcium-activated potassium channel KCa3.1 in the mammalian central nervous system. Pflugers Arch Eur J Physiol. 2014; 467: 311–328. https://doi.org/10.1007/s00424-014-1523-1 PMID: 24797146

70. Devaux JJ, Kleopa K a, Cooper EC, Scherer SS. KCNQ2 is a nodal K+ channel. J Neurosci. 2004; 24: 1236–44. https://doi.org/10.1523/JNEUROSCI.4512-03.2004 PMID: 14762142

71. Rasband MN. Clustered K+ channel complexes in axons. Neurosci Lett. 2010; 486: 101–106. https://doi.org/10.1016/j.neulet.2010.08.081 PMID: 20816921

72. Bastianelli E. Distribution of calcium-binding proteins in the cerebellum. Cerebellum. 2003; 2: 242–62. https://doi.org/10.1080/14734220310022289 PMID: 14964684

73. Pepke S, Kinzer-Ursem T, Mihalas S, Kennedy MB. A dynamic model of interactions of Ca2+, calmodulin, and catalytic subunits of Ca2+/calmodulin-dependent protein kinase II. PLoS Comput Biol. 2010;6. https://doi.org/10.1371/journal.pcbi.1000675 PMID: 20168991

74. Gao Z, Proietti-Onori M, Lin Z, ten Brinke MM, Boele H-J, Potters J-W, et al. Excitatory Cerebellar Nucleocortical Circuit Provides Internal Amplification during Associative Conditioning. Neuron. 2016; 89: 645–657. https://doi.org/10.1016/j.neuron.2016.01.008 PMID: 26844836

75. Kanichay RT, Silver RA. Synaptic and Cellular Properties of the Feedforward Inhibitory Circuit within the Input Layer of the Cerebellar Cortex. J Neurosci. 2008; 28: 8955–8967. https://doi.org/10.1523/JNEUROSCI.5469-07.2008 PMID: 18768689

76. Ankri L, Husson Z, Pietrajtis K, Proville R, Léna C, Yarom Y, et al. A novel inhibitory nucleo-cortical circuit controls cerebellar Golgi cell activity. Elife. 2015; 4: 1–26. https://doi.org/10.7554/eLife.06262 PMID: 25965178

77. Brickley SG, Misra C, Mok MHS, Mishina M, Cull-Candy SG. NR2B and NR2D subunits coassemble in cerebellar Golgi cells to form a distinct NMDA receptor subtype restricted to extrasynaptic sites. J Neurosci. 2003; 23: 4958–66. https://doi.org/10.1523/JNEUROSCI.23-12-04958.2003 PMID: 12832518

78. Santucci DM, Raghavachari S. The effects of NR2 subunit-dependent NMDA receptor kinetics on synaptic transmission and CaMKII activation. PLoS Comput Biol. 2008;4. https://doi.org/10.1371/journal.pcbi.1000208 PMID: 18974824

79. Keramidas A, Harrison NL. The activation mechanism of α1β2γ 2S and α3β3γ2S GABAA receptors. J Gen Physiol. 2010; 135: 59–75. https://doi.org/10.1085/jgp.200910317 PMID: 20038526

80. Peng H, Ruan Z, Long F, Simpson JH, Myers EW. V3D enables real-time 3D visualization and quantitative analysis of large-scale biological image data sets. Nat Biotechnol. 2010; 28: 348–353. https://doi.org/10.1038/nbt.1612 PMID: 20231818

81. Gall D, Prestori F, Sola E, D'Errico A, Roussel C, Forti L, et al. Intracellular calcium regulation by burst discharge determines bidirectional long-term synaptic plasticity at the cerebellum input stage. J Neurosci. 2005; 25: 4813–22. https://doi.org/10.1523/JNEUROSCI.0410-05.2005 PMID: 15888657

Chapter 5

General Discussion

Connectivity, dynamics, and information are three domains that contribute to the brain complexity. The nature of a complex system is generated by the interaction of many elements that are linked through a sophisticated network of connections, organized at different levels.

Over the years, the cerebellar complexity raised a lot of interest due to the fairly simple architecture, and the functionality related to the anatomical structure. The wide molecular and physiological heterogeneity of neuronal types, excitatory and inhibitory dynamics, and the signal transmitted among the cerebellar layers have been evaluated to highlight the role of the cerebellum in motor coordination, high–ordered cognitive, emotional, and perceptual processing (D'Angelo, 2018; Schmahmann, 2019). There are some open questions about cerebellar information processing related to (i) the process of the incoming signals; (ii) the performance of the forward controller operation; (iii) the contribution to the prediction and the precise timing. Here, we show two different approaches, experimental and computational, to gain a deeper insight into cerebellar network information processing. *Ex vivo* experimental assessments are important to study cerebellar cortex responsiveness at different input

frequencies and explore the cerebellar frequency-dependent processing involved in complex brain states. HD- MEAs is a powerful tool that features a high spatiotemporal resolution, and the recorded extracellular signal at each electrode enables the observation of neuronal activity network. The extensive amount of data obtained experimentally can support the reconstruction of the biophysical model of neurons and synapses, embedded in a realistic microcircuit.

The realistic model of detailed neurons reported in the second part of this thesis, suggested new directions for the experimental studies, providing a view to investigate the subcellular organization of neurons and synapses, and how they contribute to network functions. This methodology can embed multilevel information about molecular properties and network organization. Therefore, realistic models required validation through experimental information. The Golgi cell model reproduced the rich pattern of electrophysiological properties taken from experimental assessment and predicted the coincidence detection of parallel fibers and mossy fibers inputs due to dendritic integration.

The suggestion to use extracellular data as a source to reconstruct realistic models is already applied to improve the optimization performance and may provide better-validated models (Buccino et al., 2022). Moreover, the multimodal approaches can be an interesting alternative to explore the high level of complexity of the cerebellar network.

In conclusion, the cerebellar network is a complex system contained in a more complex system, the brain. The faster computational power carried out by an interlinked network of different neuronal types, makes the cerebellum an interesting object of study with multi-modal strategies to understand how connection shape dynamics and how dynamics generate integrated information.

References

Albus JS (1971) A theory of cerebellar function. Math Biosci 10:25–61.

Apps R et al. (2018) Cerebellar Modules and Their Role as Operational Cerebellar Processing Units. The Cerebellum 2018 17:5 17:654–682.

Apps R, Garwicz M (2005) Anatomical and physiological foundations of cerebellar information processing. Nat Rev Neurosci 6:297–311.

Apps R, Hawkes R (2009) Cerebellar cortical organization: A one-map hypothesis. Nat Rev Neurosci 10:670–681.

Arleo A, Nieus T, Bezzi M, D'Errico A, D'Angelo E, Coenen OJMD (2010) How synaptic release probability shapes neuronal transmission: information-theoretic analysis in a cerebellar granule cell. Neural Comput 22:2031–2058.

Attwell PJ, Rahman S, Ivarsson M, Yeo CH (1999) Cerebellar cortical AMPA-kainate receptor blockade prevents performance of classically conditioned nictitating membrane responses. J Neurosci 19 Available at: https://pubmed.ncbi.nlm.nih.gov/10594089/ [Accessed February 22, 2023].

Azevedo FAC, Carvalho LRB, Grinberg LT, Farfel JM, Ferretti REL, Leite REP, Filho WJ, Lent R, Herculano-Houzel S (2009) Equal numbers of neuronal and nonneuronal cells make the human brain an isometrically scaled-up primate brain. J Comp Neurol 513:532–541.

Bagnall MW, Zingg B, Sakatos A, Moghadam SH, Zeilhofer HU, Du Lac S (2009) Glycinergic Projection Neurons of the Cerebellum. Journal of Neuroscience 29:10104–10110.

Bastian AJ (2006) Learning to predict the future: the cerebellum adapts feedforward movement control. Curr Opin Neurobiol 16:645–649 Available at: https://pubmed.ncbi.nlm.nih.gov/17071073/ [Accessed January 15, 2023].

Burroughs A, Wise AK, Xiao J, Houghton C, Tang T, Suh CY, Lang EJ, Apps R, Cerminara NL (2017) The dynamic relationship between cerebellar Purkinje cell simple spikes and the spikelet number of complex spikes. J Physiol 595:283–299.

Buzsáki G, Llinás R (2017) Space and time in the brain. Science 358:482–485.

Castellazzi G, Bruno SD, Toosy AT, Casiraghi L, Palesi F, Savini G, D'Angelo E, Wheeler-Kingshott CAMG (2018) Prominent changes in cerebro-cerebellar functional connectivity during continuous cognitive processing. Front Cell Neurosci 12.

Cayco-Gajic NA, Silver RA (2019) Re-evaluating Circuit Mechanisms Underlying Pattern Separation. Neuron 101:584–602.

Cerminara NL, Lang EJ, Sillitoe R V., Apps R (2015) Redefining the cerebellar cortex as an assembly of non-uniform Purkinje cell microcircuits. Nat Rev Neurosci 16:79–93.

Cesana E, Pietrajtis K, Bidoret C, Isope P, D'Angelo E, Dieudonné S, Forti L (2013) Granule cell ascending axon excitatory synapses onto Golgi cells implement a potent feedback circuit in the cerebellar granular layer. J Neurosci 33:12430–12446.

Chadderton P, Margie TW, Häusser M (2004) Integration of quanta in cerebellar granule cells during sensory processing. Nature 428:856–860.

Courtemanche R, Chabaud P, Lamarre Y (2009) Synchronization in primate cerebellar granule cell layer local field potentials: Basic anisotropy and dynamic changes during active expectancy. Front Cell Neurosci 3:6.

Courtemanche R, Lamarre Y (2005) Local field potential oscillations in primate cerebellar cortex: synchronization with cerebral cortex during active and passive expectancy. J Neurophysiol 93:2039–2052.

Courtemanche R, Robinson JC, Aponte DI (2013) Linking oscillations in cerebellar circuits. Front Neural Circuits 7.

D'Angelo E (2011) Neural circuits of the cerebellum: hypothesis for function. J Integr Neurosci 10:317–352.

D'Angelo E (2018) Physiology of the cerebellum, 1st ed. Elsevier B.V.

D'Angelo E, Casali S (2012) Seeking a unified framework for cerebellar function and dysfunction: From circuit operations to cognition. Front Neural Circuits 6.

D'Angelo E, De Zeeuw CI (2009) Timing and plasticity in the cerebellum: focus on the granular layer. Trends Neurosci 32:30–40.

D'Angelo E, Nieus T, Maffei A, Armano S, Rossi P, Taglietti V, Fontana A, Naldi G (2001) Theta-Frequency Bursting and Resonance in Cerebellar Granule Cells: Experimental Evidence and Modeling of a Slow K+-Dependent Mechanism. Journal of Neuroscience 21:759–770.

D'Angelo E, Rossi P (1998) Integrated regulation of signal coding and plasticity by NMDA receptors at a central synapse. Neural Plast 6:8–16.

Davie JT, Clark BA, Häusser M (2008) The Origin of the Complex Spike in Cerebellar Purkinje Cells. The Journal of Neuroscience 28:7599.

de Solages C, Szapiro G, Brunel N, Hakim V, Isope P, Buisseret P, Rousseau C, Barbour B, Léna C (2008) High-frequency organization and synchrony of activity in the purkinje cell layer of the cerebellum. Neuron 58:775–788.

de Zeeuw CI, Hoebeek FE, Bosman LWJ, Schonewille M, Witter L, Koekkoek SK (2011) Spatiotemporal firing patterns in the cerebellum. Nat Rev Neurosci 12:327–344 Available at: http://dx.doi.org/10.1038/nrn3011.

de Zeeuw CI, Hoebeek FE, Schonewille M (2008) Causes and consequences of oscillations in the cerebellar cortex. Neuron 58:655–658 Available at: https://pubmed.ncbi.nlm.nih.gov/18549777/ [Accessed January 16, 2023].

De Zeeuw CI, Lisberger SG, Raymond JL (2021) Diversity and dynamism in the cerebellum. Nat Neurosci 24:160–167.

Dean P, Porrill J (2008) Adaptive-filter models of the cerebellum: computational analysis. Cerebellum 7:567–571.

D'Errico A, Prestori F, D'Angelo E (2009) Differential induction of bidirectional long-term changes in neurotransmitter release by frequency-coded patterns at the cerebellar input. J Physiol 587:5843–5857.

Diedrichsen J, Maderwald S, Küper M, Thürling M, Rabe K, Gizewski ER, Ladd ME, Timmann D (2011) Imaging the deep cerebellar nuclei: a probabilistic atlas and normalization procedure. Neuroimage 54:1786–1794.

Dugué GP, Brunel N, Hakim V, Schwartz E, Chat M, Lévesque M, Courtemanche R, Léna C, Dieudonné S (2009) Electrical coupling mediates tunable low-frequency oscillations and resonance in the cerebellar Golgi cell network. Neuron 61:126–139.

Eccles JC, Llinás R, Sasaki K (1966) Intracellularly recorded responses of the cerebellar Purkinje cells. Exp Brain Res 1:161–183 Available at: https://pubmed.ncbi.nlm.nih.gov/5943696/ [Accessed February 22, 2023].

Forti L, Cesana E, Mapelli J, D'Angelo E (2006) Ionic mechanisms of autorhythmic firing in rat cerebellar Golgi cells. Journal of Physiology 574:711–729.

Gall D, Prestori F, Sola E, D'Errico A, Roussel C, Forti L, Rossi P, D'Angelo E (2005) Intracellular Calcium Regulation by Burst Discharge Determines Bidirectional Long-Term Synaptic Plasticity at the Cerebellum Input Stage. Journal of Neuroscience 25:4813–4822.

Galliano E, Gao Z, Schonewille M, Todorov B, Simons E, Pop AS, D'Angelo E, Van Den Maagdenberg AMJM, Hoebeek FE, De Zeeuw CI (2013) Silencing the majority of cerebellar granule cells uncovers their essential role in motor learning and consolidation. Cell Rep 3:1239–1251.

Gandolfi D, Lombardo P, Mapelli J, Solinas S, D'Angelo E (2013) Theta-frequency resonance at the cerebellum input stage improves spike-timing on the millisecond time-scale. Front Neural Circuits 7:64.

Gandolfi D, Pozzi P, Tognolina M, Chirico G, Mapelli J, D'Angelo E (2014) The spatiotemporal organization of cerebellar network activity resolved by two-photon imaging of multiple single neurons. Front Behav Neurosci 8:92.

Harvey RJ, Napper RMA (1991) Quantitative studies on the mammalian cerebellum. Prog Neurobiol 36:437–463.

Horn KM, Pong M, Gibson AR (2010) Functional relations of cerebellar modules of the cat. J Neurosci 30:9411–9423 Available at: https://pubmed.ncbi.nlm.nih.gov/20631170/ [Accessed February 22, 2023].

Hull C (2020) Prediction signals in the cerebellum: beyond supervised motor learning. Elife 9.

Jaeger D, De Schutter E, Bower JM (1997) The Role of Synaptic and Voltage-Gated Currents in the Control of Purkinje Cell Spiking: A Modeling Study. The Journal of Neuroscience 17:91.

Jörntell H, Ekerot CF (2006) Properties of somatosensory synaptic integration in cerebellar granule cells in vivo. J Neurosci 26:11786–11797.

Keller GB, Mrsic-Flogel TD (2018) Predictive Processing: A Canonical Cortical Computation. Neuron 100:424–435.

Khaliq ZM, Gouwens NW, Raman IM (2003) The Contribution of Resurgent Sodium Current to High-Frequency Firing in Purkinje Neurons: An

Experimental and Modeling Study. Journal of Neuroscience 23:4899–4912 Available at: https://www.jneurosci.org/content/23/12/4899 [Accessed February 22, 2023].

Koziol LF, Lutz JT (2013) From movement to thought: the development of executive function. Appl Neuropsychol Child 2:104–115.

Llinás R, Sugimori M (1980) Electrophysiological properties of in vitro Purkinje cell dendrites in mammalian cerebellar slices. J Physiol 305:197–213 Available at: https://onlinelibrary.wiley.com/doi/full/10.1113/jphysiol.1980.sp013358 [Accessed February 22, 2023].

M. Bower J (2010) Model-founded explorations of the roles of molecular layer inhibition in regulating Purkinje cell responses in cerebellar cortex: more trouble for the beam hypothesis. Frontiers in Cellullar Neuroscience 4.

Manto M, Gruol DL, Schmahmann JD, Koibuchi N, Rossi F (2013) Handbook of the cerebellum and cerebellar disorders. Handbook of the Cerebellum and Cerebellar Disorders:1–2424.

Mapelli J, D'Angelo E (2007) The spatial organization of long-term synaptic plasticity at the input stage of cerebellum. Journal of Neuroscience 27:1285–1296.

Mapelli J, Gandolfi D, D'Angelo E (2010a) High-pass filtering and dynamic gain regulation enhance vertical bursts transmission along the mossy fiber pathway of cerebellum. Front Cell Neurosci 4.

Mapelli J, Gandolfi D, D'Angelo E (2010b) Combinatorial responses controlled by synaptic inhibition in the cerebellum granular layer. J Neurophysiol 103:250–261.

Mapelli L, Solinas S, D'Angelo E (2014) Integration and regulation of glomerular inhibition in the cerebellar granular layer circuit. Front Cell Neurosci 8:1–13.

Marr D (1969) A theory of cerebellar cortex. J Physiol 202:437–470.

Masoli S, Tognolina M, Laforenza U, Moccia F, D'Angelo E (2020) Parameter tuning differentiates granule cell subtypes enriching transmission properties at the cerebellum input stage. Commun Biol 3.

Medina JF, Mauk MD (2000) Computer simulation of cerebellar information processing. Nat Neurosci 3:1205–1211.

Middleton SJ, Racca C, Cunningham MO, Traub RD, Monyer H, Knöpfel T, Schofield IS, Jenkins A, Whittington MA (2008) High-Frequency Network Oscillations in Cerebellar Cortex. Neuron 58:763–774.

Mitchell SJ, Silver RA (2003) Shunting inhibition modulates neuronal gain during synaptic excitation. Neuron 38:433–445.

Nguyen TM, Thomas LA, Rhoades JL, Ricchi I, Yuan XC, Sheridan A, Hildebrand DGC, Funke J, Regehr WG, Lee W-CA (2023) Publisher Correction: Structured cerebellar connectivity supports resilient pattern separation. Nature 2023:1–1.

Nieus T, Sola E, Mapelli J, Saftenku E, Rossi P, D'Angelo E (2006) LTP regulates burst initiation and frequency at mossy fiber-granule cell synapses of rat cerebellum: Experimental observations and theoretical predictions. J Neurophysiol 95:686–699.

Nieus TR, Mapelli L, D'Angelo E (2014) Regulation of output spike patterns by phasic inhibition in cerebellar granule cells. Front Cell Neurosci 8.

O'Connor SM, Berg RW, Kleinfeld D (2002) Coherent electrical activity between vibrissa sensory areas of cerebellum and neocortex is enhanced during free whisking. J Neurophysiol 87:2137–2148.

Ohyama T, Nores WL, Murphy M, Mauk MD (2003) What the cerebellum computes. Trends Neurosci 26:222–227.

Palay SL, Chan-Palay V (1974) Cerebellar Cortex. Available at: http://link.springer.com/10.1007/978-3-642-65581-4.

Pellerin JP, Lamarre Y (1997) Local field potential oscillations in primate cerebellar cortex during voluntary movement. J Neurophysiol 78:3502–3507.

Person AL, Raman IM (2012) Synchrony and neural coding in cerebellar circuits. Front Neural Circuits 6:1–32.

Popa D, Spolidoro M, Proville RD, Guyon N, Belliveau L, Léna C (2013) Functional Role of the Cerebellum in Gamma-Band Synchronization of the Sensory and Motor Cortices. The Journal of Neuroscience 33:6552.

Powell K, Mathy A, Duguid I, Häusser M (2015) Synaptic representation of locomotion in single cerebellar granule cells. Elife 4.

Purves D, Augustine GJ, Fitzpatrick D, Katz LC, LaMantia A-S, McNamara JO, Williams SM (2001) Neuroscience. :1–2.

Raman IM, Bean BP (2001) Inactivation and recovery of sodium currents in cerebellar Purkinje neurons: Evidence for two mechanisms. Biophys J 80:729–737 Available at: http://www.cell.com/article/S0006349501760523/fulltext [Accessed February 22, 2023].

Rancz EA, Ishikawa T, Duguid I, Chadderton P, Mahon S, Häusser M (2007) High-fidelity transmission of sensory information by single cerebellar mossy fibre boutons. Nature 450:1245–1248.

Rasmussen A, Jirenhed DA, Wetmore DZ, Hesslow G (2014) Changes in complex spike activity during classical conditioning. Front Neural Circuits 8.

Raymond JL, Medina JF (2018) Computational Principles of Supervised Learning in the Cerebellum. Annu Rev Neurosci 41:233–253.

Ros T, Moseley MJ, Bloom PA, Benjamin L, Parkinson LA, Gruzelier JH (2009) Optimizing microsurgical skills with EEG neurofeedback. BMC Neurosci 10:1–10.

Rössert C, Solinas S, D'Angelo E, Dean P, Porrill J (2014) Model cerebellar granule cells can faithfully transmit modulated firing rate signals. Front Cell Neurosci 8.

Schmahmann JD (2019) The cerebellum and cognition. Neurosci Lett 688:62–75.

Schonewille M, Luo C, Ruigrok TJH, Voogd J, Schmolesky MT, Rutteman M, Hoebeek FE, De Jeu MTG, De Zeeuw CI (2006) Zonal organization of the mouse flocculus: physiology, input, and output. J Comp Neurol 497:670–682.

Schwartz EJ, Rothman JS, Dugue GP, Diana M, Rousseau C, Angus Silver R, Dieudonne S (2012) NMDA Receptors with Incomplete Mg2+ Block Enable Low-Frequency Transmission through the Cerebellar Cortex. The Journal of Neuroscience 32:6878.

Shin SL, Hoebeek FE, Schonewille M, de Zeeuw CI, Aertsen A, de Schutter E (2007) Regular Patterns in Cerebellar Purkinje Cell Simple Spike Trains. PLoS One 2:e485 Available at: https://journals.plos.org/plosone/article?id=10.1371/journal.pone.0000485 [Accessed February 22, 2023].

Silva NT, Ramírez-Buriticá J, Pritchett DL, Carey MR (2022) Neural instructive signals for associative cerebellar learning. bioRxiv:2022.04.18.488634.

Sola E, Prestori F, Rossi P, Taglietti V, D'Angelo E (2004) Increased neurotransmitter release during long-term potentiation at mossy fibre–granule cell synapses in rat cerebellum. J Physiol 557:843–861.

Solinas (2008) Computational reconstruction of pacemaking and intrinsic electroresponsiveness in cerebellar golgi cells. Front Cell Neurosci 1.

Solinas S, Nieus T, D'Angelo E (2010) A realistic large-scale model of the cerebellum granular layer predicts circuit spatio-temporal filtering properties. Front Cell Neurosci 4.

Sugihara I, Shinoda Y (2004) Molecular, topographic, and functional organization of the cerebellar cortex: a study with combined aldolase C and olivocerebellar labeling. J Neurosci 24:8771–8785.

Tang T, Xiao J, Suh CY, Burroughs A, Cerminara NL, Jia L, Marshall SP, Wise AK, Apps R, Sugihara I, Lang EJ (2017) Heterogeneity of Purkinje cell simple spike–complex spike interactions: zebrin- and non-zebrin-related variations. J Physiol 595:5341–5357.

Van Essen DC, Donahue CJ, Glasser MF (2018) Development and Evolution of Cerebral and Cerebellar Cortex. Brain Behav Evol 91:158–169.

Voogd J (2011) Cerebellar Zones: A Personal History. Cerebellum 10:334.

Warnaar P, Couto J, Negrello M, Junker M, Smilgin A, Ignashchenkova A, Giugliano M, Thier P, De Schutter E (2015) Duration of Purkinje cell complex spikes increases with their firing frequency. Front Cell Neurosci 9.

White JJ, Arancillo M, Stay TL, George-Jones NA, Levy SL, Heck DH, Sillitoe R v. (2014) Cerebellar Zonal Patterning Relies on Purkinje Cell Neurotransmission. The Journal of Neuroscience 34:8231 Available at: /pmc/articles/PMC4051975/ [Accessed February 22, 2023].

Wise AK, Cerminara NL, Marple-Horvat DE, Apps R (2010) Mechanisms of synchronous activity in cerebellar Purkinje cells. J Physiol 588:2373–2390 Available at: https://onlinelibrary.wiley.com/doi/full/10.1113/jphysiol.2010.189704 [Accessed February 24, 2023].

Žárský V (2012) Jan Evangelista Purkyně/Purkinje (1787-1869) and the establishment of cellular physiology--Wrocław/Breslau as a central European cradle for a new science. Protoplasma 249:1173–1179 Available at: https://pubmed.ncbi.nlm.nih.gov/22543689/ [Accessed February 22, 2023].

Zhou H, Lin Z, Voges K, Ju C, Gao Z, Bosman LWJ, Ruigrok TJ, Hoebeek FE, de Zeeuw CI, Schonewille M (2014) Cerebellar modules operate at different frequencies. Elife 3 Available at: https://pubmed.ncbi.nlm.nih.gov/24843004/ [Accessed January 16, 2023].